APPLICATION OF SINGLE WALLED CARBON NANOTUBES IN ENVIRONMENTAL ENGINEERING: ADSORPTION AND DESORPTION OF ENVIRONMENTALLY RELEVANT SPECIES STUDIED BY INFRARED SPECTROSCOPY AND TEMPERATURE PROGRAMMED DESORPTION

by

Xue Feng

B.S. in Polymer Engineering, Shanghai Jiaotong University, China, 1999

M.S. in Environmental Engineering, Shanghai Jiaotong University, China, 2002

Submitted to the Graduate Faculty of

School of Engineering in partial fulfillment

of the requirements for the degree of

Doctor of Philosophy

University of Pittsburgh

2005

UNIVERSITY OF PITTSBURGH

SCHOOL OF ENGINEERING

This dissertation was presented

by

Xue Feng

It was defended on

November 21, 2005

and approved by

Leonard W. Casson, Associate Professor, Department of Civil and Environmental Engineering

J. Karl Johnson, Professor, Department of Chemical and Petroleum Engineering

Robert Ries, Assistant Professor, Department of Civil and Environmental Engineering

Dissertation Co-Director: Eric Borguet, Associate Professor, Department of Chemistry, Temple University

Dissertation Director: Radisav D. Vidic, Professor, Department of Civil and Environmental Engineering

APPLICATION OF SINGLE WALLED CARBON NANOTUBES IN ENVIRONMENTAL ENGINEERING: ADSORPTION AND DESORPTION OF ENVIRONMENTALLY RELEVANT SPECIES STUDIED BY INFRARED SPECTROSCOPY AND TEMPERATURE PROGRAMMED DESORPTION

Xue Feng, Ph.D.

University of Pittsburgh, 2005

This study evaluated the environmental applications of carbon nanotubes through the adsorption and desorption of representative environmentally relevant adsorbates; ammonia, hydrogen sulfide and acetone under ultra high vacuum (UHV) and high pressure conditions. The results showed that functionalities/defects sites on nanotube surfaces play an important role on the interaction between molecules and carbon nanotubes.

The oxygen containing functional groups on single-walled carbon nanotubes (SWNTs) are studied by Fourier Transform Infrared (FTIR) spectroscopy under vacuum. Vacuum heating to ~ 1300 K removes most of the functionalities in the samples. The similarities in the infrared spectra of the Rice Tubes after a 1400 K treatment with spectra for HiPco nanotubes suggest the observation of intrinsic SWNT IR bands.

Ammonia adsorption on single walled carbon nanotubes (SWNTs) was studied in order to investigate the environmental application of nanotubes, mainly possible uses as sensors. At 94 K, vacuum annealed SWNTs showed no detectable ammonia uptake. However, the ammonia adsorption was found to be sensitive to the functionalities and defects on the nanotube surfaces.

NH_3 desorbed from those nanotubes above 140 K, indicating a weak adsorbate-nanotube interaction (~30 kJ/mol). This work suggests the influence of functionalities and/or defect densities on the sensitivity of SWNT chemical gas sensors.

Both physisorption and chemisorption of acetone on nanotubes were observed. It was found that H_2S adsorbed on nanotube surfaces at cryogenic temperature but not at room temperature. The low desorption temperature suggests only physisorption of H_2S on nanotubes.

In this study, low concentration of functionalities on carbon material surfaces was detected by fluorescent labeling technique. Florescent labeling indicated the presence of COOH and CHO groups on the ACF 25 fiber surface. Neither the infrared spectrum nor the X-ray photoelectron spectrum showed evidence of the existence of those low concentration groups.

The key findings of this work make it possible that applying scientific information obtained from studies under ideal conditions to industrial sorbents/sensors under realistic process conditions. Nanotube surfaces can be modified chemically to enhance their affinities for certain kinds of gas molecules.

TABLE OF CONTENTS

LIST OF TABLES

LIST OF FIGURES

ACKNOWLEDGEMENTS

First, I am especially grateful to my research advisors, Dr. Eric Borguet and Dr. Radisav D. Vidic, for the rewarding experience of working with them.

I express appreciation to the committee members, Dr. Karl Johnson, Dr. Leonard W. Casson and Dr. Robert Ries, for their comments and help in the proposal and preparation of the final draft.

I would like to express a special acknowledgement to Dr. John T. Yates, Jr. and his group, especially Oleg Byl, for the benefit of their experiences in vacuum surface science. Thanks also go to Jeff, Dennis and Tom, in the machine shop and Chuck, in the electronic shop, in the Department of Chemistry at the University of Pittsburgh for manufacturing the IR chamber and other useful materials for my research.

Many thanks go to my colleagues in the Department of Civil and Environmental Engineering at the University of Pittsburgh and the Chemistry Department at the Temple University: Wayne, Joon, Nicole, Nikolay, Yufan, Satoshi, Ali and Kyoungja.

Special acknowledgments go to Dr. Chris Matranga at the National Energy Technology Laboratory for his patient help at the beginning of my research work.

The contributions of the Morukuma group at Emory, especially Dr. Stephan Irle, in providing microscopic insight into the processes investigated are gratefully acknowledged.

The research was made possible by generous financial support from the U.S. Department of Energy.

Finally, this work is dedicated to the love of my husband, Yangjun, my daughter, Ai tian and my parents.

1.0 INTRODUCTION

In 2004, US Environmental Protection Agency (EPA) announced that research was needed to identify opportunities and applications of nanoscale science and technology to address environmental problems [1]. Three research topics were identified

Environmental benign manufacturing and processing,

Remediation/treatment,

Sensors.

Nanotechnology refers to the use of materials and structures of nanoscale dimensions. Nanotubes are relatively new but broadly studied materials in the nanotechnology field. Due to their outstanding mechanical, electronic and chemical properties, carbon nanotubes offer great promise of delivering new and improved environmental technologies as sensors and sorbent materials to detect and treat existing contaminants and prevent new pollution which are significant challenges to environmental scientists and engineers [2]. Nanotubes, present as small particulate material, may also present environmental hazards in their own right[2]. Clearly nanotechnology brings many opportunities and challenges that scientists have only just begun to explore.

Environmental control agencies, researchers and the general public are concerned about the increasing mobilization and release of trace elements to the environment. Substances of significant concern in the remediation of soils, sediment and ground water include heavy metals

(e.g. mercury, lead, cadmium) and organic compounds (e.g. benzene, chlorinated solvents, and toluene). Although nanotubes have been applied to adsorb several kinds of trace contaminants, [3, 4] from water, there is a lack of fundamental understanding of the physics and chemistry of nanotube surfaces related to sorbent capacity, and interference of other components in the gas mixture.

The objective of this study was to investigate possible environmental applications of nanotubes through adsorption and desorption study of environmentally interesting molecules including ammonia, hydrogen sulfide and acetone. This study describes the effects of surface functional groups and different nanotube production methods on the adsorption and desorption of molecules from nanotube surfaces. The study suggests an integrated approach that may provide conditions by which adsorption process can be optimized on nanotube surfaces. The key findings of these studies will then be extended to more complex systems. Additionally, nanotubes present a relatively well defined degree of porosity and functionality that can also serve as a model for more complex nanoporous carbons such as activated carbon and activated carbon fiber (ACF). A long term goal of the study is to design more efficient and cost-effective sorbents, e.g. nanotubes, for pollution control through the basic understanding of molecular interactions with these materials.

2.0 LITERATURE REVIEW

2.1 CARBON NANOTUBES AND THEIR ENVIRONMENTAL APPLICATIONS

Carbon nanotubes have been the focus of much research since their discovery in the early 90s'[5]. Simply speaking, a carbon nanotube is analogous to a sheet of graphite rolled into a cylinder closed at either end with caps containing pentagonal rings. Depending on the twist direction of the graphite sheet, nanotubes can be metallic or semiconducting. Cartoons in Figure 2- 1[6, 7] illustrate the idea of rolling. Due to their special structure, perfect carbon nanotubes are light, flexible, thermally stable and chemically inert [8]. Several methods have been applied to produce nanotubes. Laser ablation and HiPco are two effective methods [6, 7] A laser is used in laser ablation technique to vaporize a composite graphite/transition metal target inside a heated quartz flow tube. Nanotubes form in the condensing vapor. HiPco stands for catalytic decomposition of CO at high pressure and temperature.

Nanotechnology could make many products lighter, stronger, cleaner, less expensive and more accurate. EPA joined the national nanotechnology initiative in FY 2002 through its STAR grant program. Nanotechnology has the potential to significantly improve environmental protection. [9]

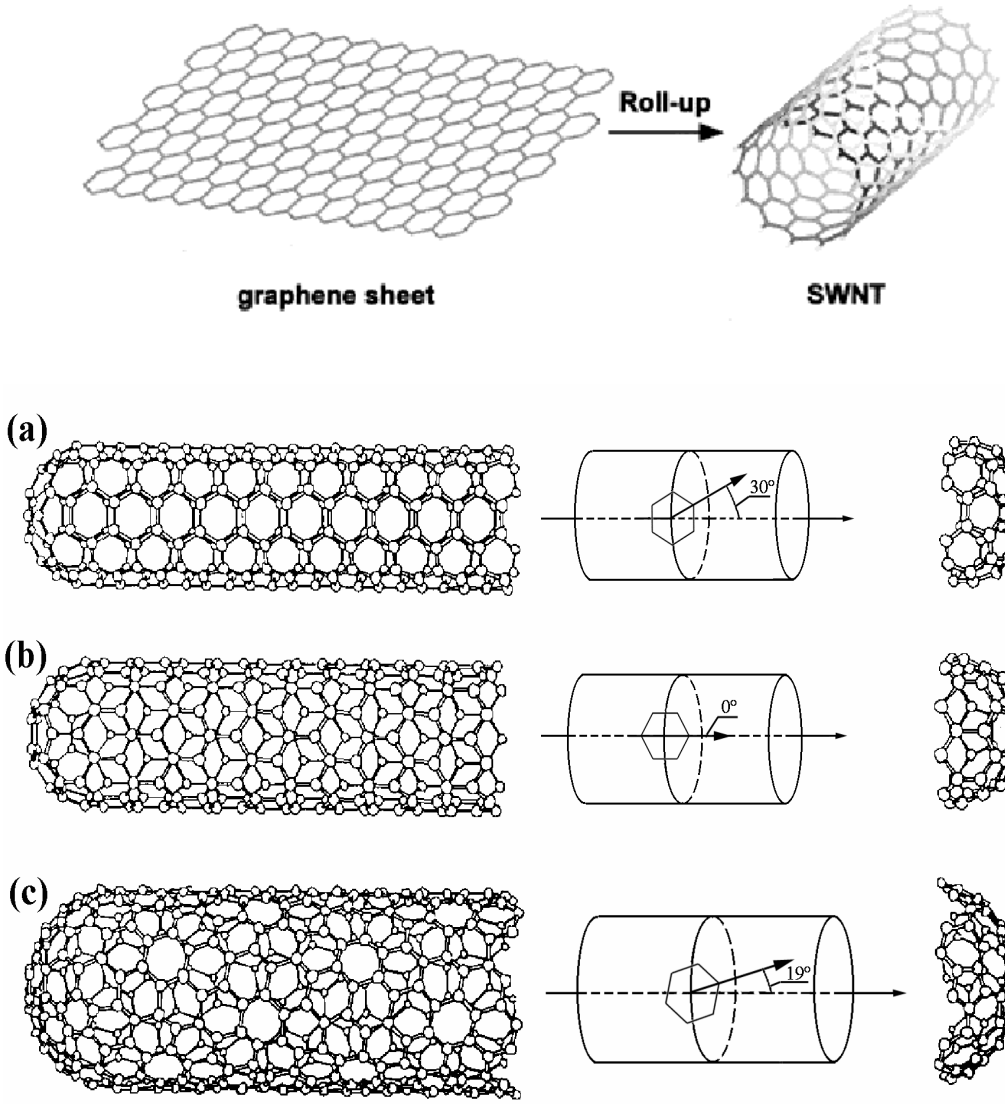

Figure 2- 1 Schematic theoretical models of single walled carbon nanotubes, their hexagon orientations and cap structures (a) armchair (5,5) nanotube; (b) zigzag (9,0) nanotube; (c) chiral (10,5) nanotube. [6, 7]

The excellent mechanical, electronic and chemical properties of carbon nanotubes have stimulated some work by environmental scientists and engineers [2]. Most work until now has been performed on the laboratory scale. So far, there are three main environmental applications of nanotubes, i.e. energy storage, sorbents and sensors. Nanotechnology has the potential to be used to develop new, "green" processing technologies that minimize or eliminate the use of toxic materials and the generation of undesirable byproducts and waste streams. However, the present cost of nanotubes, at hundreds of dollars per gram, limits large-scale applications of nanotubes in the near future. Novel production techniques may change this in the future.

Although currently expensive, carbon nanotubes are also considered promising materials for hydrogen storage, an application that will be crucial in the development of efficient hydrogen-based vehicles.[10] The reversible storage of hydrogen on nanotubes has attracted much attention from the energy and environmental protection field. Using hydrogen as an alternative energy carrier is rapidly developing due to an increasing demand for renewable and environmentally friendly energy sources[11-15]. It is reported that crystalline SWNTs have a capacity for hydrogen sorption of 5-10 wt. % at pressures less than 1 bar near room temperature[16]. Such a hydrogen storage capacity would be a significant advance for the use of hydrogen as a fuel as high gravimetric density of hydrogen is a figure of merit. The Department of Energy (DOE) target for vehicular fuel cells is 6 wt.% for gravimetric and 60 kg/m^3 for volumetric densities[17]. Simonyon et.al have presented a review of experimental and theoretical work on hydrogen adsorption in graphite nanofibers and single walled carbon nanotubes[18]. They found that adsorption of hydrogen onto alkali-metal doped nanotubes increased in comparison to the identical bundle without the metal and concomitant charge transfer. However, the total adsorption of hydrogen on metal-doped SWNT bundles is still a

rather modest 2 wt.% which is significantly smaller than the DOE target[18]. Extensive exploration of hydrogen storage has been performed by several research groups. However, the claimed hydrogen uptake capacity varied from less than 0.5% up to 10%.[18] Nanotubes are produced by different methods and under different conditions such as pressure and temperature make comparisons sometimes difficult. However, the uniform pore size distribution, high surface area and excellent electronic properties make nanotubes promising materials for hydrogen storage[18].

Storage of other fuels in nanotubes also has been studied. Natural gas (methane is the primary constituent) adsorbed on porous materials is a promising alternative to compressed natural gas as a clean vehicular fuel, and for bulk transportation. The adsorption of methane gas on isolated SWNTs and idealized carbon slit pores at 303 K was studied by nonlocal density functional theory. [19-21] Based on the research already done, [19-21] nanotubes appear to be promising materials for energy storage.

The early impact of nanotube research has been mostly in remediation and end-of-pipe treatment technologies. Highly toxic, persistent, and difficult to treat and/or access pollutants present particular challenges. Nanotechnology applications that would result in improved treatment options might include removal of the minute concentrations of contaminants from water and air and “smart” materials or reactive surface coatings that destroy or immobilize toxic compounds. Substances of significant concern in the remediation of soils, sediment and ground water include heavy metals and organic compounds [1]. EPA STAR researchers at Lehigh University are optimizing the synthesis of nano-sized particles for use in groundwater cleanup. [9] The potential benefit of this technology for remediation stems from the fact that it is

portable, the nanoparticles are highly reactive, and it can be scaled to fit the pollution problem. [9]

Carbon nanotubes have been proposed as superior sorbents for dioxin removal.[22] Due to the extreme toxicity of dioxins, it is desirable to have a more efficient sorbent than activated carbon so that the dioxin emissions can be reduced to lower levels. Long et al. found the interactions of dioxins with carbon nanotubes are much stronger than that with activated carbon.[22] The origin of these strong interactions is not clear but the authors suggest that it may be attributed to the unique structure and electronic properties of carbon nanotubes.[22] Because of the higher bond energy between dioxin and carbon nanotubes compared to other sorbents (315 kJ/mol for nanotube vs. 119 kJ/mol for ZX-4 carbon), the removal efficiency for dioxin by carbon nanotubes is much higher than other sorbents. Nanotubes can also be used as aqueous phase adsorbents. Peng et al. used as-grown nanotubes and graphitized nanotubes as adsorbents to remove toxic 1,2-dichlorobenzene (DCB) from water.[23] Nanotubes can be used as adsorbents in a wide pH range (3-10).[23] The experiments demonstrated that it takes only 40 minutes for nanotubes to attain equilibrium and that the adsorption capacity is relatively high, thereby making carbon nanotubes good adsorbents for the removal of DCB from water. Nanotubes were also evaluated as adsorbents for trapping volatile organic compounds from environmental samples. For example, Li and coworkers, found that nanotubes have much higher breakthrough volumes for toluene, xylene, dichloromethane, 1,2-dichloroethane and so on than graphitized carbon black with the same surface area.[24]. This was ascribed to the more porous structure of SWNTs. The results indicate that nanotubes are potential useful adsorbents for direct trapping VOCs from air samples.

The adsorption of heavy metals by nanotubes has been studied by Li group[3, 4]. They found that nanotubes show exceptional adsorption capability and high adsorption efficiency for lead removal from water. The adsorption is significantly influenced by the pH value of the solution and the nanotube surface status. Their work also showed that the oxidation dramatically increase the cadmium adsorption capacity. The Cd (II) adsorption capacity of the as grown nanotubes is much smaller than H_2O_2, HNO_3 and $KMnO_4$ oxidized nanotubes.

Using carbon nanotubes in computer displays[2] may further diminish environmental impacts by eliminating toxic heavy metals and dramatically reducing material and energy use requirement. Moreover, multi-walled nanotubes demonstrated good properties as solid phase extraction adsorbents for the extraction and quantification of several chemicals in water including bisphenol A, 4-n-nonylphenol, 4-tert-octylphenol and phthalate esters. [25]

Novel monitoring technologies and devices are needed for pollutants and microbial detection. Protection of human health and ecosystem requires rapid, precise sensors capable of detecting pollutants at the molecular level. The EPA is interested in remote, *in situ*, and continuous monitoring devices that yield real-time information and can detect pollutants at very low concentrations [1]. EPA STAR researchers at the University of California-San Diego are developing new, selective, solid-state sensors that use nanotechnology to detect toxic forms of chromium and arsenic in water.[9] Recently, several papers about nanotube sensors have been published [26-30]. The electrical resistance of semi-conducting SWNTs is dramatically changed upon exposure to ammonia and nitrogen dioxide molecules [28]. This result provided the basis for research into the use of nanotubes as chemical sensors. Goldoni and coworkers showed that gas molecules could directly affect the nanotube properties via physisorption or chemisorption, but they could also have an indirect effect by interacting with contaminants bonded to the

nanotubes[29]. Residual contaminants in purified single-walled carbon nanotube bundles may be responsible for the reported sensitivity of the electronic and transport properties to oxygen[29]. Strong sensitivity to NO_2, SO_2 and NH_3 was observed which confirmed the possible application of nanotubes as powerful sensors capable of measuring environmentally significant levels of toxic gases.

2.2 OXYGEN CONTAINING FUNCTIONALITIES ON NANOTUBE SURFACE AND THEIR DETECTION

The presence of functional groups or adsorbed oxygen species on single-walled carbon nanotubes (SWNTs) is known to affect properties of these materials [30, 31]. Functionalities influence the electronic properties of SWNTs by disrupting the graphitic-like sp^2 network of carbon in the SWNTs. This disruption produces local sp^3 defects which can introduce an impurity state near the Fermi level[32] and perturb the electronic spectra of these materials [33]. The conductivity[32] and solubility [34, 35] of SWNTs have also been shown to change as a result of functionalization. Ultimately, the performance of SWNTs as adsorbents[36], catalysts[37], capacitors[38], microscopy tips [39-41] and sensors [42] depends on understanding and controlling surface functionalities.

Normally, as-received nanotubes contain few heteroatom functional groups. However, during various purification steps, oxygen containing functional groups are introduced [43, 44]. Some purification procedures use aggressive oxidizers like HNO_3, H_2SO_4, or H_2O_2 to crack the passivating carbon shells encapsulating residual catalyst particles and to remove unwanted carbons [45-47]. Newer procedures use more gentle steps which expose the catalyst by heating

in moist air followed by an acid wash for catalyst removal[48]. As one might expect, the amount and type of functional groups introduced by these purification steps vary drastically with each different type of procedure employed.

Many applications of carbon materials, including activated carbon, activated carbon fibers and carbon nanotubes are based on the presence of oxygen containing surface functional groups[49-54]. For example, the dynamic adsorption of hexane by activated carbons under humid conditions was found to be mainly governed by the quantity of acidic surface functional groups[55]. It is reported that oxygen surface complexes, possibly lactones and carbonyl groups, were the active sites for Hg-0 capture[56]. An increase in the number of some acid functional groups and surface wetting quality was helpful to microorganism fixing[57].

Several methods have been applied to detect and quantify oxygen functional groups on carbon surfaces[58-61]. Infrared spectroscopy (IR) [62-68], X-ray photoelectron spectroscopy (XPS) [50, 55, 62, 63, 68, 69], thermal desorption spectroscopy (TPD)[62, 65, 70], elemental analysis [50, 71, 72] and Boehm titration [62, 63, 72-74] are the most frequently used methods. Although the Boehm titration is a valuable technique, it is limited to special functional groups[61, 75]. TPD does not provide detailed information about the type of functionality as it only probes the products of their decomposition. Quantitative analysis of XPS and IR is not straightforward[61]. The time-consuming titration[58], the difficulty in assigning the peaks, and the influence of experimental parameters (such as the heating rate in TPD) highlight the need for new methods. Furthermore, these techniques do not reveal the location of the functional groups. For example, they do not distinguish between functional groups located within small pores and functional groups located in large pores and on the external surface.

Some new methods, e.g., inverse gas chromatography (IGC)[76, 77], diffuse reflectance infrared Fourier transform spectroscopy (DRIFTS)[78], combining DRIFTS with transient kinetic (TK) and TPD techniques[79], and electro kinetic measurements (zeta potential)[80], have been applied to investigate the surface properties of activated carbons and carbon fibers. Scanning tunneling and atomic force microscopes (STM/AFM) have also been used to study surfaces functional groups in some cases[81].

Fluorescent labeling has been used to identify and quantify functionalities on self-assembly monolayer[82] and polymer surfaces[83, 84]. Recently, the interactions between functional groups (defects sites) on single walled carbon nanotubes (SWNTs) and their performances in various fields have been explored actively by several groups. Changing the quantity or type of functional groups will make obvious differences to the solubility[34, 85], adsorption behaviors [4, 14, 86-89] of SWNTs and their performance as catalysts [90], capacitors [91] electrolytic transporters [92] and biosensors[42].

Attaching molecules to the SWNTs through functional groups also can modify the surface of SWNTs[93, 94] and make SWNTs work as sensor [95] and carbon SWNTs AFM probes.[39] However, covalent chemical attachments to the functional groups will decrease the maximum buckling force of SWNTs by about 15% regardless of tubule helical structure or radius of SWNTs.[96]

Identification and quantification of those functional groups have become key issues for the field of SWNT materials topic.[97-99]. XPS [100-102], IR[15, 100, 101, 103, 104] and Raman [105] are the main techniques used to detect functional groups on SWNTs surfaces. Scientists try to develop new methods to detect functional groups more effectively.

Scanning tunneling microscopy (STM) and TEM were applied to analyze carbon nanotubes covered with functional groups attached to their exterior wall [106] Jiang and his colleagues selectively attached gold nanoparticles to the nanotubes.[94, 107] This approach provided an efficient method to attach other nanostructures to carbon nanotubes and can be used as a detection method of the functional groups on carbon nanotube surfaces. SWNTs produced by plasma laser vaporization (PLV) and containing oxidized surface functional groups were studied for the first time with NEXAFS in 2001.[104] By measuring the evolution of CO_2(g) and CO(g), the fraction of oxidized carbon sites present were determined on heating to 1273 K [108].

Fluorescence detection is a technique that has been broadly used in the biological field. Recently, it was introduced into research work of carbon nanotube in several aspects[109-115]. Several groups studied the attachment of interesting fluorescent molecules through linkage with functional groups on nanotube surface[116-120]. Fluorescence microscopy was used to make carbon nanotubes visible [121, 122]. Georgakilas reported an approach to the organic functionalization of nanotubes with a fluorescent moiety (pyrene), which has led to high level of solubility of the resulting products. Zhu and his colleagues incorporated a naphthalimide fluorescence molecule onto SWNT via amidation. [123] Those modifications can change the electronic structure of nanotubes. [123] Several papers have shown that the chromophore emission can be significantly quenched by the attached nanotubes[122, 123] which makes the quantification of chromophores on nanotubes surface complicated.

2.3 INFRARED STUDY OF CARBON NANOTUBES

The vibrational spectrum of a molecule is considered to be a unique physical property and is characteristic of the molecule. As such, the infrared spectrum can be used as a fingerprint for identification by the comparison of the spectrum from an "unknown" with previously recorded reference spectra. It is possible to detect whether a specific functional group is present. If detected, it is also possible to determine local orientation of the group and its local environment [124].

Infrared spectroscopy has proved to be a powerful technique to study carbon nanotubes[103, 125-127]. Both theoretical and experimental work showed that infrared active phonon modes around 1590 and 850 cm^{-1} appear in all symmetries almost independent of the diameter and are therefore expected to produce clearly recognizable structures in absorbance or reflectance spectra of a variety of single walled carbon nanotubes [128].

In addition to the study of the intrinsic structure of nanotubes, infrared spectroscopy has been widely applied to the investigation of interactions between nanotubes and molecules in the physical, environmental and biological fields. [24, 28, 29, 129, 130]

There are many possible sites for a molecule to adsorb on nanotube bundles. There are four adsorption sites on nanotube bundles from a strictly geometric point of view. They are the tube interior (endohedral), the interstitial channels, the external grooves and the outer surfaces as shown in Figure 2- 2[131]. Infrared spectroscopy has proved an effective technique to differentiate molecule adsorption sites on nanotube bundles. Matranga et al. have investigated carbon dioxide, generated during the decomposition of functional groups, trapped in nanotube bundles using infrared spectroscopy[132, 133] . Experimental and simulation studies point to a sequential filling of adsorption sites in open nanotubes with adsorption in interstitial sites

preceding adsorption in endohedral sites. The limited number of sites available to the trapped carbon dioxide species is used to facilitate a tentative assignment of vibrational peaks to specific sites in the nanotube bundles. Furthermore, they studied the displacement of carbon dioxide by Xe on nanotube bundles with FT-IR and grand canonical Monte Carlo (GCMC) simulations. [132, 133] Both experimental and simulation work showed that the molecules in endohedral sites are initially displaced by Xe before molecules in groove/external surface sites. Yim and coworkers[134] used molecular simulations to show a range of shifts for the asymmetric stretching mode from about -6 to -20 cm^{-1} for internally bound CO_2 and a range from -4 to -16 cm^{-1} for externally bound CO_2 at low densities. Byl et.al [135, 136] used infrared spectroscopy to discriminate molecules such as CF_4 and NO, bound by physisorption on the exterior surface of nanotubes and molecules bound in the interior. These results suggest that Infrared spectroscopy is a useful and effective method to determine the adsorption sites on nanotube bundles.

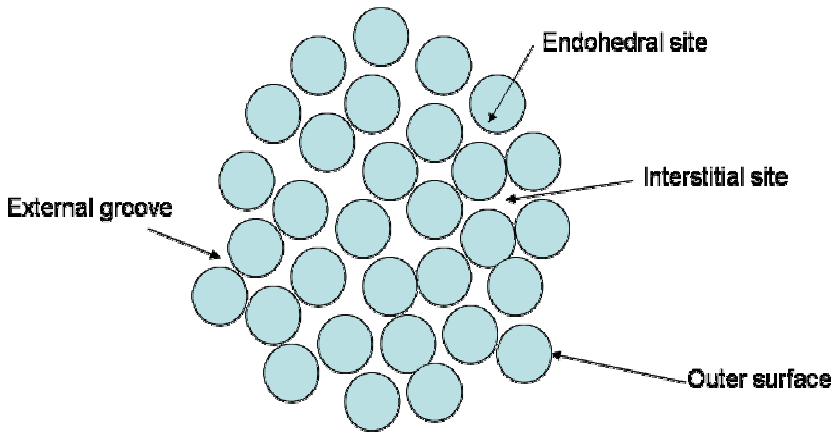

Figure 2- 2 Cartoon of available adsorption sites on nanotube bundles

Functional groups introduced, on nanotube surfaces during purification or oxidation processes play important role in nanotube performances. The presence of functional groups on single walled carbon nanotubes (SWNTs) is known to affect properties of these materials [31]. The performance of SWNTs as adsorbents[137], catalysts[138], capacitors[38], microscopy tips [39-41] and sensors [42] depends on understanding and controlling surface functionalities. Again, infrared spectroscopy has proved to be an extremely powerful tool to study functional groups. It was applied to understand the photodesorption mechanism of aligned carbon nanotubes thin film by impedance spectroscopy[139]. It was found that the photodesorption strongly depends on the polar impurities adsorbed on the nanotube surfaces. FT-IR transmission spectra of as-grown nanotubes detected large amounts of OH, CH_2 and CH_3 functional groups. Through the investigation by Raman and FT-IR, it was confirmed that the release of the trapped OH polar molecules was a dominant light molecular desorption mechanism[139].

This study focused on the Fourier Transform infrared (FTIR) studies of the functional groups present on nanotube samples produced by HiPco and laser ablation techniques. In particular, it was found that the air/HCl treatment is as effective in reducing the metal content of HiPco samples as HNO_3 refluxing, but it does not functionalize the sample whereas the HNO_3 treatment does. It was also found that vacuum heating to above 1000 K is effective in removing most of the functionalities created in HNO_3 treated HiPco samples. The details of this work will be presented in chapter 4.

A number of other chemical species adsorbed on SWNTs have been investigated. Reflectance FT-IR spectra revealed that catalase, xanthine oxidase and glucose oxidase adsorbed onto the SWNT surfaces[29, 140, 141]. The direct electrochemistry of redox-active bio-macromolecules can be improved through the use of carbon nanotubes[29, 140, 141]. The

catalytic activity of these molecules isn't drastically perturbed by adsorption on the nanotubes [29, 140, 141].

During the study of adsorption of ammonia and nitrogen dioxide on nanotubes at room temperature, Ellison et al.[142] suggested that ammonia adsorbs via both its lone pair and hydrogen atoms at room temperature and that nitrogen dioxide adsorbs in an asymmetric configuration via at least one of the oxygen atoms. However, as will be shown in Chapter 4, no ammonia adsorption was observed on nanotubes at room temperature.

Infrared spectroscopy has been effectively applied to study molecular interactions and functional groups on nanotube surfaces. Moreover, this powerful technique can also been used to study the structures of tubes.

2.4 KINETICS OF DESORPTION FROM SOLID SURFACES

Temperature programmed desorption (TPD) spectroscopy is one of the simplest quantitative techniques for studying interactions of chemical species with surfaces [143]. The basic idea of TPD is illustrated in Figure 2- 3. After molecules adsorb on the sample surfaces, samples are heated to elevated temperature and desorbed species are monitored by a mass spectrometer. TPD can be used to determine the activation energy for desorption which, in the absence of an activation energy for adsorption, corresponds to the binding energy between the absorbate and the adsorbent. The relative sticking coefficient can be deduced from a series of desorption spectra with different initial doses. TPD can also provide information about the kinetics of adsorption and desorption. The thermal desorption rate can be interpreted by an Arrhenius

formula, which assumes that the desorption rate constant, k, is independent of surface coverage, as follows;

$$-\frac{d\theta}{dt} = k_d \theta^n = \nu\theta^n \exp\left(-\frac{E_d}{RT}\right)$$

Where, $-d\theta/dt$ is the rate of desorption, k_d is the rate constant, θ is the surface coverage, T is the temperature, t is the time, ν is the pre-exponential factor of desorption, and n is the desorption order. E_d and R are desorption activation energy and ideal gas constant, respectively. By fitting the experimental peak shape, one may deduce the best values of energy, order and pre-exponential factor.

Zero order kinetics (n=0) are often indicative of desorption from a multilayer where the rate of desorption is independent of surface coverage. A number of approximate methods of analysis have also been developed because they are rapid and easily formulated. The leading edge analysis, developed by Habenschaden and Kűpper [144], is a frequently used method for the interpretation of TPD peaks, especially for zero order desorption.

First order kinetics is typical of monolayer or sub monolayer coverage of non-interacting surface species. The rate of desorption during heating will change as a function of coverage. In order to determine the kinetic parameters, it is convenient to refer to a simpler relationship derived by Redhead [145].

$$E = RT_p (\ln (\nu T_p/\beta)-3.64)$$

Where, T_p is the temperature at which the maximum desorption rate is achieved and β is the heating rate (dT/dt).

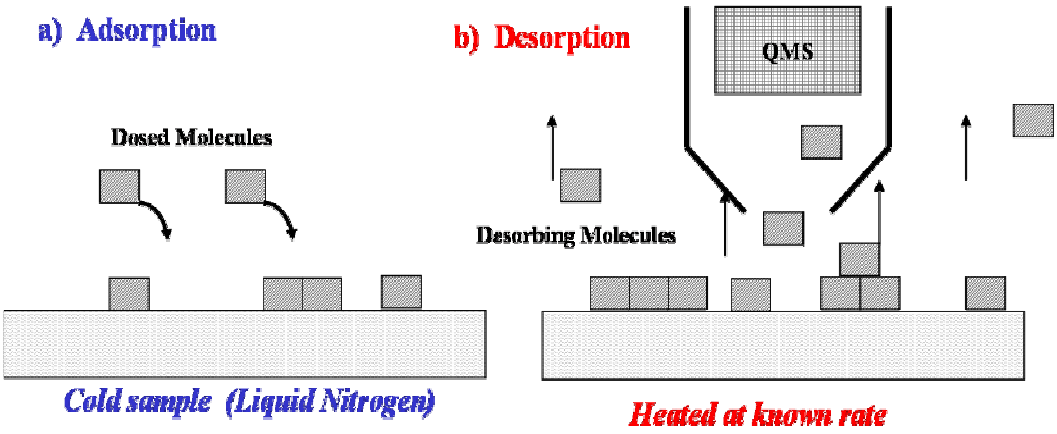

Figure 2- 3 Schematic of the temperature programmed desorption (TPD) experiment

2.5 RESEARCH OBJECTIVES

The overall goal of this study is to understand the fundamental phenomena involved in molecular adsorption on the surface of nanotubes, a new and important nanomaterial, and to optimize the adsorption process and operating conditions for effective pollution control. Understanding molecular interactions with nanotubes is also likely to impact the usefulness of nanotubes as environmental sensors. Infrared spectroscopy and temperature programmed desorption technique were combined in order to achieve this goal.

3.0 EXPERIMENTAL

3.1 ULTRA HIGH VACUUM SETUP

3.1.1 Infrared cell

A stainless steel ultra high vacuum (UHV) cell (Figure 3- 1) was designed and constructed for the infrared study. A turbo molecular pump (Leybold, Turbovac151) backed by a mechanical pump (Leybold, Trivac D4B) provided a 2 X 10^{-9} torr base pressure measured by a Bayard-Alpert ionization gauge (10^{-10} -10^{-3} torr) via a controller (Stanford Research system, IGC100). A tungsten grid (Alfa Aesar, 100 mesh size), which provided 64% transmittance, was used as sample holder because of its high melting point, thermal conductivity and resistivity (see appendix A). The grid was fixed onto nickel clamps which were connected to the copper wires of a power supply/thermocouple feed through which was mounted at the end of a liquid nitrogen dewar. Constant temperature heating can be obtained by computer interfaced (Labview, National Instruments) power supply and a type K thermocouple (chromel-alumel) spot welded to the top of the tungsten grid. With this setup, the tungsten grid can be cooled to 90 K with liquid nitrogen, and heated to 1400 K by resistive heating. Uniform glowing of the sample was observed when the tungsten grid was heated above 1000 K suggesting even heat distribution on the sample.

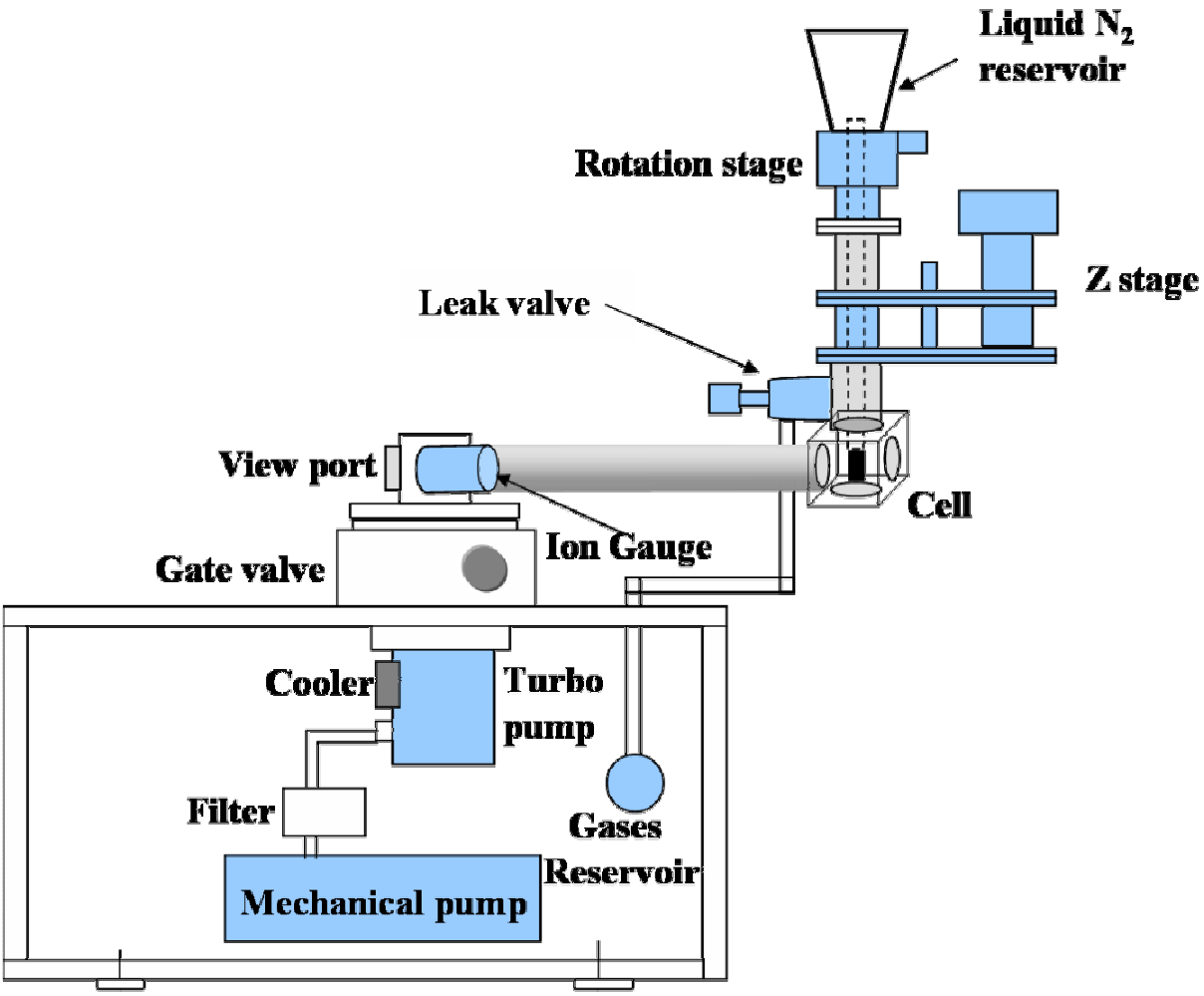

Figure 3- 1 Vacuum cell for infrared spectroscopy

The sample holder is connected to a rotation stage (MDC) (~ 240 degrees rotation) and a Z translation stage (MDC) (1 inch vertical displacement). The whole system is purged continuously with nitrogen. A simple tube-like attachment[125] between the KBr windows of the cell to the optical opening of the infrared spectrometer provided a well controlled water and CO_2 free environment for the IR beam path.

Nanotubes suspended in solvent were deposited directly onto the top part of the tungsten grid to form a 1cm X 2cm rectangular film through a drop and dry method. The nanotubes are very stable on the tungsten grid and cannot be completely removed even with sonication. The amount of nanotubes was controlled to get an optical density (O.D.) of about 1 at ~ 2300 cm^{-1}. Increasing the amount sample will increase the absorbance. However, the number of IR photons reaching the detector will be decreased by adding more carbon nanotubes, so that detector noise can begin to dominate the signal. 1 O.D is selected as an optimal point compromise. The lower part of the blank tungsten grid without nanotubes was used as a reference.

The gas exposure is recorded as Langmuir ($1L=10^{-6}$ torr s). After the desired exposure has been reached, all the gases were pumped out from the chamber to the base pressure before the sample spectrum was taken.

3.1.2 Temperature programmed desorption chamber

A stainless steel ultra high vacuum (UHV) chamber (Figure 3- 2), pumped by a turbo molecular pump backed by a mechanical pump, provides a base pressure of 5×10^{-10} torr after bake out. Samples can be cooled lower than 100K by liquid nitrogen and heated up to1300 K with 2.5 K/s ramping rate. A detailed description was provided previously [146-148].

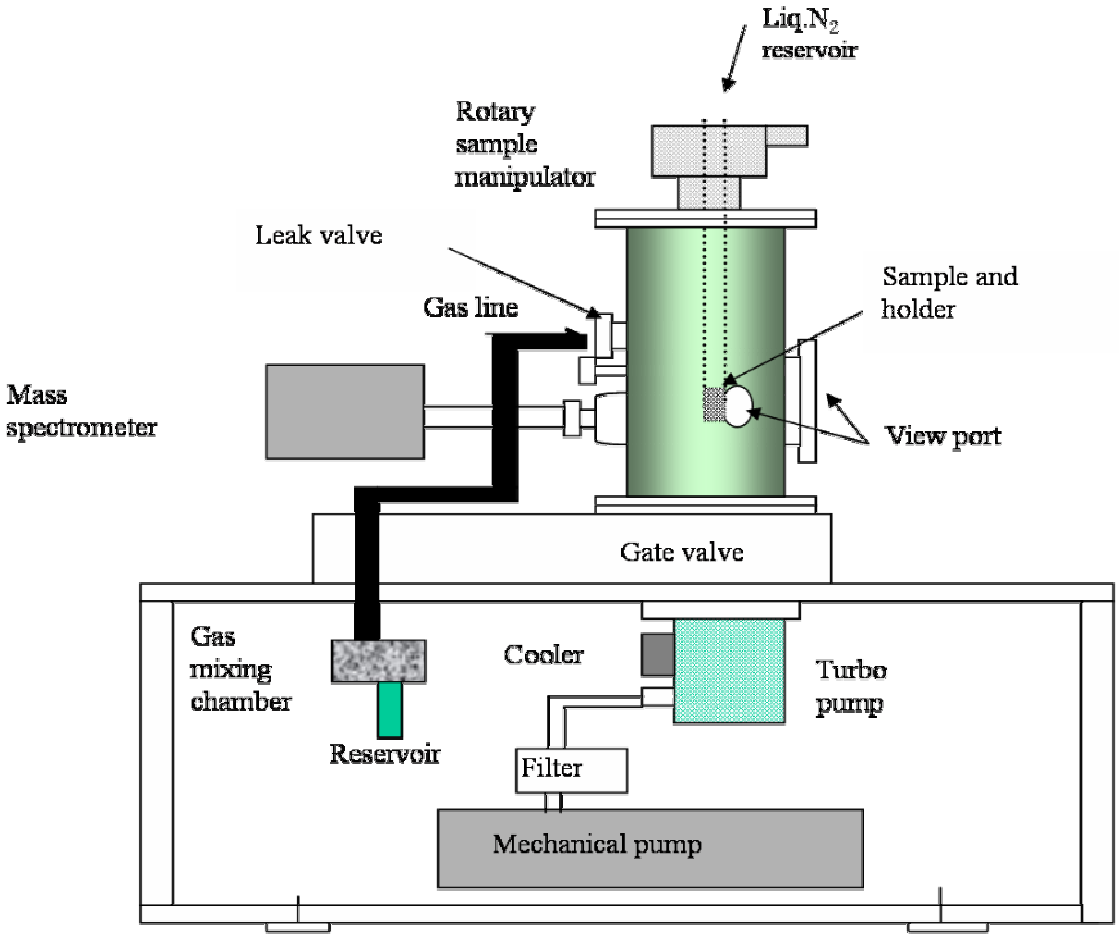

Figure 3- 2 Vacuum chamber for temperature programmed desorption (TPD)

The SWNTs were dispersed in solvents by sonication. The nanotubes sample for TPD was made by depositing nanotubes on a W grid through drop and dry method. Control experiment was performed on an identical W grid that could be independently heated, mounted in tandem in the UHV chamber.

3.2 SAMPLE PREPARATION

3.2.1 Activated carbon fiber

Activated carbon fiber (ACF), which has relatively well defined structure, provides a simple model of industrial sorbents for this study. The commercially available activated carbon fiber, ACF-25, used in this study was supplied by Nippon Kynol, Japan. Fibers made by acid-catalyzed cross-linking of melt-spun novolac resin to form a fully cross-linked, three-dimensional, amorphous "network" polymer structure similar to that of thermo-setting phenolic resins. Kynol^{TM} novoloid fibers are transformed into activated carbon fibers by a one-step process combining both carbonization and activation [149]. The specific surface area of the ACF was measured by nitrogen gas adsorption at 77K. The adsorption measurements were conducted with Quantachrome Autosorb Automated Gas Sorption System (Quantachrome Corporation). Before the adsorption test, the ACF samples were heated for 24 hours at 120^{o}C with flowing nitrogen.

3.2.2 Single walled carbon nanotubes

SWNTs produced by the HiPco process were obtained from Carbon Nanotechnologies Incorporated as an unpurified solid. Thermo Gravimetric Analysis (TGA) of this as received HiPco sample shows approximately 18 weight % (grams Fe/grams sample x 100%) of residual iron catalyst, in agreement with previous reports for these samples [150].

The as-received HiPco SWNTs were purified by a procedure reported in the literature [150]. This included flowing moist air (0.2L/min) through the sample for four hours at 498 K in a quartz tube furnace. Then the nanotubes were sonicated in a 3M HCl solution for another 4 hours. After acid extraction, the nanotubes were filtered and rinsed with deionized water until the rinse water was pH neutral. The sample was dried and dispersed in toluene by sonication. TGA of the sample shows that the residual Fe content is approximately 5 weight %.

A second purification procedure was used for the HiPco sample which involved refluxing the as received HiPco material in 3M HNO_3 for 8 hours; allowing the sample to sit unheated in the nitric acid overnight with continued refluxing for another 8 hours on the following day[132]. The sample was then rinsed with deionized water until the rinse was pH neutral and the still damp sample was then dispersed in acetone. TGA of this sample shows approximately 3 weight % of residual iron.

SWNTs prepared by the laser ablation technique, were purchased from Tubes@Rice as a "Purified Grade" suspended in toluene. They were called Rice Tubes in this study. These tubes have been oxidized/purified by a nitric acid and sulfuric acid mixture by the manufacturer[151]. TGA analysis shows that the residual metal content of this material is approximately 8 weight % of a 1:1 mixture of Ni and Co [152].

3.2.3 Adsorbates

An adsorbate physical properties chart is shown in appendix B.

The ammonia gas (AIRCO special gases), hydrogen sulfide gas (Matheson gas products) were used without further purification.

Acetone used in this study was research grade and was degassed by freeze – pump – thaw cycle before dosing. For freezing of acetone, a 195 K bath which lowers the temperature below freezing point of acetone (T_{melt} = 239 K) was prepared with dry ice and acetone. MTBE, Hexanes, Toluene were research grade and were from Aldrich.

3.3 TEMPERATURE PROGRAMMED DESORPTION

A clean surface exposed to a gas at fixed pressure and constant surface temperature provides steady state condition. Surface cleaning was accomplished by sample degassing. Prior to TPD experiments, the sample was positioned to face the QMS and the QMS aperture was brought close to the sample (< 1mm). As the temperature was increased at a constant rate during the desorption cycle, the mass spectrometer was used to detect the type and the amount of species desorbing from the surface.

In a typical degassing experiment, the sample was heated to a desired temperature at 5 K/sec and separately evolved gas species were monitored by the QMS. The masses typically monitored were 16 atomic mass unit (amu), 18 amu, 28 amu and 44 amu, corresponding, for example, to gas compounds such as CH_4, H_2O, CO and CO_2, respectively. After degassing of the sample, the QMS shield was retracted to allow dosing. Once the exposure (L) reached the

desired value, the QMS shield aperture was brought close to the sample and the sample was heated at a known rate (typically at 2.5 K/sec) while monitoring temperature and partial pressure of absorbate as a function of time.

In a full spectrum temperature programmed desorption (TPD), the sample was heated to a desired temperature and every evolved gas species between 1amu to 100amu was monitored by the QMS. In a full spectrum TPD, QMS scan speed was much faster than during the typical TPD. The sample temperature increased 10 K during one spectrum scan at a heating rate of 2.5 K/s.

3.4 INFRARED SPECTROSCOPY

The vacuum cell is positioned into the sample compartment of a Brüker Optics Tensor 27 series FTIR spectrometer. A liquid nitrogen cooled MCT (HgCdTe) detector was used to record the infrared signal from the nanotube sample from 700 to 4000 cm^{-1} with 4 cm^{-1} resolution. Reference spectra were taken on the blank tungsten grid before the nanotube sample scans. 500 scans were typically averaged for both background and sample. During thermal annealing, unless otherwise mentioned, the sample was kept at the desired heating temperature for 2 minutes. Then the power was turned off and sample was allowed to cool to ~ 90 K slowly (in approximately 10 minutes). Because this slow process possibly caused the adsorption of background gases onto the sample another heating step to 423 K, at 2 K/s, was required in order to get rid of physisorbed impurities. Subsequent cooling to 90 K took 10 minutes. Spectra were taken at 90 K after the second heating.

In order to show the spectra clearly, manual baseline subtraction was applied in the data analysis of this study using Brüker OPUS software. The baseline was a series of straight lines. Difference between the FTIR spectra of raw materials and materials after thermal annealing revealed the changes in the peaks that were induced by heat treatment. An example of baseline subtraction for the sample made by the laser ablation technique after a 700 K treatment is shown in Figure 3- 3.

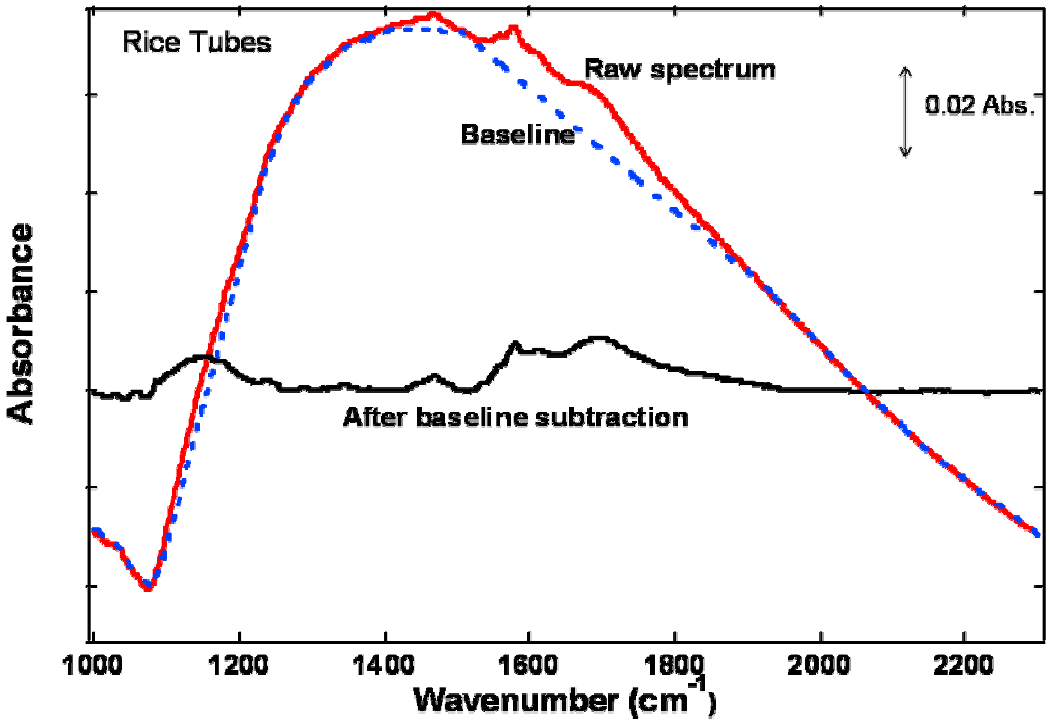

Figure 3- 3 Example of SWNT FTIR spectrum and baseline subtraction: Rice Tubes after 700 K treatment

3.5 FLUORESCENCE LABELING EXPERIMENT

In order to identify and quantify functional groups on activated carbon fiber and nanotube surfaces, the fluorescence labeling of surface species (FLOSS) technique was applied. Three chromophores with appropriate functionalities were selected to covalently label CHO, COOH and OH groups, respectively, as shown in Figure 3- 4. mM solutions of 1-pyrenemethylamine (95%, Aldrich) in ethanol (ACS grade, Pharmaco), triphenylmethylchloride in DMF (ACS grade, Baker) or 1-napthaleneethanol (99%, Aldrich) in acetonitrile (ACS grade, Fisher) were prepared for this study. The reactions (between fibers or nanotubes and chromophores) for the first two chromophores were performed at room temperature for two hours. The last reaction was performed by refluxing for two hours with catalytic amount of hydrochloric acid (CMOS grade, Baker).

In order to differentiate the fluorescence signals of chemisorbed chromophores from physisorbed chromophores, control experiments, using unfunctionalized chromophores, i.e., naphthalene, triphenylmethane and pyrene instead of 1-1-napthaleneethanol, triphenylmethylchloride and pyrenemethylamine, were performed. Post reaction cleaning following the chromophore grafting was performed by rinsing the sample several times with neat solvents used in each reaction to get rid of non-covalently bound molecules.

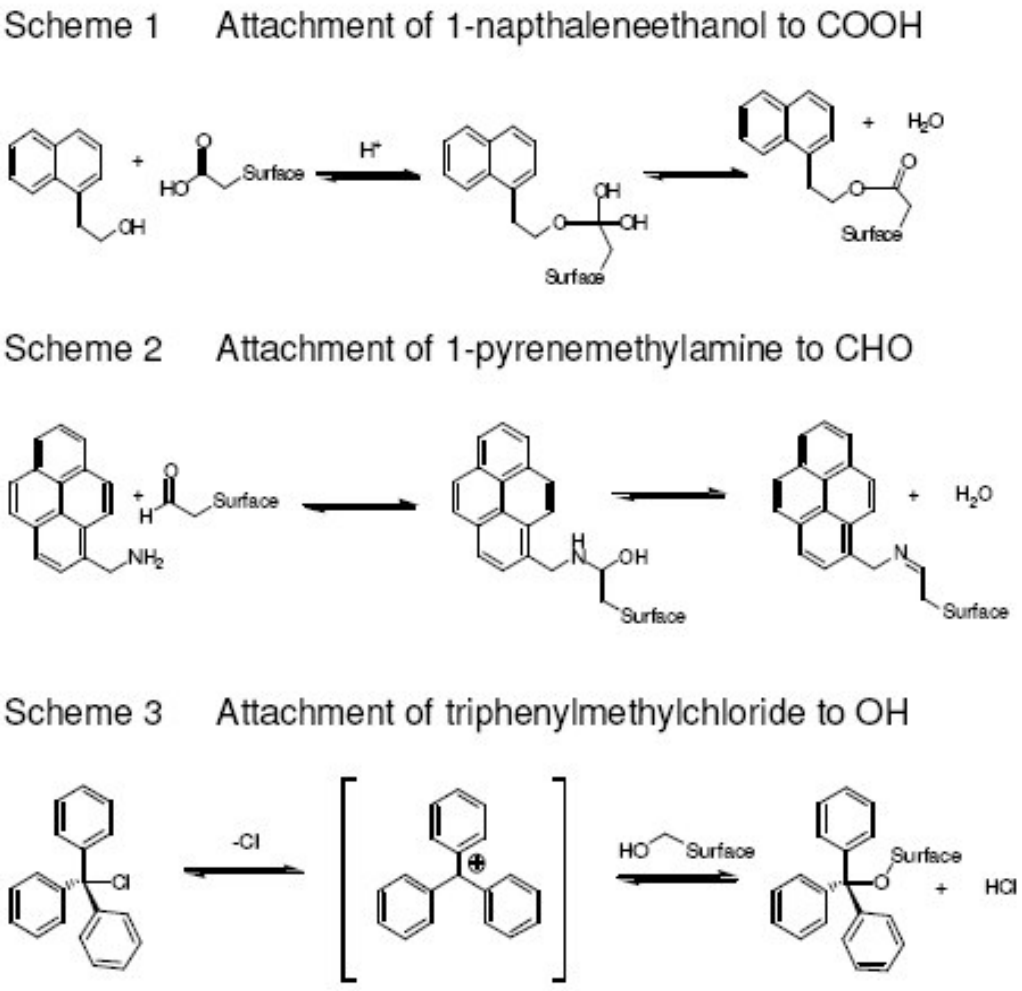

Figure 3- 4 Reaction schemes of covalent attachment of chromophores to different functional groups

The detection of fluorescence signals from fiber/nanotube surface was performed on a silicon wafer substrate. The fiber/nanotube was dispersed in the reaction solvent after the post reaction cleaning. They were deposited on a silicon wafer through the drop and dry method. Silicon wafers were previously cleaned with SC1 solution (NH_4:H_2O_2:H_2O, 1:1:4) at 80ºC for 45 minutes. Fluorescence measurements were performed on a Jobin Yvon Horiba Spex Fluorolog 3 with 5nm band pass and 3 scan averages with samples oriented at a 45º incident angle. Detection was accomplished using a photomultiplier tube (PMT). Fluorescence signals for all samples were corrected for lamp fluctuations by recording the ratio of the sample fluorescence signal to the source reference photodiode.

FLOSS depletion experiment After the reaction, the amount of pyrenemethylamine left in the reaction solution, instead of chromophores bound to the fibers, was determined using UV absorption at 324 nm. The reacted fibers were rinsed four times with neat solvent and the supernatant solution was transferred to a volumetric flask every time by pipette after the fibers settled to the bottom of the reaction container. In this manner, in principle, only chemisorbed chromophores were retained by the fibers.

3.6 OTHER TECHNIQUES USED IN THE STUDY

Raman Measurement A Nicolet Almega Dispersive Raman System with a 532 nm excitation source was used to obtain the Raman spectra at NETL. Samples were dispersed on a W grid. Estimated spectrum resolution is 6-10 cm^{-1} over the spectral range of 100-4000 cm^{-1}. A one second acquisition time, added over 30-50 acquisitions, was used for each Raman spectrum.

Boehm Titration The titration method suggested by Boehm [153] was used to calculate the concentration of acid groups on the ACF surface under the assumption that NaOH neutralizes carboxylic, phenolic and lactonic groups; Na_2CO_3 neutralizes only carboxylic and phenolic groups; $NaHCO_3$ only neutralizes carboxylic groups.

About 0.2g of activated carbon fiber was mixed with 25ml solution (0.025N) of NaOH, $NaHCO_3$, Na_2CO_3 and HCl respectively, for 24 hours with continuous stirring. 10ml of each filtrate was used for the excess acid and base titration by 0.025N NaOH and 0.025N HCl. The phenolic group content on the carbon surface was determined as the amount of 0.025N $NaHCO_3$ consumed by the carbon sample. Lactonic group content was calculated as the difference between the amounts of 0.025N Na_2CO_3 and 0.025N $NaHCO_3$ consumed by the carbon. Carboxyl group content was obtained by subtracting the amount of 0.025N Na_2CO_3 consumed by the carbon from the amount of 0.025N NaOH consumed. Multiple experiments were performed to determine the experimental error.

X-ray photoelectron spectroscopy X-ray photoelectron spectroscopy was performed on a Physical Electronics Model 550, equipped with a cylindrical, double pass energy analyzer. The ACF sample was attached to a tantalum surface by a conductive silver paste (LADD Research Industries).

4.0 RESULTS AND DISCUSSION

4.1 INFRARED STUDY OF THE FATE OF FUNCTIONAL GROUPS ON NANOTUBE SURFACES DURING THERMAL ANNEALING

Stability of Oxygen Containing Functionalities during Vacuum Heating. The infrared spectra of the as-received HiPco materials are shown in Figure 4- 1. The broad peak around 1700 cm^{-1} is assigned to the C=O vibration of carboxylic acid groups [154]. Features assigned to C=C vibrations around 1600 cm^{-1} and C-O bands around 1150 cm^{-1} are also seen in the spectrum before heating [154]. Heating the sample to 1300 K does not create any significant change in the infrared spectrum. A similar result has been noted for this sample after vacuum heating to 700 K [132].

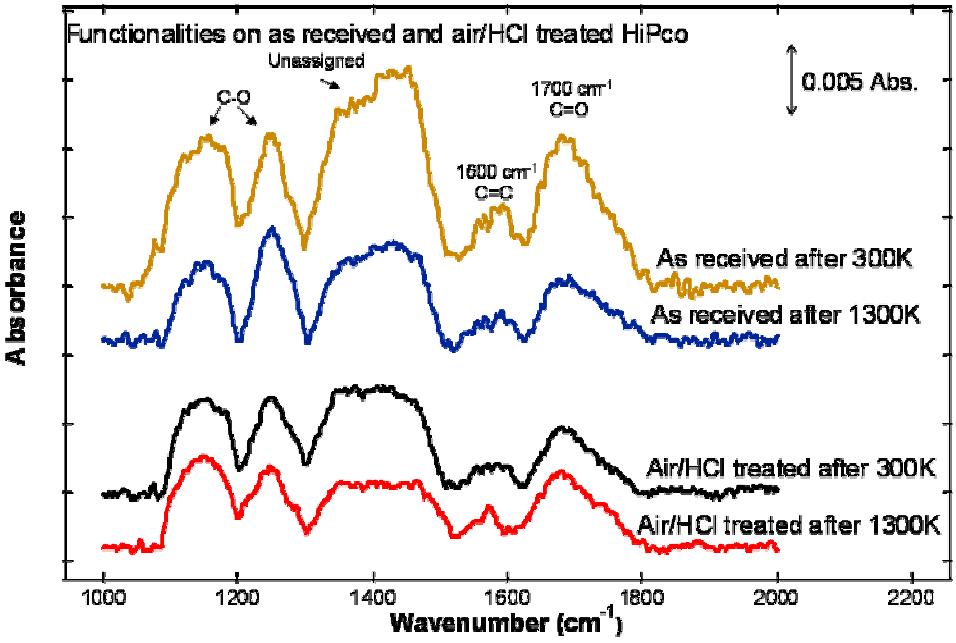

Figure 4- 1 IR peak evolution of as-received HiPco and air/HCl treated HiPco samples during vacuum heating

Infrared spectra for the air/HCl treated HiPco samples do not show any significant differences from the as-received HiPco samples (Figure 4- 1). This finding indicates that the air/HCl purification procedure does not introduce any detectable functionality onto the sample. The lack of functionality on the Air/HCl treated tubes is most likely a result of the mild oxidation temperature used during the air oxidation and the mild acid used to extract the residual catalyst. Vacuum heating of the air/HCl treated sample does not cause any observable change in the infrared spectra.

The lack of functionalities in this sample is significant since the TGA results indicate that the air/HCl purification is as effective in reducing the metal content of samples as the other

purification method studied here, HNO_3 oxidation. It was also found that few changes in the Raman spectra (see below) of these samples after air/HCl treatments indicating that this purification step does not introduce defects in the nanotubes sp^2 network of carbon. The results on the air/HCl purified sample show that this procedure is highly effective in reducing metal impurities without the complication of adding functionalities or other types of defects as do other purification steps (see below).

The infrared spectra of the nitric acid treated HiPco samples are shown in Figure 4- 2. The main infrared features of Figure 4- 2 are assigned to C=O (~ 1770 cm^{-1}), C=C (~ 1600 cm^{-1}) and C-O (~ 1250 cm^{-1}) vibrations [132]. As noted previously[132], the integrated intensity from these oxygen containing functionalities is about a factor of 20 higher than from what is seen in this spectral region for the as-received and air/HCl treated HiPco samples. Since the absorbance of each sample was controlled at approximately 1 O.D. for all the samples around 2300 cm^{-1}, this intensity increase cannot be easily accounted for by sample-to-sample variations of the film thickness. Instead, it must be related to a higher density of functionalities in the HNO_3 treated sample. This high density of functionalities shows that the HNO_3 refluxing done on these samples is an effective method of functionalizing SWNTs.

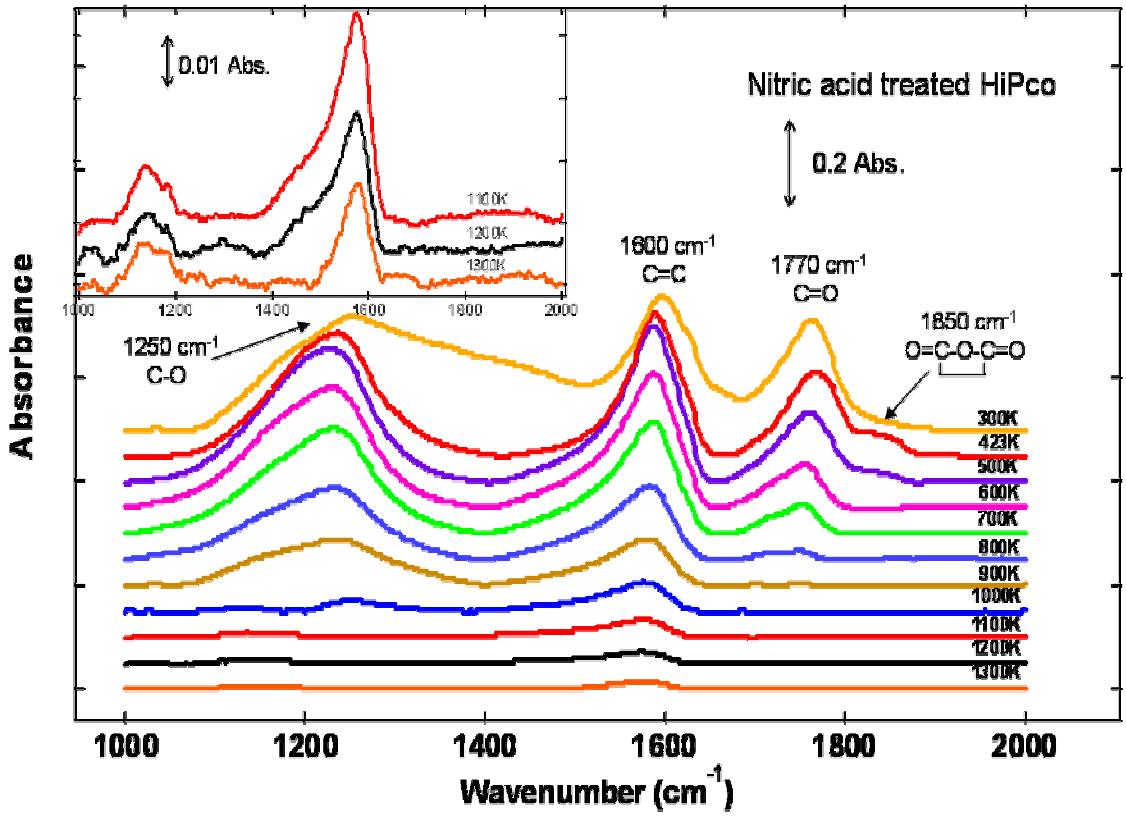

Figure 4- 2 IR peak evolution of nitric acid treated HiPco samples during vacuum heating from 300 K to 1300 K.(inset shows the enlarged spectra for samples annealed to higher temperatures)

The functionalities, seen in Figure 4- 2, change drastically during thermal annealing. The carbonyl band develops a shoulder around 1850 cm^{-1} upon heating to 423 K which was tentatively assigned to a C=O stretch in a cyclic anhydride group[155]. The temperature where this change occurs (above 423 K) suggests that the anhydride may form from the coupling of two carboxylic acid groups with the loss of H_2O (dehydrolysis). The formation of anhydride functionalities is likely when the reactant groups are near each other and these observations suggests a high local density of carboxylic acid groups on the HNO_3 refluxed samples. A report by Li [156] shows that the concentration of carboxylic acid groups is larger at the ends, the curves and the connecting regions of SWNTs bundles.

The anhydride groups evidenced in Figure 4- 2 are only observed in the nitric acid treated HiPco sample. Due to the six carbon ring structure of carbon nanotubes, the anhydrides should be cyclic in form, consistent with the peak seen at 1850 cm^{-1} in Figure 4- 2. This compares with linear anhydrides which are expected to have carbonyl bands in the range from 1760-1820cm^{-1}. The intensity of this 1850 cm^{-1} shoulder decreases with increasing temperature and ultimately disappears after 600 K.

The other carbonyl peak at 1770 cm^{-1} in Figure 4- 2 also loses intensity upon heating and is completely diminished after 800 K. This change is accompanied by a frequency shift from 1770 cm^{-1} to 1752 cm^{-1}. The band at 1597 cm^{-1}, associated with C=C bonds, decreases in intensity during heating and eventually evolves into a broad band at 1579 cm^{-1} which is typically associated with the IR active phonon of graphitic carbons [157]. Heating to 1300 K caused the C-O functionalities to decompose, as indicated by the dramatic reduction in absorbance around 1200 cm^{-1}, leaving behind a band at around 1138 cm^{-1}. An enlargement of the spectrum for the higher temperatures (from 1100 K to 1300 K) is shown as the inset of Figure 4- 2 to highlight the

residual peaks. Most of the functionalities on this sample have been removed after 1300 K heating, as shown by the IR intensity decrease seen for this spectral region.

The infrared spectra for the Rice Tubes produced by the laser ablation technique are shown in Figure 4- 3. Carbonyl and carbon-carbon double bond peaks are seen between 1500 and 1900 cm^{-1}. The spectra show a C-O peak at 1150 cm^{-1} and an unassigned region at ~ 1450 cm^{-1} [157] . Vacuum heating causes significant changes in these functionalities. The whole process can be divided into three steps:

1) In the first step (below 500 K), the spectra do not change significantly. Only a small intensity decrease was observed for the carbonyl peak (1744 cm^{-1}) and the C=C peak (1610 cm^{-1}).

2) In the second step (600 K to 1100 K), heating causes an intensity loss of the carbonyl peak which is accompanied by a frequency shift from 1710 cm^{-1} to 1678 cm^{-1} [154]. The peak at 1610 cm^{-1} decreases in intensity revealing 3 peaks in this region at 1610, 1578, and 1556 cm^{-1}. The 1610 cm^{-1} peak has previously been assigned to intercalated NO_3^- [158]. However, this peak is not observed for the nitric acid treated HiPco samples in this study, which possibly should also have intercalated NO_3^-.

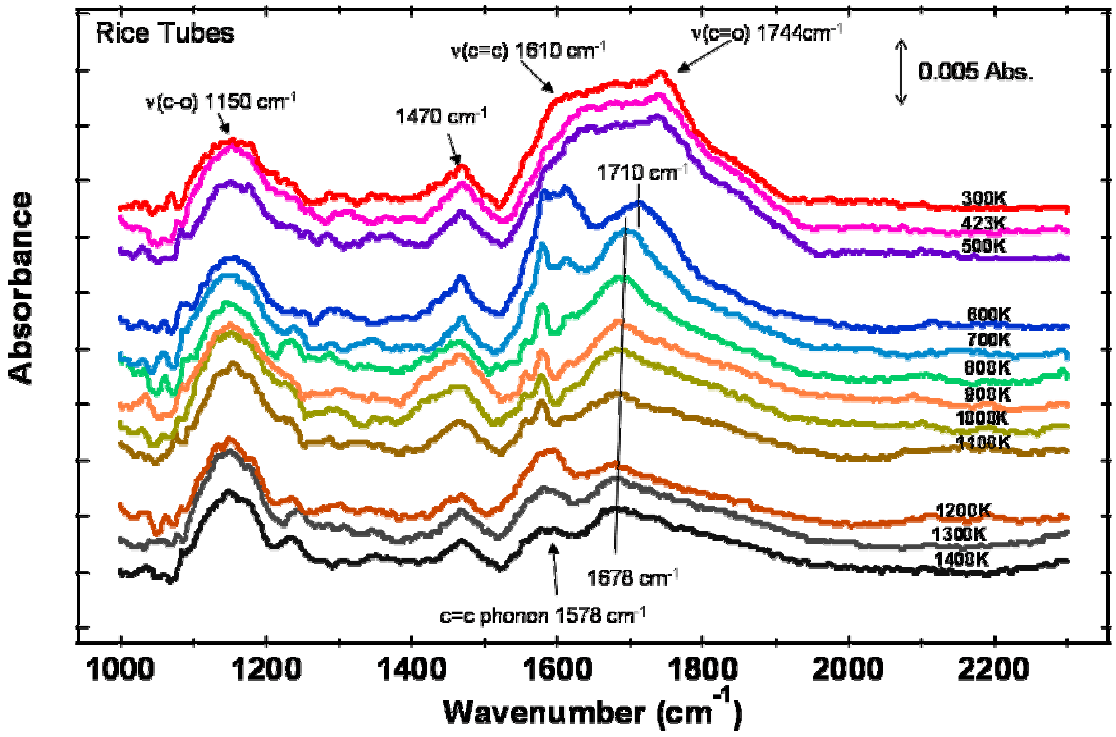

Figure 4- 3 IR peak evolution of Rice Tubes during vacuum heating from 300K to 1300K

The feature centered at 1578 cm^{-1} is similar to what is typically associated with the IR active phonon mode in nanotubes[157] and other C=C type vibrations. The features at 1556 and 1578 cm^{-1} start to merge at ~ 900-1100 K and form a single, broad band near 1580 cm^{-1}. A similar behavior for the merging of these 2 bands was observed in a previous IR study[157]. The single broad feature formed at 1580 cm^{-1} was assigned to the IR active phonon. [157]

3) The third step, from 1100 to 1300 K, begins with an intensity decrease of the 1470 cm^{-1} peak. A small decrease is observed for the relatively broad phonon mode at 1580 cm^{-1}. No significant change of the 1150 cm^{-1} peak occurs during the whole annealing process.

One interesting result from this work is that many similarities were found in the infrared spectra of the Rice Tubes after a 1400 K treatment with spectra for the as-received and air/HCl treated HiPco nanotubes (Figure 4- 4). This suggests that the heating step defunctionalizes the Rice Tubes producing a sample that is similar to the air/HCl purified and unprocessed HiPco samples. A previous study reported that heating of acid purified PLV (plasma laser vaporization) SWNTs produces C K-edge near edge X-ray absorption fine structure (NEXAFS) spectra which are very similar to those seen for unprocessed HiPco materials [43]. The NEXAFS result seems to agree with the infrared findings. If indeed all the functionalities are removed, then the remaining IR features should be tentatively assigned to intrinsic IR modes of the SWNT. Further experiments and calculations will be necessary to confirm this assignment.

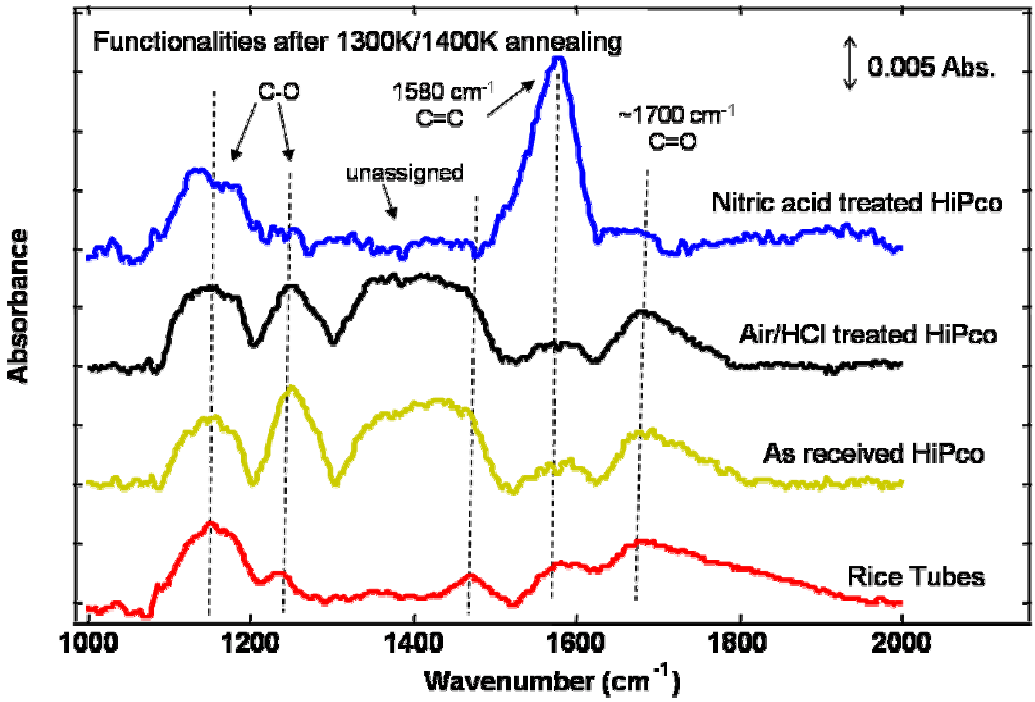

Figure 4- 4 IR spectra of 1000-2000 cm^{-1} region for as-received, air/HCl treated, nitric acid treated HiPco and Rice Tubes after 1300 K/1400 K annealing

Ex-situ Raman spectroscopy was performed before and after the infrared experiments to check the integrity of the samples (Figure 4- 5). The Raman spectra show G bands (~ 1400-1650 cm^{-1}) and radial breathing modes (RBMs) (< 350 cm^{-1}) for each sample indicating that the overall SWNT structure is intact both before and after the infrared experiments. Most of the changes with the G bands caused by purification and heating are subtle with the exception of the HNO_3 treated HiPco sample which shows drastic broadening in comparison with the as-received HiPco sample. This change was also noted in recent work[132, 159]. Associated with this is a drastic intensity increase in the D band near 1350 cm^{-1}. This D band intensity increase is consistent with the disruption of the sp^2 network of the SWNT sidewalls and is likely caused by sidewall functionalization during the HNO_3 oxidation step as evidenced in the infrared spectra of Figure 4- 2.

Overall, the Raman data presented in Figure 4- 5 shows conclusively, that the tubular structure of the samples is not disrupted by the purification or vacuum heating steps of the experiments. This indicates that the IR spectra presented here likely occur from functionalities on the nanotubes and not on some other form of carbon impurity present in the sample.

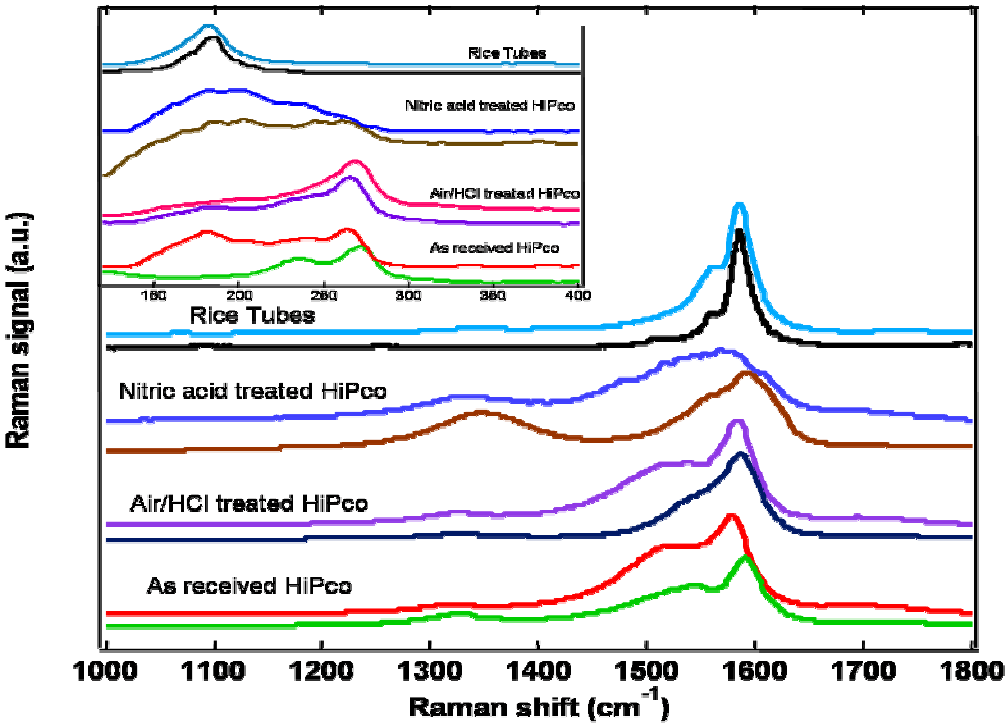

Figure 4- 5 Raman spectra of G band and RBM mode (inset) for as-received, air/HCl treated, nitric acid treated HiPco and Rice Tubes both before (lower line) and after 1300 K/1400 K annealing (upper line)

Trapped CO_2. The IR detection of physically trapped CO_2 which is generated by oxygen containing functional groups during the thermolysis of nanotubes has been reported [132, 154]. The entrapment of CO_2 was suggested to involve the rearrangement of functionalities at defect sites as they decompose, locking the generated CO_2 into endohedral and interstitial pores in the bundle[132, 154] . Rearrangements of the bundle itself due to the annealing effect of vacuum heating were also suggested to play a role [132, 154] .

The ν_3 modes for trapped CO_2 are expected to be in the region of 2330 cm^{-1} [132, 154]. The spectra of this region for as-received HiPco and lightly oxidized HiPco samples following thermal treatment did not show any peaks attributable to trapped CO_2. Since oxygen containing functionalities are responsible for the evolution of carbon dioxide, the lower degree of functionalities on these samples may not be capable of generating trapped CO_2 in amounts that can be detected by infrared spectroscopy [132, 154] .

For the nitric acid treated HiPco sample, a peak attributable to trapped CO_2 peak is seen at 2329 cm^{-1} just after heating the sample to 423 K (Figure 4- 6). The peak intensity increases with each heating step, reaching a maximum at 700 K. Above 700 K, the CO_2 peak decreases, presumably because this trapped species starts to be released from the nanotubes. No trapped CO_2 was detected after 1100 K treatment. The data shows that the peak intensity changes were accompanied by a frequency shift from 2329 cm^{-1} at 423 K, to 2334 cm^{-1} between 500 and 800 K and finally to 2338 cm^{-1} between 900 K and 1000 K. The peak around 2330 cm^{-1} has been tentatively assigned to CO_2 trapped in endohedral sites [132, 154].

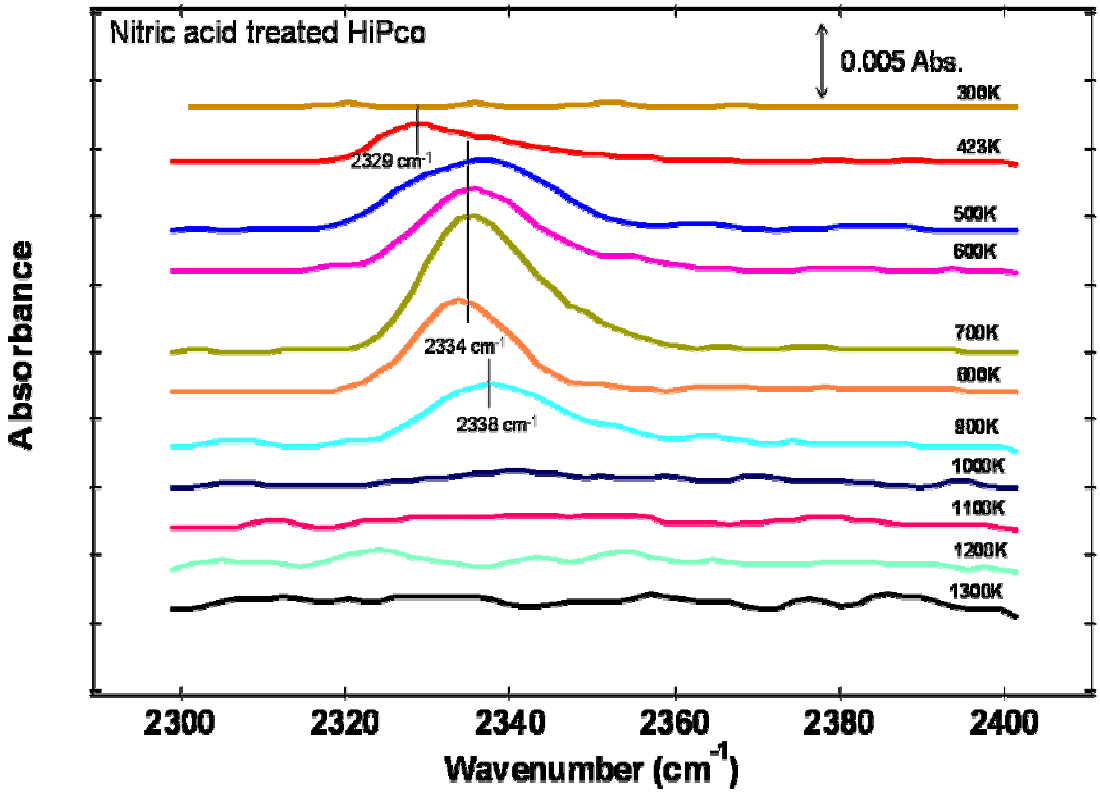

Figure 4- 6 IR spectra for the trapped CO_2 created from the decomposition of functionalities on nitric acid treated HiPco samples

The fate of the trapped carbon dioxide in the Rice Tubes during heating cycles is shown in Figure 4- 7. The integrated IR absorbance associated with trapped CO_2 (Figure 4- 8) gives two maxima around 700 and 1100 K. The appearance of trapped CO_2 can be correlated with the decomposition of oxygen containing functionalities as shown by the IR intensity decrease between 1000 cm^{-1} and 2000 cm^{-1} (Figure 4- 8). Previous infrared and temperature programmed desorption work has seen a maximum in functional group decomposition between 623 and 723 K which is consistent with the results presented in Figure 4- 7 and Figure 4- 8 [157].

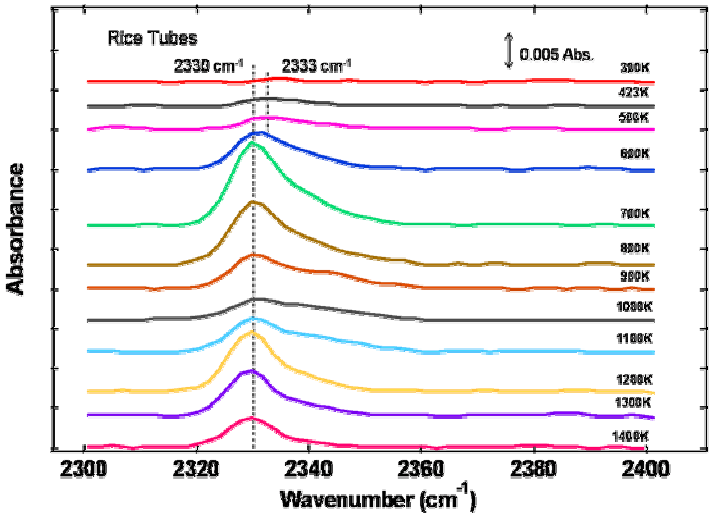

Figure 4- 7 IR spectra for the trapped CO_2 created from the decomposition of functionalities in Rice Tubes

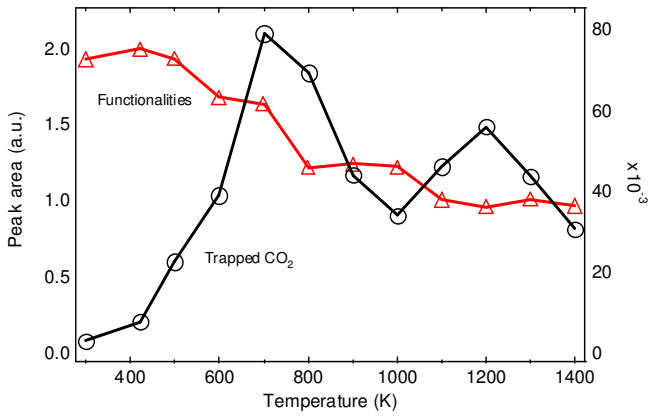

Figure 4- 8 The integrated intensity of peaks from 1000^{-1} to 2000 cm^{-1} (in Figure 4-6) and trapped CO_2 peaks (in Figure 4-7) for Rice Tubes during thermal annealing from 300 to 1400 K

In Figure 4- 7, the ν_3 mode at 2330 cm^{-1} has been attributed to CO_2 in endohedral sites [132, 154]. There is a high energy tail extending up to 2340 cm^{-1} which indicates that other adsorption sites might be populated. The peak at 2340 cm^{-1} has been attributed to CO_2 trapped in large interstitial spaces [132, 154]. Even after a 1400 K annealing, CO_2 is not completely removed from the Rice Tubes, suggested that there is a high energy barrier preventing its release. It has been suggested that steric rearrangements of functionalities responsible for generating the trapped CO_2 are responsible for locking it into the nanotubes[132, 154]. These functionalities could provide such a barrier.

Summary and Conclusions The following is a summary of the main findings of this study.

1) Nitric acid oxidation/purification generates functionalities and defects sites on nanotube surfaces. Vacuum heating decomposes most of those groups. The as-received HiPco

sample has less functionality than the nitric acid treated HiPco sample. Nitric acid refluxing is a highly effective method of functionalization.

2) Vacuum heating of nitric acid treated HiPco sample appears to lead to the formation of cyclic anhydride groups as indicated by the appearance of spectral features in the 1850 cm^{-1} region. The cyclic anhydride group decomposed and ultimately disappeared after thermal annealing to 600 K.

3) Air/HCl treatment is a relatively mild purification method. The iron content decreased from 18% to 5% after purification. But there is not much difference between as-received and air/HCl treated HiPco infrared spectra. This shows that the air/HCl purification is highly effective in reducing metal impurities without the complication of adding functionalities or other types of defects as do other purification steps.

4) There are many similarities in the infrared spectra of the Rice Tubes after a 1400 K treatment with spectra for the as-received and air/HCl treated HiPco nanotubes.

5) The drastic increase in the D band near 1350 cm^{-1} for nitric acid treated HiPco spectrum is consistent with the disruption of the sp^2 network of the SWNT sidewalls caused by the HNO_3 oxidation step. Thermal annealing under vacuum condition leads to a recovery of the as-received tube character.

6) The RBM data show that the tubular structure of the nanotube samples is not disrupted by the purification or the vacuum heating steps of the experiments.

7) The trapped CO_2 is completely released from nitric acid treated HiPco after 1100 K treatment. However, the existence of CO_2 in Rice Tubes after 1400 K treatment suggests the existence of high energy desorption barrier and the obvious influence of production methods and purification process on their adsorption abilities.

4.2 FLUORESCENCE LABELING OF SURFACE SPECIES ON CARBON MATERIAL SURFACES

4.2.1 Detection of low concentration oxygen containing functional groups on activated carbon fiber surfaces through fluorescent labeling

Fluorescent labeling of surface functional groups The presence of COOH groups on fiber surface is indicated in the data shown in Figure 4- 9. The dominant peak near 340nm is associated with monomer emission of naphthaleneethanol[82]. One open question was whether this peak came from chemisorption (naphthaleneethanol that reacted with COOH group) or from non-specific physisorption of chromophores on the fiber surface. Estimation of residual, non-specific adsorption on the fiber surface was made by repeating the functionalization experiment with unsubstituted naphthalene. The spectrum from this control is also shown in Figure 4- 9 (dashed line). The absence of a monomer peak at 340 nm for the fiber mixed with naphthalene suggests that the peak in the spectrum of naphthaleneethanol reacted sample really corresponds to chemisorbed chromophores. The low intensity of the dimer emission peak at 410-420 nm suggests little or no chromophore aggregation on the surface, which is consistent with the FLOSS result that the concentration of COOH groups is very low. The lack of a dimer also suggests that the naphthaleneethanol does not cluster and therefore that COOH groups are isolated, i.e., they are further than 3.3Å away from each other on average[160].

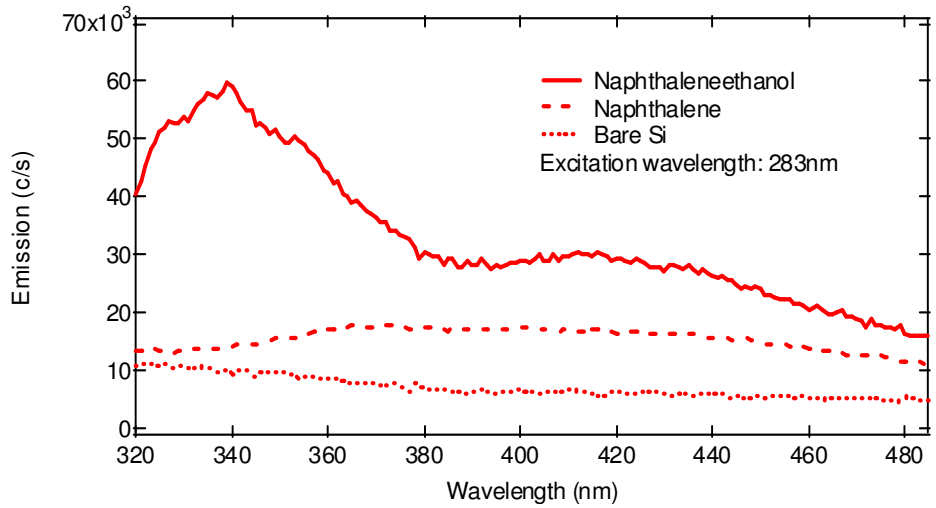

Figure 4- 9 FLOSS for COOH groups. Emission spectra of naphthaleneethanol (solid), naphthalene (dashed) reacted activated carbon fiber on silicon and bare silicon (dotted line)

The fiber used in this study was derived from a phenol-aldehyde polymer. It is reasonable to expect residual aldehyde groups from the raw material. The presence of CHO groups on the fiber surface is revealed by the fluorescence spectra that resulted from covalent attachment of 1-pyrenemethylamine to CHO, as shown in Figure 4- 10. The dominant peak near 398nm is associated with monomer fluorescence[82]. The lack of emission peak at 398nm for physisorbed-unfunctionalized chromophore (pyrene) suggested that the peak in 1-pyrenemethylamine spectrum is from chemisorbed fluorophores.

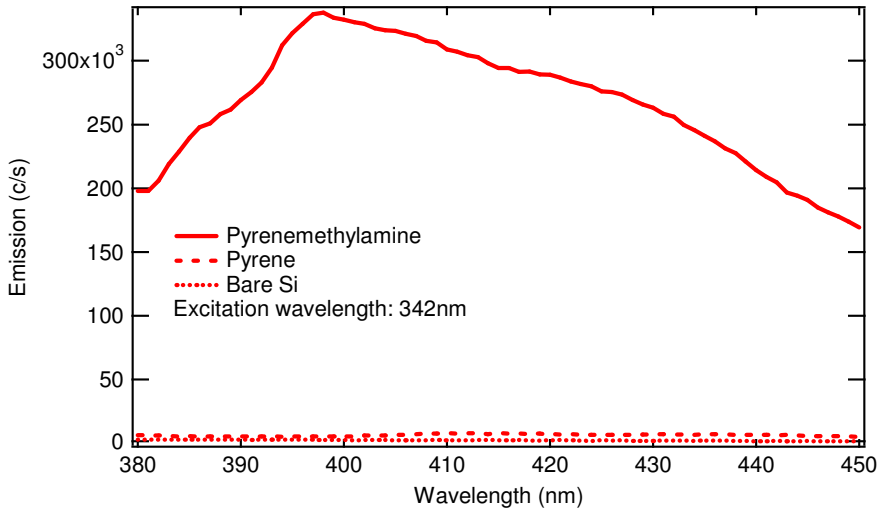

Figure 4- 10 FLOSS for CHO groups. Emission spectra of pyrenemethylamine (solid), pyrene (dashed) reacted activated carbon fiber on silicon and bare silicon (dotted line)

The detection of OH was performed using triphenylmethylchloride, which is known to react with hydroxyl groups[82]. The fluorescence spectra for fibers exposed to triphenylmethylchloride are shown in Figure 4- 11. The fibers exposed to non-functionalized chromophore (triphenylmethane) showed almost the same signal level (Figure 4- 11).

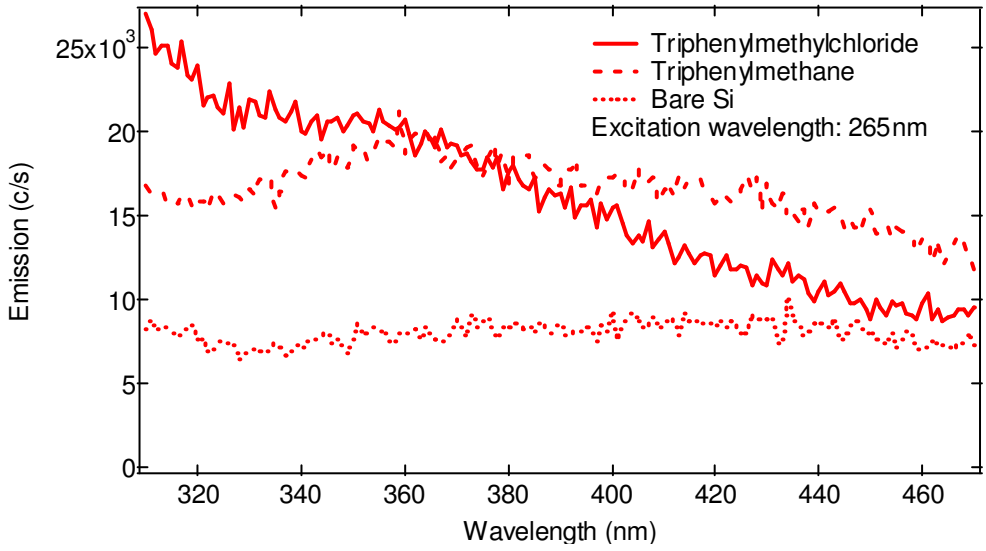

Figure 4- 11 FLOSS for OH groups. Emission spectra of triphenylmethylchloride (solid), triphenylmethane (dashed) reacted activated carbon fiber on silicon and bare silicon (dotted line)

XPS and IR data XPS was used to detect functionalities on activated carbon fiber surface. The difference in binding energies for atoms in various environments is very small and deconvolution of the peaks is necessary to analyze XPS data[58] [161]. The curve fitting and deconvolution of C1s region XPS spectra of ACF 25 are shown in Figure 4- 12. The dominant peak at 284.8 eV was assigned to graphitic carbon in the fiber[63, 68, 161]. However, the asymmetric shape of the peak suggests the existence of another peak as shown in the deconvolution. The 286.2 eV peak was assigned to the carbon in -C-O- structures[63, 68, 161]. The binding energy of carbon in carbonyl groups is 287.5~288.1eV[68]. No obvious evidence of carbonyl groups was detected in the C1s XPS.

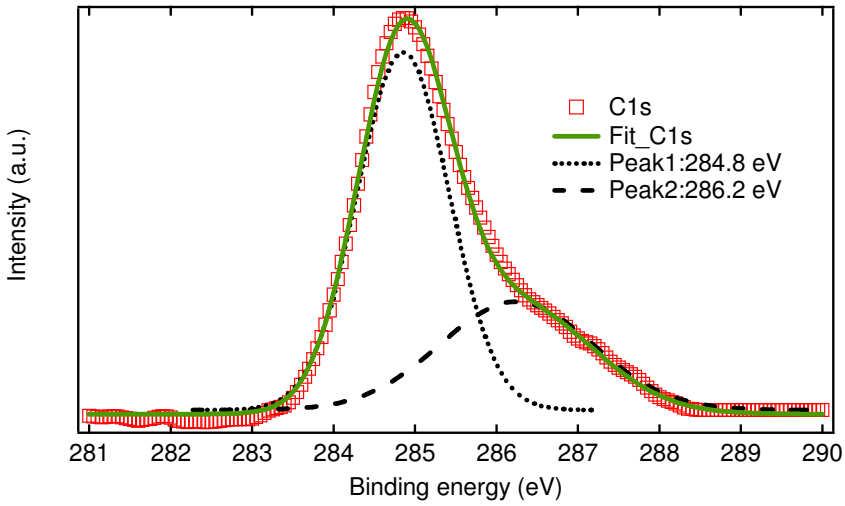

Figure 4- 12 C1s XPS spectrum of activated carbon fiber (□ is experimental data; Solid line is fitted experimental data; dotted line is 284.8eV peak; dashed line is 286.2eV peak)

The O1s feature shown in Figure 4- 13 is composed of two peaks. One is at 533.4eV, which corresponds to oxygen in -C-O- groups[161]. The smaller peak with higher binding energy of 535.6 eV was assigned to chemisorbed oxygen and/or oxygen in the remaining fiber moisture[68]. The oxygen double bond carbonyl peak was expected to be at 530.4-530.8 eV[68]. Existence of carbonyl groups, that could either be characteristic of aldehyde or carboxylic acid functionality, could not be detected by XPS in this case.

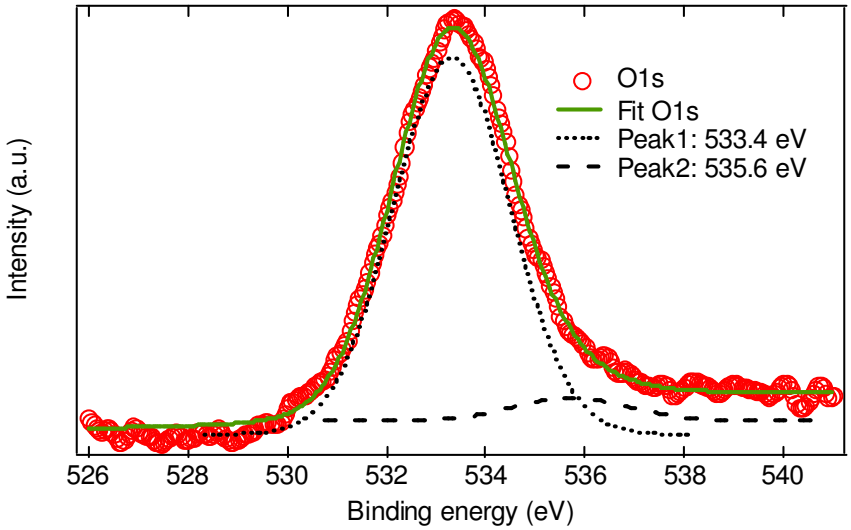

Figure 4- 13 O1s XPS spectrum of activated carbon fiber (o is experimental data; solid line is fitted experimental data; dotted line is 533.4eV peak; dashed line is 535.6eV peak)

The infrared spectrum from 1100 to 1800 cm^{-1} shown in Figure 4- 14 does not reveal any evidence of carbonyl groups (usually in the 1700 cm^{-1} region) on the fiber surface[66, 162]. The IR results are in good agreement with XPS results. The peak in the 1200-1250 cm^{-1} region was associated with ether type structures (C-O-C). Peak at 1500-1600 cm^{-1} region is assigned to aromatic C=C band and various substitution modes of the aromatic ring [162]. The amount of fiber used for the transmission IR experiment was limited by the high absorbance of carbon materials [58] and loss of light due to scattering process. While more ACF would have resulted in a greater fractional IR absorbance, loss of light due to scattering would render the experiment detector noise limited.

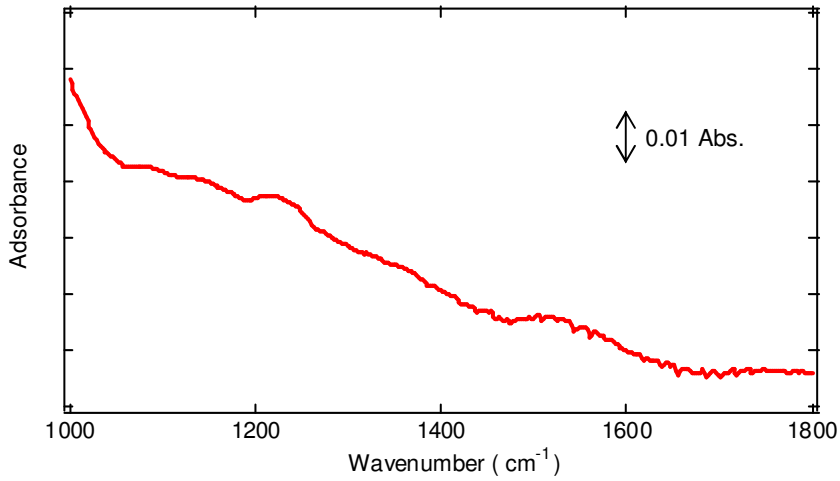

Figure 4- 14 IR spectra of activated carbon fiber in the range of 1100-1800 cm^{-1}

Quantification of functional groups by FLOSS Quantification of functional groups by FLOSS (+/-20%) was carried out by establishing a calibration curve formed by measuring the peak fluorescence intensities for known amounts of chromophores on a silicon surface which was covered by a self-assembled monolayer of alkylsiloxane[82]. The error was determined by the multiple experiments performed for the calibration curve. It was assumed that the functional groups are homogeneously distributed on the fiber surface and that the fiber is homogeneously distributed on the silicon wafer. Fibers exposed to naphthaleneethanol gives a signal of 60000 counts/second in Figure 4- 9, which corresponds to 8.65×10^{11} COOH groups/cm^2 of fiber surface based on the calibration curve provided in the previous paper[82]. The results are determined knowing the mass of ACF deposited on the Si wafer, typically ~5 µg, and the specific surface area of this sample (1950 m^2/g). Fibers reacted with functionalized pyrene molecules gave a signal of 340000 counts/second (Figure 4- 10) which corresponds to 1.33×10^{12} CHO groups/cm^2

of fiber surface. Similar calculations were performed for OH groups. The signal level shown in Figure 4- 11is 18000 counts/second at 400 nm where the triphenylmethane emission peak is supposed to be. The intensity is close to the zero level on the calibration curve[82]. Therefore, the concentration of the OH group on the fiber was below the present detection limit of FLOSS (~10^{10} molecules/cm^2).

In order to compare the number of functionalities determined by FLOSS with data from another independent technique, FLOSS depletion experiments were performed. UV spectra of the supernatant of the pyrenemethylamine solution before and after reaction with the ACF are shown in Figure 4- 15. The reaction induced change in solution absorbance at 324 nm is 0.47 O.D., corrected for scattering from residual fiber ~ 0.07 O. D.. The molar extinction coefficient of pyrenemethylamine at 324 nm was determined by the UV absorbance to be 26500 $mol^{-1}\cdot L\cdot cm^{-1}$. The amount of chromophore reacted with fibers was determined to be 1.56×10^{12} (+/-15%) molecules/cm^2 of fiber surface**,** corresponding to a density of aldehyde groups on the fiber surface of about $1.56\times10^{12}/cm^2$. This number is in good agreement with the data determined by FLOSS, which is 1.33×10^{12} /cm^2.

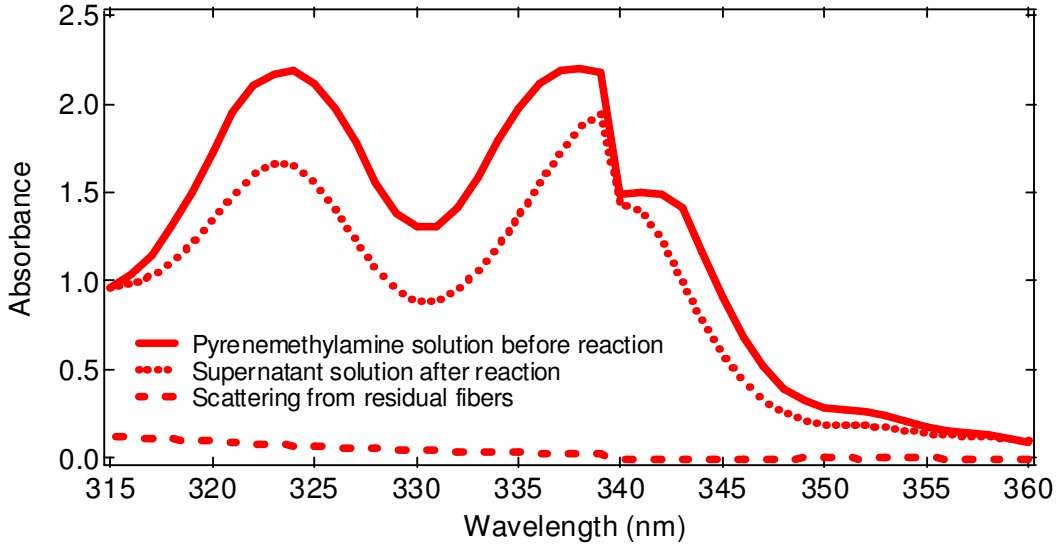

Figure 4- 15 UV-Vis spectra of pyrenemethylamine solution before and after reaction

The Boehm titration results (+/-7%) shown in Table 4- 1 suggest that there are 1.05×10^{13} carboxyl groups/cm^2 of fiber surface and 3.11×10^{13} carbonyl groups/cm^2 of fiber surface. The total acid determined by the Boehm titration includes phenolic, lactonic, carboxylic and carbonyl groups[75]. Since the precursor of the fiber is a phenol-aldehyde polymer,* it is likely that the carbonyl groups determined by Boehm titration correspond to aldehyde groups. Compared with Boehm titration, FLOSS underestimated the total amount of both COOH (8.65×10^{11} vs 1.05×10^{13}) and CHO (1.33×10^{12} vs 3.11×10^{13}) groups on the fiber surface. Several issues could contribute to this discrepancy. First, the narrowest diameter of chromophores, as calculated by the Chemsketch software (Advanced Chemistry Development Inc.), is around 10 Å for naphthaleneethanol molecule. This neglects solvent shell that might be necessary for reaction.

* http://www.kynol.com

While the pore size distribution analysis suggest that pores larger than 10 Å account for less than 50% of the total surface area as shown in Figure 4- 16. Thus not all the functional groups were accessible to the chromophores while the bases used in Boehm titration are small enough to diffuse into most micro pores.

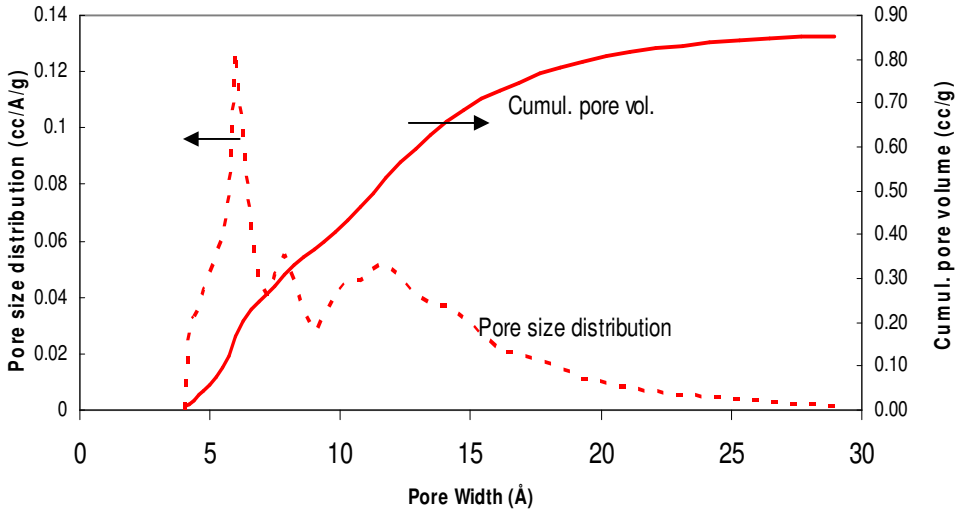

Figure 4- 16 Pore size distribution and cumulative pore volume of ACF 25

The pores of fibers are important in applications that involve separations for example. However, for many other applications, e.g. composite material formation, the larger pores and external surface are the key components. The sensitivity of FLOSS to these surfaces provides a unique application to FLOSS. The aldehyde groups determined by pyrenemethylamine are expected to be even more underestimated compared with carboxylic acid groups, which are determined by naphthaleneethanol, because pyrenemethylamine is larger than

naphthaleneethanol. Therefore, it is reasonable to expect that the FLOSS data would give lower values than the Boehm titration approach for the analysis of COOH group.

Table 4- 1 Surface acidic functional groups of activated carbon fiber determined by Boehm titration

Surface functional groups based on surface area (number/cm^2 ACF 25)				
Phenolic	Lactonic	Carboxylic	Carbonyl	Total Acidic
2.50×10^{12}	4.20×10^{12}	1.05×10^{13}	3.11×10^{13}	4.83×10^{13}

Summary and Conclusions FLOSS is an effective method to detect and quantify low concentrations of functional groups on carbon surfaces, especially when IR and XPS data are not conclusive regarding the existence of COOH and CHO groups. The presence of COOH and CHO groups was indicated by the fluorescence signal from covalently bound chromophores. The surface concentration of OH groups was estimated at less than 10^{10} molecules/cm^2 of fiber surface. Compared with other methods, i.e. Boehm titration, FLOSS is highly surface sensitive and is valuable for determining specific functional groups,. FLOSS is not limited to COOH, CHO and OH groups studied here. Other groups can be detected by selection of suitable chromophores.

4.2.2 Fluorescence labeling of surface functional groups on single walled carbon nanotube surfaces

Fluorescence detection of functional groups FLOSS technique was applied to determine COOH group on single walled carbon nanotube surface. Fluorescence spectra were recorded from 320nm to 480nm for naphthalene molecules. The presence of naphthalene molecules on both as-received and purified HiPco SWNTs was revealed in Figure 4- 17 with the dominant monomer peak was at 340nm and dimer peak at 430nm, respectively. One open question was whether this peak came from chemisorption, i.e., naphthaleneethanol molecules reacted with COOH groups, or from physisorption of chromophore on the surface.

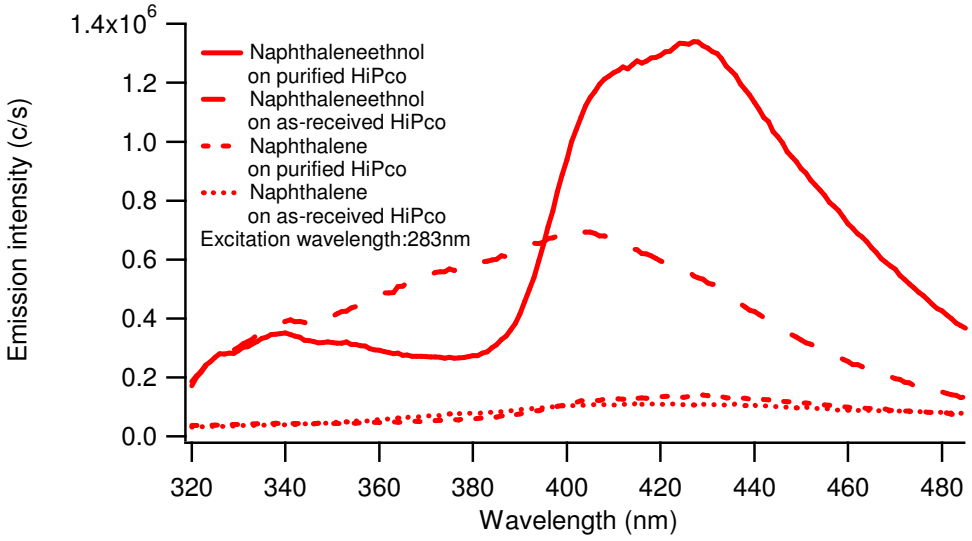

Figure 4- 17 Emission spectra of naphthalene on purified and as received HiPco

The estimation of residual, non-specific adsorption was attempted made by adsorbing unsubstituted naphthalene to the fiber surface, which is also shown in Figure 4- 17. The absence of obvious peaks for the nanotubes mixed with naphthalene suggests that the peak for naphthaleneethanol corresponded to chemisorbed chromophores alone.

The spectra in Figure 4- 17 provide evidence of the existence of COOH groups on both as-received and purified HiPco SWNTs. For both nanotube samples, two peaks are visible at 340 and 420 nm, representing monomers and dimers in the spectra. The dimer peak suggests a high local concentration of fluorescence molecules, i.e. a heterogeneous distribution of fluorescence molecules, and therefore COOH functional groups. It is well known that most of the functional groups on nanotubes surface exist on defects sites which are unlikely to be homogeneously distributed on the surface. These results are in a goon agreement with previous studies. After purification, the monomer intensity didn't change and the enhancement of dimer peak was observed. Because same amount of nanotubes were put for these two samples, the COOH group concentration increased after purification. According to the source of the dimer peak, the increasing of dimer peak should come from the increasing of the local concentration of COOH groups. That means new COOH groups typically form near the existing COOH groups i.e. near existing defects sites It is commonly accepted to understand that the defects are easier to be attacked than perfect structure.[163]

The presence of CHO groups is revealed by the fluorescence signal of pyrene Figure 4-18. The concentration of CHO groups on as-received is too small to be detected by fluorescence labeling. OH groups were barely observed on as-received nanotubes, as shown in Figure 4- 19. Both CHO and OH groups are introduced during the purification process as revealed by both

monomer peak at 395nm and dimer peak at 418nm of pyrene molecules in Figure 4- 18 and the monomer peak of triphenylmethane at 410nm in Figure 4- 19.

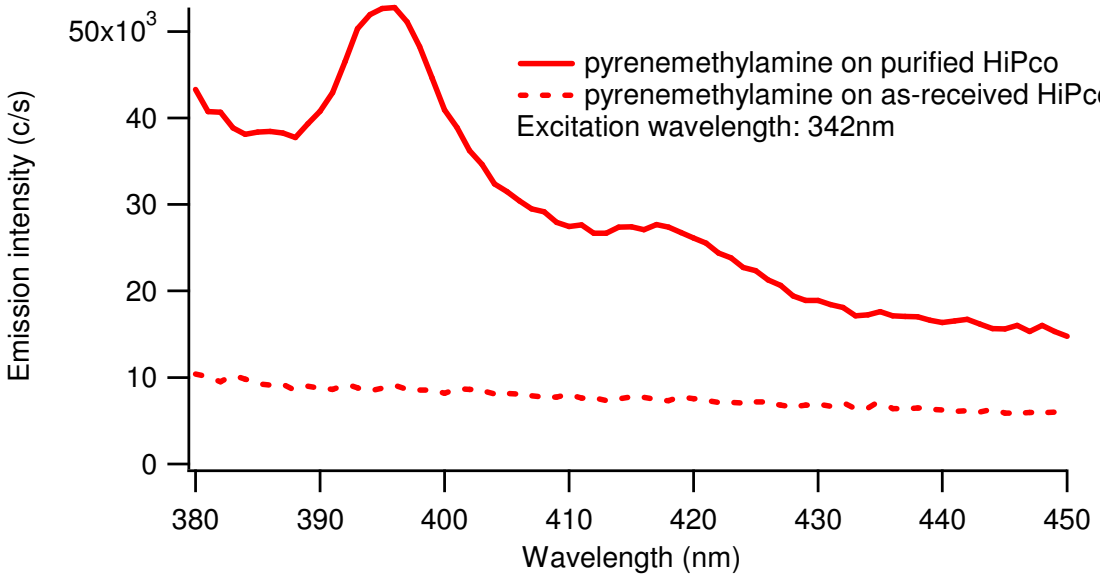

Figure 4- 18 Emission spectra of pyrenemethylamine on purified (solid) and as-received (dashed) HiPco

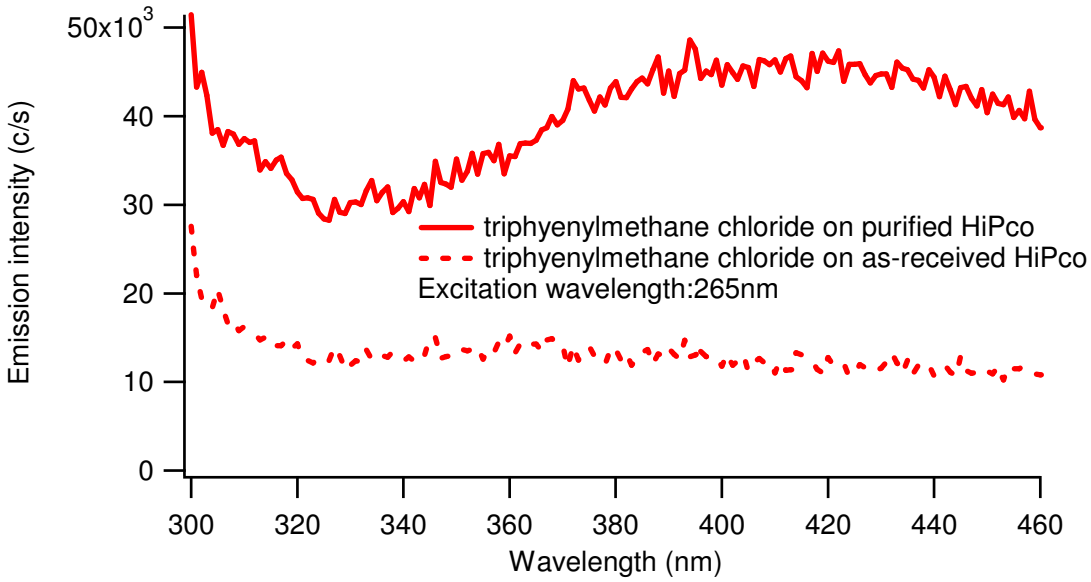

Figure 4- 19 Emission spectra of triphenylmethylchloride on purified (solid) and as-received (dashed) HiPco

These results lead us to draw a rough picture for the purification process. HiPco nanotubes were made by the catalytic decomposition of CO at high pressure and temperature. Iron particles remain as the catalyst of production. There are COOH groups and negligible amounts of CHO and OH groups on as-received HiPco SWNT. After purification, 90% of the iron was removed due to the acid extraction. Functional groups appear on the defects sites from the flowing of moist air. It is also reported [137] by other group that oxygen-based functional groups (detected by XPS) were introduced to the nanotube surface by either a one-step purification process with HCl-washing or a two-step process with HCl-washing after air oxidation.

Because of its higher purity, HiPco SWNTs are studied by more and more nanotube researchers [164-167] reported that single-walled nanotubes produced by the HiPco process, and

not treated with oxidizing acids, exhibit an O/C ratio of 1.9% and do not exhibit either pi*(CO) or sigma*(CO) resonances at the detection limit of NEXAFS. Low concentration of functional groups on the as received nanotube surface set a challenge to the detection technique. FLOSS is an effective method from this point of view. Moreover, it gave additional information on the morphology of the groups on the nanotube surface.

Summary and Conclusion FLOSS has been proved as an effective tool for detection of oxygen containing functional groups on as-received and purified HiPco SWNTs. FLOSS revealed the existence of COOH groups on as-received sample while concentrations CHO and OH groups were under the present detection limit. Purification processes introduced more groups to purified nanotubes. Moreover, FLOSS showed that the functional groups are distributed heterogeneously on the nanotube surface. New functional groups favorably grew on the defects sites through purification process, which was revealed by the increase of dimer peak in fluorescence spectra.

4.3 AMMONIA ADSORPTION ON, AND DESORPTION FROM NANOTUBES

SWNTs have been suggested as the basis of novel monitoring technologies and devices for pollutant detection. [168] Understanding the interaction between small molecules, such as H_2, Xe, CO_2, NH_3 and NO_2[132, 169-172] and nanotubes will help to reveal the mechanisms of molecular sensing. Of particular interest is ammonia, one of the first species shown to affect SWNT conductivity. [28]

The interaction of ammonia with SWNTs is somewhat controversial. Ammonia was shown to dramatically change the electrical resistance of semi-conducting SWNTs by Kong et al.

[28] Recently, infrared and temperature programmed desorption (TPD) were used to study the interaction of ammonia with heterogeneous bundles of as-received HiPco nanotubes at room temperature. [172] The authors reported that ammonia adsorbed on nanotubes at room temperature and could be thermally desorbed with a broad TPD peak around 430 K, indicative of a strong interaction[172] Valentini et.al also found that the increase of the electrical resistance of SWNT sensors when exposed to a mixture of interfering gases, NH_3, ethanol as well as 80 % relative humidity, at different operating temperatures between 25 and 250 ^oC. [173] Because of the presence of multiple gases, the interaction of specific molecules, e.g. ammonia, with the nanotubes was unclear. On the other hand, it is suggested that the interaction of ammonia with nanotubes is environment (humid) sensitive. [174]

In apparent contrast, several theoretical studies showed that ammonia molecules bind to carbon nanotubes via physisorption. [171, 175, 176] Only weak electron charge transfer (~0.03 electron) was reported. [175]

The apparent conflict about whether the interaction between ammonia and nanotubes is chemisorption or physisorption, weak or strong as reported by different research groups motivated us to investigate the influence of sample preparation methods, purification and oxidation processes on the properties of nanotubes. New theoretical studies were performed by the collaborators at Emory of ammonia adsorption on pristine, defect, and oxidized tubes.

In this work the IR investigation of ammonia adsorption on SWNTs and the sensitivity to the presence of functional groups or defect sites on the nanotubes was reported. The weak interaction between nanotubes and ammonia molecules is suggested by the observation of complete desorption above 140 K. Theoretical studies indicate very weak adsorption of ammonia to defect-free and defective nanotubes containing missing carbon atoms, but stronger

interaction with oxidized tubes. No adsorption is observed by infrared spectroscopy at room temperature with up to 80 torr ammonia dosing pressure. This work suggests that the sensitivity of nanotube gas sensors may be enhanced through functionalization (particularly oxidation) and defect generation.

Computational modeling of NH_3 adsorption on nanotubes was performed at Emory with the self-consistent charge density functional tight binding method (SCC-DFTB). [177] This method has been successfully employed for instance in the description of DNA strands [178] and the formation mechanism of fullerene cages from randomly oriented ensembles of C_2 molecules[179] To capture weak dispersion forces occurring in physisorption, a Heitler-London-term was added to the SCC-DFTB energies and gradients following the methodology described in Ref. . [178, 180] A methodological comparison was presented between SCC-DFTB and *ab initio* MP2 and CCSD (T) results of Bauschlicher *et al.* [11] for simple ammonia-benzene and ammonia-coronene systems.

Ammonia adsorption on HNO_3-treated HiPco nanotube surface An infrared spectrum of ammonia adsorbed on HNO_3-treated nanotubes at 94 K (Figure 4- 20) shows four main additional peaks overlapped on the spectrum of the nanotubes. The strong band at 3376 cm^{-1} is assigned to the N-H asymmetric stretch. [181] The symmetric stretch peak at 3290 cm^{-1} is very weak. [181] A shoulder is present on this feature at lower frequency. The N-H bending vibration at 1651 cm^{-1} is weak[181] The umbrella mode (symmetric deformation) [181] splits into multiple peaks (1057, 1105 and 1116 cm^{-1}) with the strongest at 1057 cm^{-1}.

The frequencies of vibrational modes of ammonia adsorbed on C_{60} at 170-180 K, [181] on carbon nanotubes at room temperature [172] and 94 K (present work) are compared with gas phase[181] and condensed phase ammonia[182] in Table 4- 2. Except for the bending mode, all

other modes of ammonia adsorbed on nanotubes at 94 K show similar frequencies and shift trends with ammonia adsorbed on C_{60} compared with gas phase modes. In the C_{60} work, [181] the authors attributed the peak shoulders to ammonia molecules adsorbed in different, less abundant sites on C_{60}. The splits (umbrella mode) and shoulder (symmetric stretch) of different bonds in Figure 4- 20 can possibly be associated with different adsorption sites on nanotube bundles, such as interstitial and endohedral sites, as suggested for other species interacting with SWNTs. [132]

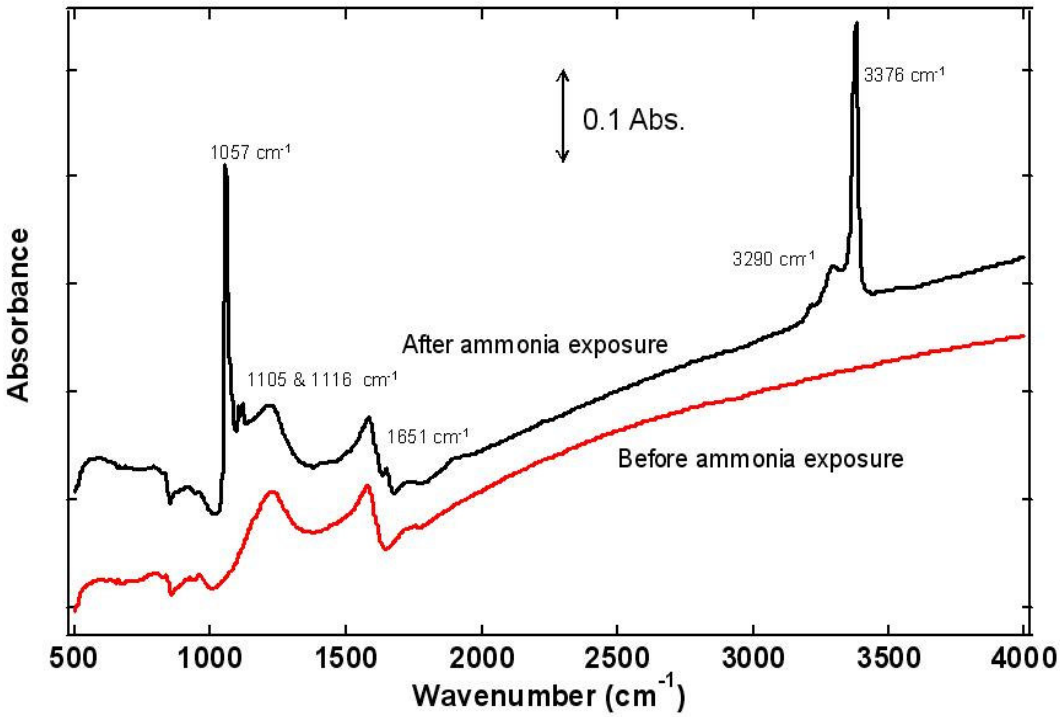

Figure 4- 20 FTIR spectra of HNO_3-treated HiPco SWNTs before and after adsorption of ammonia at 94 K (Exposure = 5,000 L). Samples were subjected to 900 K thermal annealing prior to experiments

Table 4- 2 Vibrational modes and frequencies (cm^{-1}) for ammonia adsorbed on C_{60} [181] and nanotubes [172] compared with gas phase [181] and condensed phase ammonia [182]

	Gas phase	Condensed phase	C_{60} (170-180K)	SWNTs (room temp.)	SWNTs (94K)
Asymmetric stretch	3414	3378	3354	3318, 3249	3376
Symmetric stretch	3337.5, 3336	3290	3222	3205, 3156	3290
Bend	1627	1650	1616	1618	1651
Umbrella	968, 932	1060	1132	1354, 1248	1057, 1105, 1116
Rock			542		

The infrared spectra of nanotube surfaces dosed with increasing ammonia exposure at 94 K are shown in Figure 4- 21. Ammonia is detectable at 30 L exposure in this study. The reported surface areas of the HiPco nanotubes are in the range from 300 to 900 m^2/g. [36, 183, 184] 1 Langmuir exposure only results in at most 0.004 monolayer on the 0.09 mg sample. The larger the specific surface area the lower the coverage will be at a given exposure. No significant frequency shift (< 2 cm^{-1}) is observed from the lowest detectable coverage (30 L) to highest exposure (5000 L) in this study. The frequencies are near the condensed phase ammonia vibration mode positions, [182] suggesting that the interaction energy between nanotubes and ammonia molecules is similar to the ammonia intermolecular interactions, and not indicative of

chemisorption. It was also reported that the NH_3-NH_3 interaction was similar in magnitude to the NH_3-graphite interaction. [185]

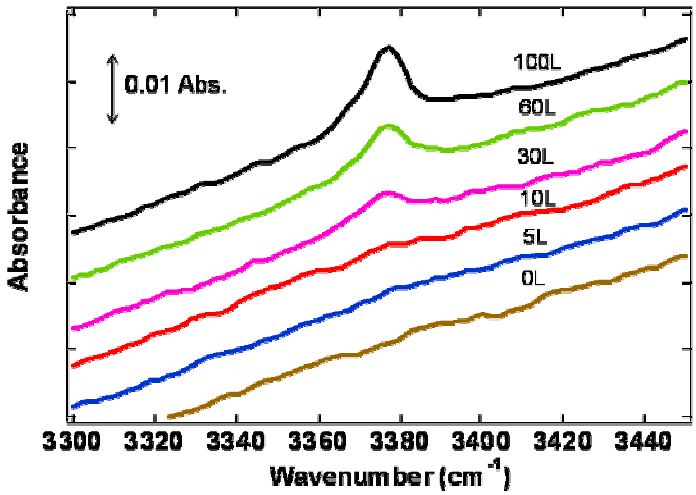

Figure 4- 21 FTIR spectra of HNO_3-treated HiPco samples with ammonia exposure 0-100 L. The samples were heated to 500 K in vacuum before ammonia exposure at 94 K

In order to investigate the strength of ammonia adsorption, the following series of experiments were performed. After 500 L ammonia exposure, the sample was flash heated (at about 3 K/s) to the desired temperature and then cooled down to 94 K. A FTIR spectrum was taken after every flash heating. The quantity of adsorbed ammonia, revealed by observing asymmetric stretch (~3376 cm^{-1}) in Figure 4- 22, remains approximately constant up to 120 K. By 140 K, however, all the ammonia appears to have desorbed.

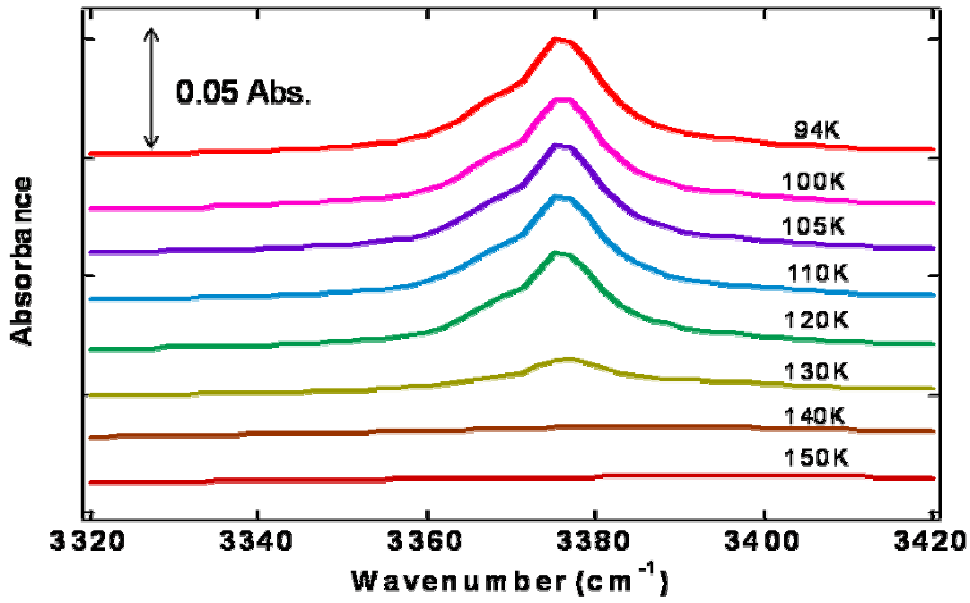

Figure 4- 22 Ammonia desorption infrared spectra from HNO_3-treated HiPco. Spectra recorded at 94 K after flashing to successively higher temperatures indicated by label on each spectrum. The samples were heated to 500 K in vacuum before ammonia exposure at 94 K (Initial ammonia exposure=500 L)

The desorption energy is estimated to be ~30 kJ/mol according to Redhead analysis assuming the maximum desorption temperature is 120 K, a first order process and a pre-exponential factor of 10^{13} s^{-1}. The desorption energy varied from 28 kJ/mol to 35 kJ/mol when the maximum desorption temperature vas varied from 120 K to 130 K and the pre-exponential factor was varied from 10^{12} s^{-1} to 10^{14} s^{-1}. [145] These values of the desorption energy suggest that the ammonia interaction with SWNTs is physisorption rather than chemisorption. {[171, 174, 175]

The apparent desorption of ammonia from HNO_3-treated HiPco SWNTs at < 140 K, while revealing a physisorbed state, does not exclude the possibility of a chemisorbed state. It is possible that a chemisorbed state exists but can only be populated at higher temperature and pressure because of an activation barrier to chemisorption. To address this issue ammonia was dosed to HNO_3-treated HiPco samples (after 500, 900 and 1300 K treatment) at pressures up to 10 torr at room temperature. No feature associated with ammonia vibrational modes larger than 1 milli. O.D. is observed (Figure 4- 23).

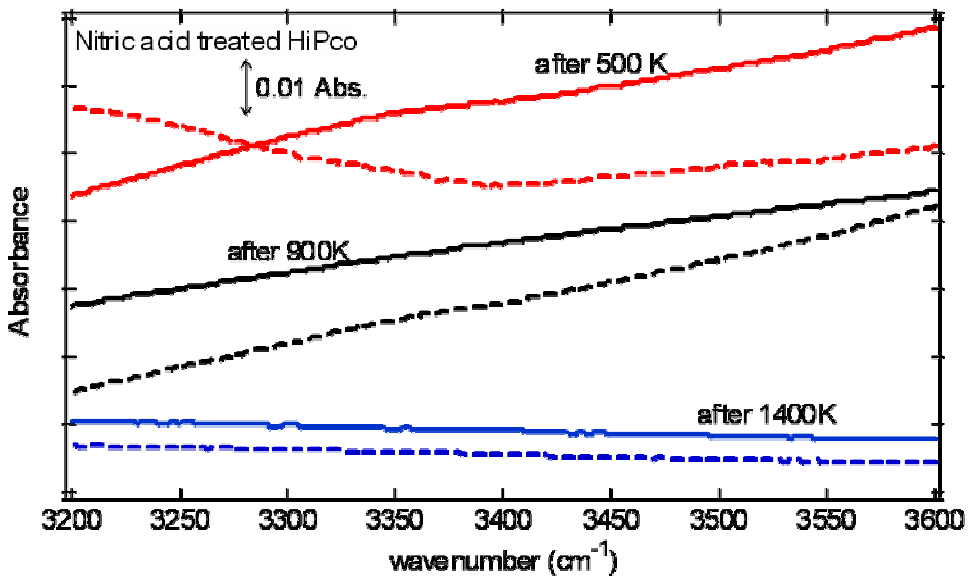

Figure 4- 23 Infrared spectra of ammonia adsorption on nitric acid treated HiPco samples at room temperature. Tubes were subjected to 500, 900 and 1400 K thermal annealing prior to experiments, as indicated in the figure. Ammonia pressure was 10 torr and exposure time was 15 minutes (Solid line is before ammonia exposure and dashed line is after exposure)

In addition to the infrared study, a temperature programmed desorption (TPD) study of nanotube samples dosed with ammonia at room temperature was also performed. The HNO_3-treated nanotube samples were exposed to 15 L ammonia at room temperature. There is no obvious peak of both 2 (H_2) and 17 (NH_3) amu species monitored from room temperature up to 650 K (Figure 4- 24). In conclusion, as discussed above, that no significant ammonia adsorption occurs at room temperature, consistent with a lack of chemisorption interaction between ammonia and nanotubes.

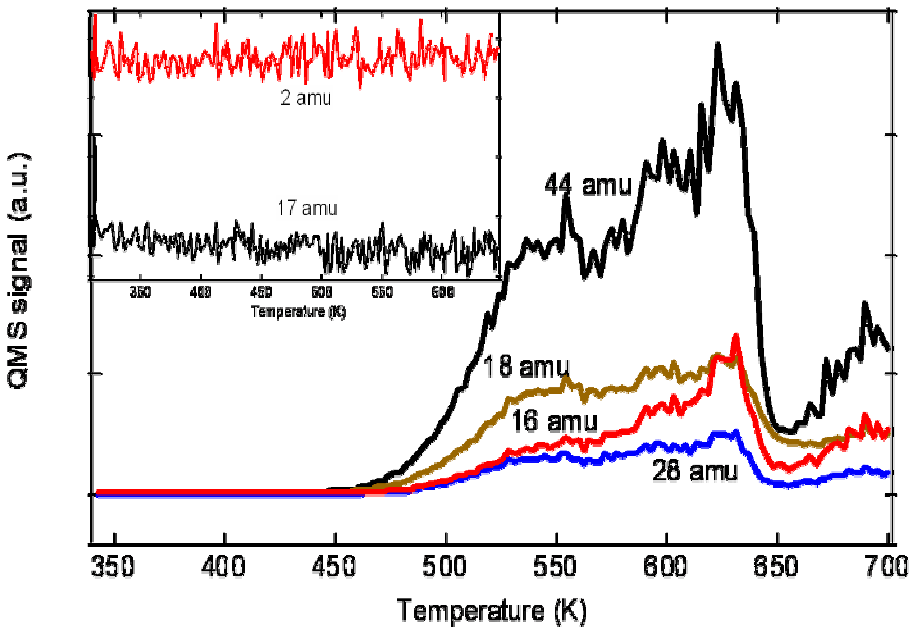

Figure 4- 24 Temperature programmed desorption (TPD) spectra of nitric acid treated HiPco nanotubes exposed to ammonia at room temperature. Exposure amount is 15 L. 2 amu is H_2 and 17 amu is NH_3

The lack of ammonia adsorption at room temperature is not inconsistent with CNT sensitivity to ammonia. A simple estimate of the equilibrium coverage, when the adsorption rate (flux of ammonia molecules from gas phase) equals the desorption rate, can be made. [186] At room temperature, assuming a pre-exponential factor for desorption of 10^{13}/s, a unity sticking coefficient and a desorption energy of 30 kJ/mol, 1 ppm ammonia (0.76 mtorr) results in an equilibrium coverage of about 10^{-5} monolayer of ammonia. While this coverage is beyond the infrared detection limit, it may be sufficient to modulate CNT conductivity. If the binding energy is 12 kJ/mol, as estimated for pristine CNTs (see theory below), the surface coverage at 1ppm ammonia is about 10^{-8} monolayer of ammonia.

In contrast to the results presented above, Ellison et al. found that ammonia adsorbed strongly on as-received HiPco at room temperature when the backfilling pressure was 50 torr. [172] This discrepancy could arise from the different sources of the nanotube materials, different purification methods and differences in experimental procedures. In an attempt to address these differences, a number of additional experiments were performed. (a) Ammonia adsorption was investigated on as-received, nominally untreated HiPco SWNTs with an ammonia dosing pressure of 80 torr, estimated from the measured decrease of ammonia in the gas line and the known volumes of the chamber and gas line. (b) The influence of water vapor (by introduction of water vapor into the chamber during ammonia adsorption), adsorption temperature (by keeping the sample at 425 K during ammonia exposure) and nanotube vacuum pre-treatment temperature (373 K and 725 K) were also evaluated. Under all the evaluated conditions, no peak greater than 1 milli. O.D., the noise level, appears in the infrared spectra (Figure 4- 25). As with the HNO_3-treated HiPco tubes, no evidence of ammonia adsorption at room temperature, within the sensitivity of these experiments, is observed.

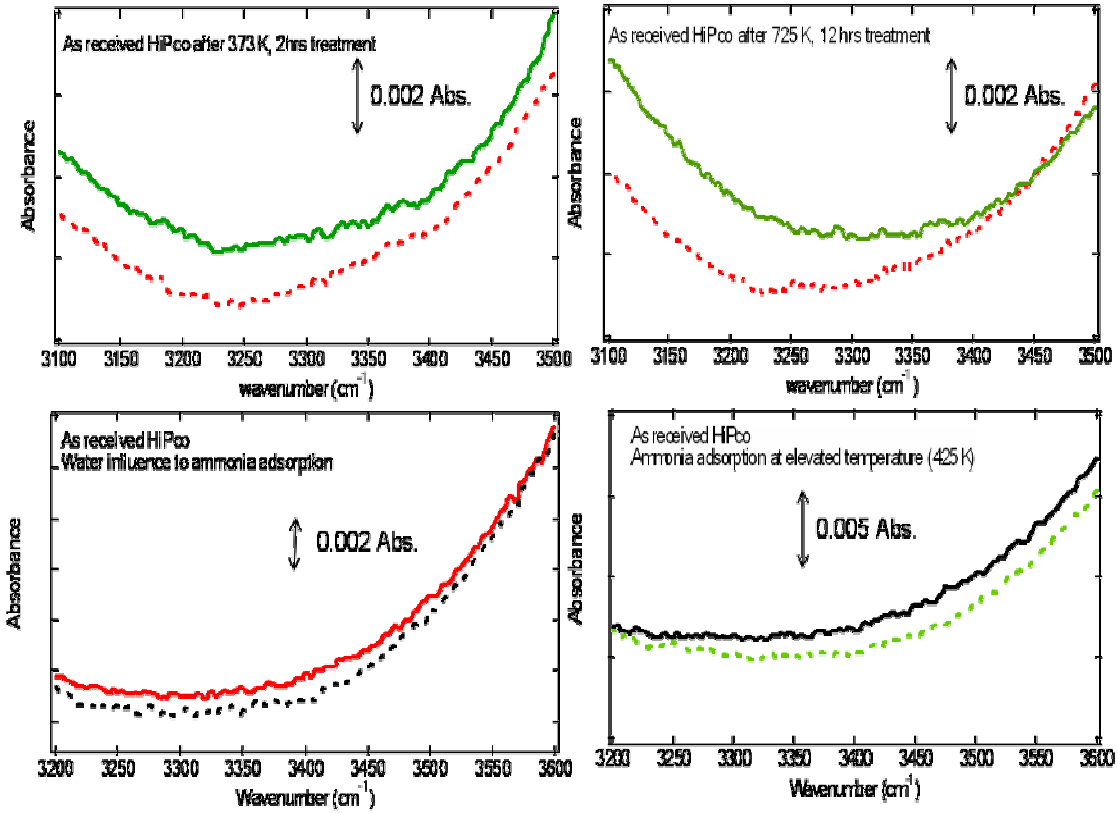

Figure 4- 25 Infrared spectra of ammonia adsorption on as received HiPco samples at room temperature under various conditions as shown in each spectrum. Ammonia pressure is 80 torr. Exposure time is 1 to 2 hours (Solid line is before ammonia exposure and dashed line is after ammonia adsorption)

Influence of annealing on NH_3 adsorption The effect of annealing of nanotube samples, from 500 K to 1400 K, on the adsorption of ammonia is shown in Figure 4- 26. In order to show the results clearly, a normalized enlargement of the ammonia asymmetric stretch region is shown in the inset. The decrease in the peak intensity, for constant exposure of ammonia, reveals a decrease of ammonia sticking probability as the annealing temperature of the surface increases. The asymmetric stretch peak intensity is completely suppressed after 1400 K treatment.

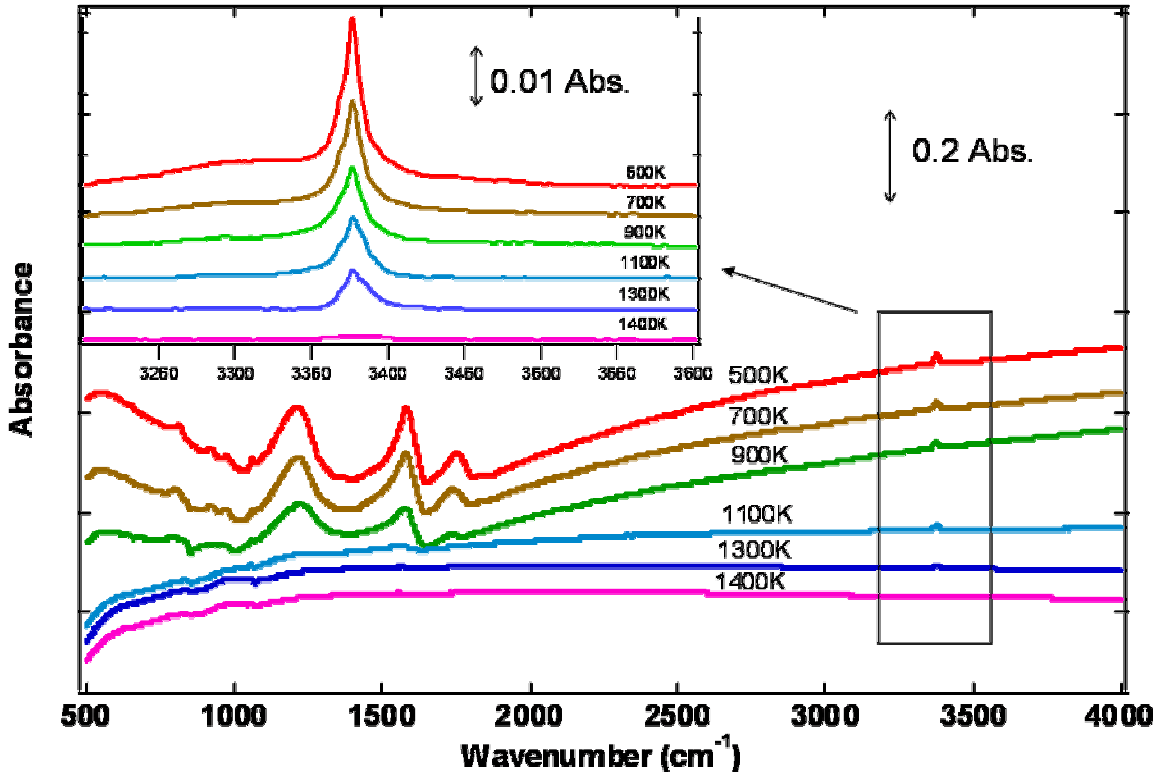

Figure 4- 26 Infrared spectra of ammonia adsorption on HNO_3-treated HiPco at 94 K after thermal annealing of SWNTs to successively higher temperatures (Ammonia exposure=200 L)

High temperature annealing has been reported to be an effective method to heal defect sites and recover the pristine tubes[33, 187-189] Raman spectra showed that vacuum thermal annealing decreased the defects (D band near 1350 cm^{-1}) intensities. [187] Most theoretical works use pristine tubes as simulation models. So it is more reasonable to compare theoretical results with experimental values from tubes similar to pristine ones. The complete suppression of ammonia uptake by nanotubes after 1400 K treatment is consistent with the 8 ± 8 kJ/mol NH_3 binding energy estimated for "pristine" nanotubes. [176] Valentini and co-workers also suggested that the interaction between oxygen and defective sites may be responsible for the reported sensitivity of nanotubes to NO_2. [190] The control of ammonia adsorption by annealing is observed not only for HNO_3-acid treated HiPco but also for as-received HiPco prior to purification processes and Rice tubes produced by the laser ablation technique. On each sample, ammonia adsorption decreases with increasing annealing temperature under conditions of constant ammonia exposure (Figure 4- 27). All the three kinds of nanotubes samples reveal the extreme sensitivity of ammonia adsorption to thermal annealing.

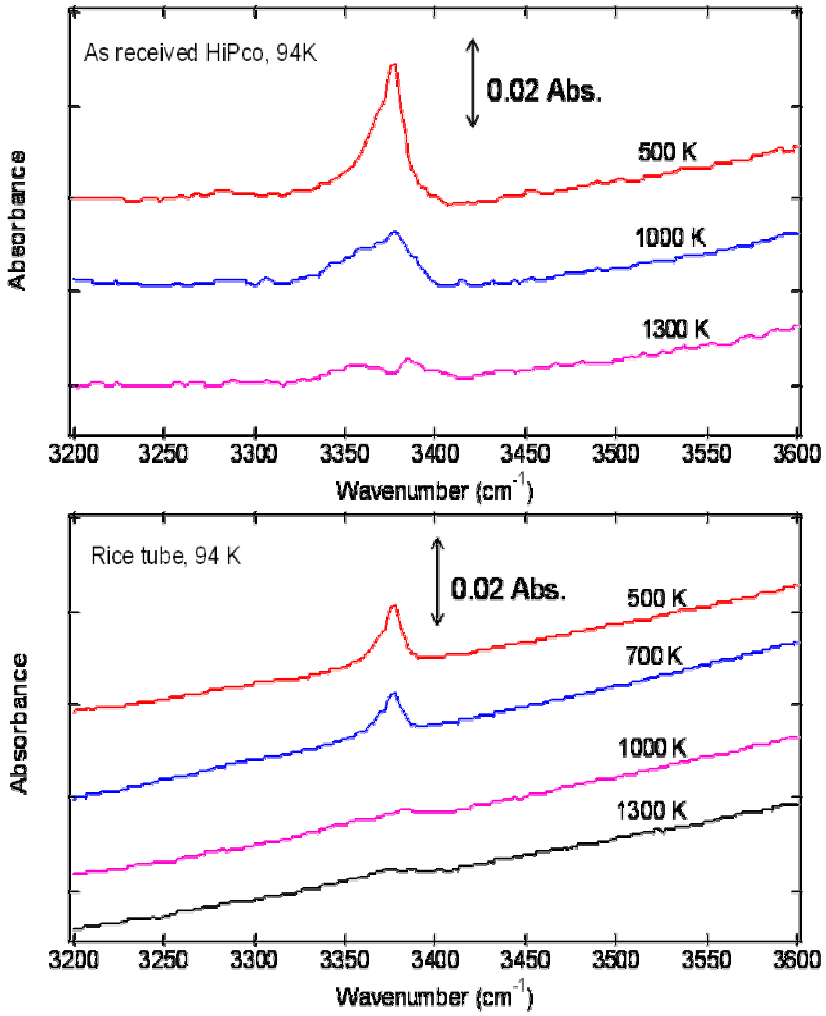

Figure 4- 27 Infrared spectra of ammonia adsorption on as received HiPco samples and Rice tubes at 94 K after thermal annealing of SWNT to successively higher temperatures (Ammonia exposure=500 L)

In addition to healing defect sites, annealing also causes removal of functional groups. [187] It is reported that functional groups on nanotube surfaces influence the electronic properties of SWNTs by disrupting the graphitic-like sp^2 network of carbon in the SWNTs. [32]This disruption produces local sp^3 defects which can introduce an impurity state near the Fermi level[32] and perturb the electronic spectra of these materials. [33, 191] The electronic characteristics of nanotubes play an important role in nanotube adsorption properties. [30, 191] It is possible that removal of functional groups changes the local electronic state, hence the affinity between ammonia and nanotubes. It was suggested that the existence of functional groups and defects provides sites for ammonia to adsorb on the surface that are energetically favorable. The role of functional groups on molecular adsorption has been reported previously. [51, 52, 192-194] For example, the presence of surface functional groups changed the binding energy, while increasing the uptake kinetics, of a polar molecule (acetone) [52] and decreased the uptake of a non-polar molecule (propane) [51], on graphite surfaces. There is evidence that accessible functional groups rather than external surface area were responsible for the ammonia uptake on the surfaces of organic materials. [192] These aforementioned studies, on a range of carbon materials, such as HOPG[51, 52], activated carbon[193] and activated carbon fiber,[194] suggest that it is not unreasonable that surface functionalities or chemistry could dramatically change the adsorption capacity of ammonia by nanotubes.

The suggested importance of functionalities does not exclude other possible impacts from annealing. Exposure of nanotube samples, thermally heated to 1400 K, to ambient laboratory air for one hour at room temperature led to the recovery of the nanotube affinity for ammonia adsorption at 94 K. The sticking probability of ammonia on nanotubes decreased again when the nanotubes were heated to 1400 K a second time under vacuum conditions. It was reported that

exposure to air or oxygen dramatically influenced the nanotube electrical resistance, thermoelectric power and local density of states.[30] It is possible that oxygen chemisorbed at defects sites where dangling bonds, generated by the annealing, were present.[195] The sample was flash heated to 423 K to drive off physisorbed impurities (such as water) after exposure to air and before exposure of ammonia at 94 K. This excluded the possible influence of water on ammonia adsorption.[174] One hypothesis is that exposing thermally-annealed nanotubes to ambient air led to the regeneration of functionalities/defects sites increasing the SWNT affinity to ammonia molecules.

Theoretical Studies The method of choice for theoretical modeling of NH_3 adsorption on carbon nanotubes is the computationally cost-effective SCC-DFTB method.[177] However, the modeling of physisorption on nanotubes in electronic structure calculations is inherently extremely difficult, since dispersion forces can only be described at the post-Hartree-Fock level of theory. An alternate way to include dispersion is to add a Heitler-London dispersion energy term to the calculated total energy as described in Ref.[178] , which is very similar to the approaches typically used in molecular mechanics force fields. In order to check the accuracy of such an approach, SCC-DFTB-D (-D meaning dispersion) optimized structures and energetics for the benzene and coronene $C_{24}H_{12}$ complexes was compared with NH_3 to the best calculated results obtained by Bauschlicher *et al.*[176] (see Table 4- 3). Investigated structures include complexes with one, two, and three hydrogen atoms, as well as the N lone pair, pointing toward the plane of benzene. SCC-DFTB-D predicts accurately all stationary points on the corresponding potential energy surfaces, and the differences in interaction energies between SCC-DFTB-D and the best level of theory applied by Bauschlicher are only about 1 kJ/mol for

the benzene-NH_3 system. In fact, SCC-DFTB-D and MP2/6-31G(d,p) frequencies was ran to verify the nature of the stationary points, and the structure with all three hydrogen atoms pointing towards benzene is a transition state for the tilting motion connecting the two tilted structures. The discrepancy between SCC-DFTB-D and Bauschlicher's interaction energies is somewhat larger for the coronene system (almost 7 kJ/mol), but again, the stationary point is predicted accurately, and Bauschlicher's value for this system was actually obtained using a much smaller basis set in their MP2 calculations compared to the benzene calculations.

Therefore the SCC-DFTB-D level of theory was applied in the study of NH_3 adsorption on nanotubes, and studied adsorption of ammonia on a pristine tube (a), defective tube (b and c), and oxidized tube (d) (see Figure 4- 28). The model system for the nanotube was a 20 Å long (5,5) armchair tube capped at both ends with C_{30} buckminsterfullerene half-spheres to prevent the ammonia molecule from being "sucked" inside. A defect was simulated by removing a carbon atom from the sidewall (at the center for system b and near the cap for system c). The defect healed in geometry optimizations to a defect site containing an opening of 9 carbon atoms plus a pentagon, where one carbon atom maintains an unfilled valence similar to triplet-methylene. The oxidized tube model (d) was derived by adding five oxygen atoms to the (5,5) tube model to yield a tube with a cyclic anhydride group with two adjacent oxygen sites, which presumably reduces ring strain due to otherwise adjacent pentagons. This model was shown by us to be much more stable than any other combination of the tube model plus 5 oxygen atoms in 34 different conformations.[196] Ammonia was placed in all calculations on top of the tube and in the vicinity of defect sites. Figure 4- 28 shows the bond distances between the ammonia hydrogen atoms to the next-neighbored C and O atoms for a-c) and d), respectively. Not unexpectedly, the interaction between a pristine tube and ammonia in a) is very similar to the

ammonia-coronene interaction with –12.1 kJ/mol. The interaction of the ammonia molecule with the unfilled valence of a defect tube is slightly increased to –15.9 kJ/mol (b and c). Yet, the presence of oxygen molecules on the tube dramatically increases this interaction energy to –40.2 kJ/mol (d), in line with the experimental observation that oxidized tubes bind ammonia significantly better than pristine tubes. Apparently, ammonia forms strong hydrogen bonds with oxygen atoms in the oxidized tubes.

Table 4- 3 Interaction energies (E) between ammonia and benzene/coronene systems. All systems have been fully optimized at the SCC-DFTB-D level (by Morokuma group, Emory University)

System	SCC-DFTB-D E [kJ/mol]	E Ref [176] [kJ/mol]
NH_3	0.00	0.00
C_6H_6	0.00	0.00
C_6H_6-NH_3 C_{3v}[a]	-7.82	-6.74
C_6H_6-NH_3 tilt2[b]	-7.87	-8.41
C_6H_6-NH_3 tilt1[c]	-8.20	-8.45
C_6H_6-NH_3 u/d[d]	-3.14	N/A
$C_{24}H_{12}$	0.00	0.00
$C_{24}H_{12}$-NH_3	-14.30	-6.90

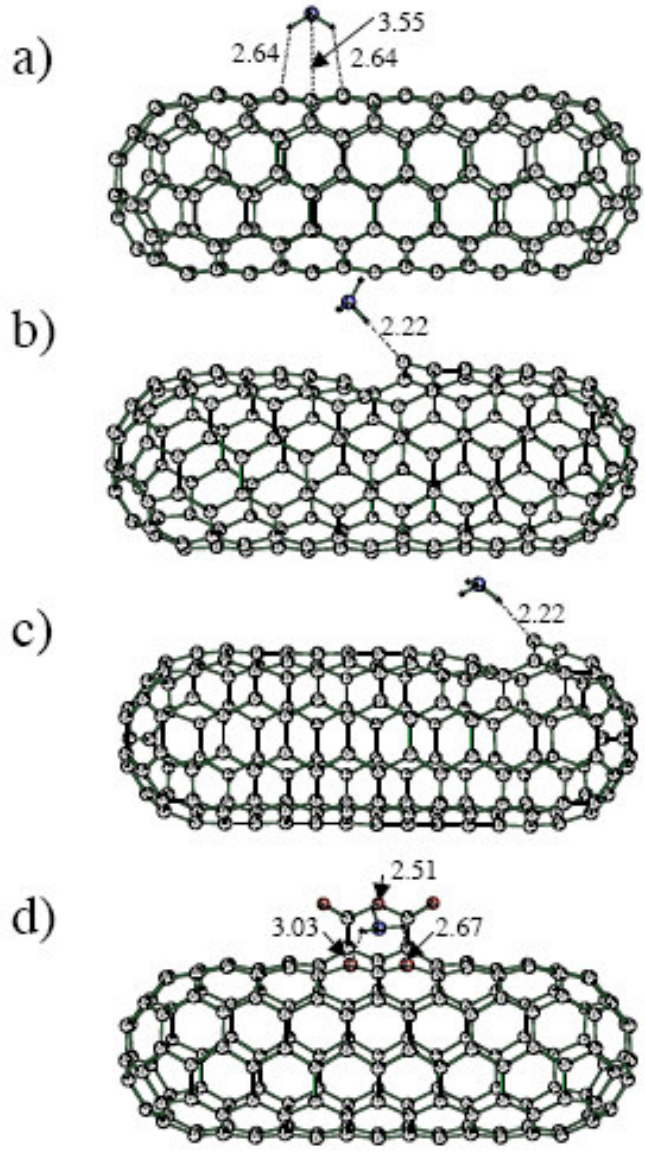

Figure 4- 28 SCC-DFTB-D optimized structures of a (5, 5) capped 20 Å long CNT model system plus one physisorbed NH_3 molecule: a) pristine, b) and c) defective (one carbon atom removed), and d) oxidized (5 oxygen atoms added). H-C (panels a-c) and H-O distances are given in Å

Summary and Conclusions Several conclusions can be drawn from this study.

I: HiPco nanotubes subjected to vacuum annealing, which tends to recover pristine tubes by healing defects sites and removing functional groups, show no detectable ammonia uptake.

II: Ammonia adsorption is detected on as-received HiPco, Rice and HNO_3-treated HiPco nanotubes (with higher degree of functionalities and defect sites) at 94 K. Nanotube surface chemistry may dramatically influence the sensitivity of nanotube sensors to trace ammonia from the environment. This finding is corroborated by computational modeling of ammonia adsorption of pristine, defective, and oxidized tubes.

III: Ammonia doesn't interact strongly with HNO_3-treated HiPco nanotubes, as revealed by the complete desorption above 140 K (~30 KJ/mol desorption energy).

IV: Exposing thermally annealed nanotubes to ambient air led to the recovery of ammonia uptake by nanotubes. This possibly occurs, as suggested in the literature, [195] through the chemisorption of oxygen at dangling bonds, leading to the regeneration of sites where NH_3 can bind.

V: Computational studies indicate that ammonia interacts more strongly with the oxidized nanotubes than with pristine or defective nanotubes, consistent with experimental observations.

VI: The lack of ammonia adsorption at room temperature is not inconsistent with CNT sensitivity to ammonia, as long as conductivity is sensitive to coverage of 10^{-5} monolayer or less.

4.4 INTERACTION BETWEEN HYDROGEN SULFIDE AND SINGLE WALLED CARBON NANOTUBES

Fixed bed activated carbon absorbers have been widely used for the control of vapor phase mercury emission [143]. It is reported that sulfur impregnated activated carbon has significantly higher mercury adsorption capacity compared with virgin activated carbon [143]. The increasing of mercury adsorption by sulfur impregnated carbon involves mercury reaction with elemental sulfur to form chemisorbed species instead of only physisorbed mercury [143]. Carbon materials impregnated by hydrogen sulfide are of particular interest because hydrogen sulfide itself is a pollutant [197], so impregnation from hydrogen sulfide is of benefit to both pollution control and the economy. The performance of activated carbon adsorption of hydrogen sulfide depends on several physical properties of the material, such as surface area and environment parameters including flue gas velocity, pressure, temperature, gas concentration, moisture content, etc. [197]. Sulfur impregnated from hydrogen sulfide showed less thermal stability than that from elemental sulfur.

An objective of this study is to understand the effect of functional groups on the ability of nanotubes to adsorb hydrogen sulfide. It is reported that heat treatments effectively removed oxygen containing functional groups from nanotube surfaces[198-201]. Heating the nanotube led to desorption of 16, 18, 28 and 44 m/e (Figure 4- 29) containing species, possibly H_2O, CO_2 and CO. In order to completely remove all the functional groups, the sample needs over 1273 K thermal treatment [148].

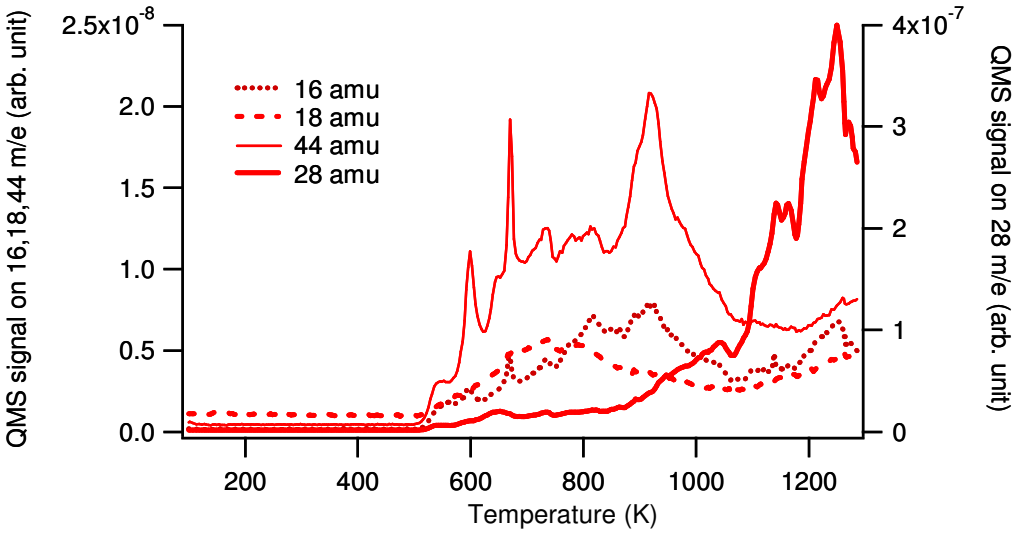

Figure 4- 29 TPD spectrum resulting from Heat treatment of purified HiPco

Influence of functional groups on the adsorption of H_2S by nanotubes at 100 K In order to probe the interaction of hydrogen sulfide with SWNTs, TPD experiments were performed on 300 degree C treated (Figure 4- 30) and 1000 degree C treated (Figure 4- 31) nanotube samples exposed to hydrogen sulfide at 100K. The partial pressure of hydrogen sulfide (monitored at 34amu) was plotted as a function of sample temperature. The area under each curve represents the relative coverage of the surface by molecules. The peak temperature is associated with the maximum desorption rate. The desorption temperatures are similar for H_2S from 300 degree C and 1000 degree C treated sample. After the functional groups were removed, desorption energy didn't change significantly.

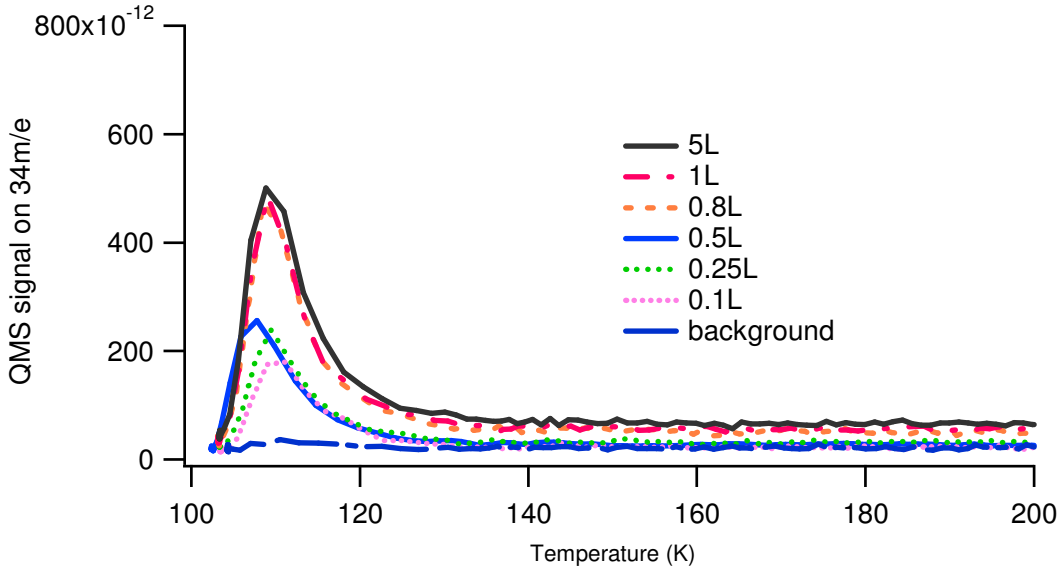

Figure 4- 30 TPD spectrum of hydrogen sulfide from nanotube samples dispersed on HOPG after 300 °C treatment (dosing at 100 K)

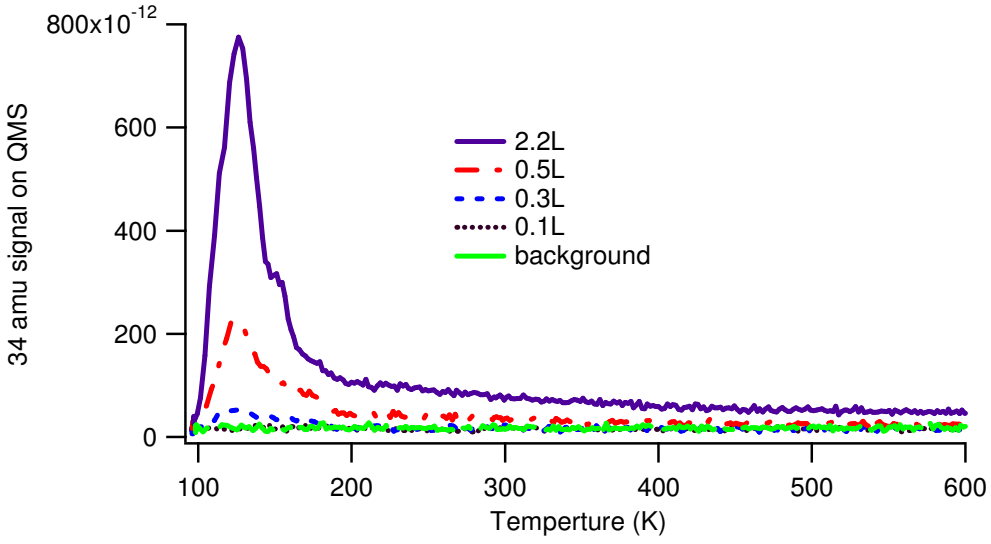

Figure 4- 31 TPD spectrum of hydrogen sulfide from nanotube samples after 1000 °C treatment (dosing at 100 K)

A comparison of uptake capacity, by integration of peak area, of nanotubes before and after 1000 degree C treatment is displayed in Figure 4- 32. The amount of H_2S adsorbed on both two nanotube samples increased over the entire exposure region. The uptake capacity of the 1000 ^oC treated sample was larger than 300 ^oC treated sample, suggesting a higher sticking probability on the former. This result suggests that removing of functional groups enhanced the uptake capacity of nanotubes to H_2S. It is possible the heating treatment opened the entrance to the endohedral sites of nanotubes for H_2S adsorption.

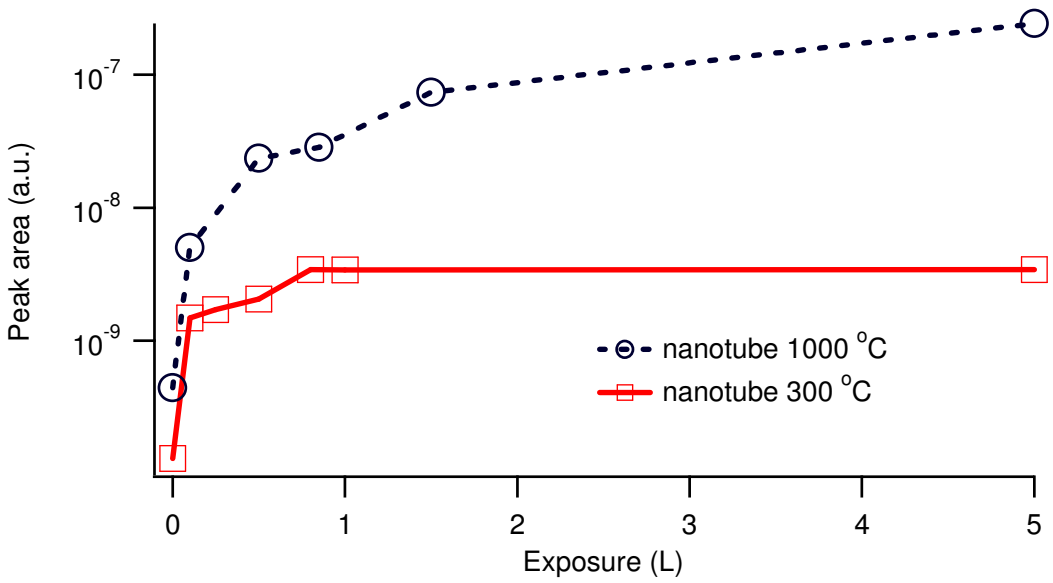

Figure 4- 32 Hydrogen sulfide uptake capacities by nanotubes after 300 and 1000 ^oC treatment

Influence of functional groups to the adsorption of H_2S by nanotubes at room temperature No obvious desorption peak was observed for 34 and 32 amu species at room temperature as shown in Figure 4- 33 even after the dosing amount reached 3600 L. The

absence of adsorption at room temperature indicated that the interaction between hydrogen sulfide and nanotube is not very strong.

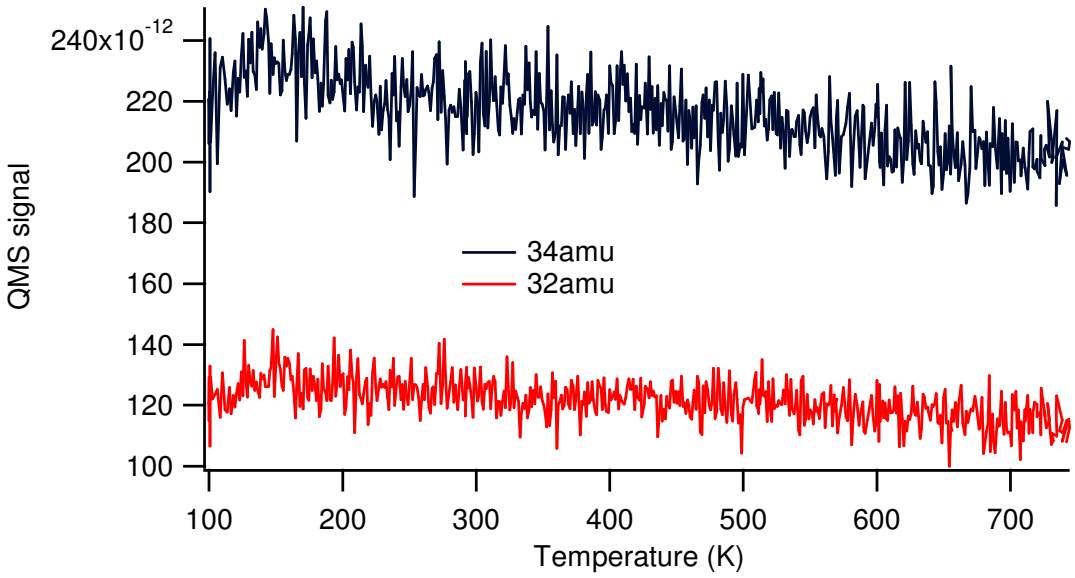

Figure 4- 33 TPD spectrum of hydrogen sulfide from nanotube samples after 1000 ^{o}C treatment (dosing at room temperature and dosing amount was 3600 L)

IR study of H_2S adsorption on nanotubes **A** preliminary infrared study of H_2S adsorption on nanotubes was performed. However, the intensity of the signal which can be observed from the infrared spectra is still less than 1 milli O.D. when the exposure amount is already more than 100 Langmuir as shown in Figure 4- 34. Detection of such low signals is a challenge for the study of adsorption by infrared spectroscopy.

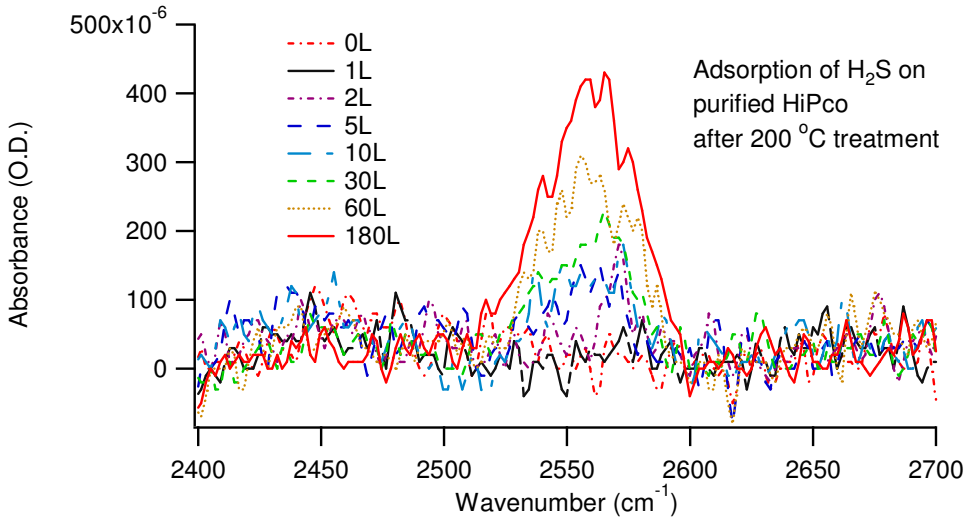

Figure 4- 34 Infrared spectra of nanotubes after serial of hydrogen sulfide exposure at 2400 to 2700 cm^{-1} region

Summary and Conclusions In summary, from TPD study, it was found that H_2S adsorbed on nanotube surfaces at cryogenic temperature but not at room temperature. The low desorption temperature suggests physisorption. Removal of functional groups from nanotube surfaces probably opened the entry port to the inside of nanotubes, increasing the uptake capacity of nanotubes.

4.5 INTERACTION BETWEEN ACETONE AND SINGLE WALLED CARBON NANOTUBES

Single walled carbon nanotubes show promise as new, miniaturized functional devices [26, 27, 202-204]. In the application of nanotubes to molecular electronics, separation materials and

sorbents, the uniform dispersion of nanotubes into solvents is an important step[205]. However, as received nanotubes are insoluble in most solvents, e.g. acetone. This makes it difficult to process SWNTs and disperse them in order to investigate their properties. Several strategies, including dispersion and suspension under special experimental conditions, chemical modification and functionalization, have been developed to disperse carbon nanotubes into solvents[205]. Sonication is a simple and effective method to stabilize nanotubes in solvents. However, the sonication process could affect the surface properties as well as the structure of nanotubes [163]. Indeed, ultrasonication is reported to be a simple way to chemically react nanotubes with organic materials [206]. The sonication induced reaction between nanotube and aniline was observed by Sun et.al [207]. Key to successful dispersion is an understanding of the interaction between solvents and nanotubes. However, this is still not well established [208].

In this work, temperature programmed desorption (TPD) and infrared spectroscopy (IR) study were applied to study the interaction between a commonly used solvent, acetone, with single walled carbon nanotube (HiPco).

TPD and IR acetone dosing experiments Figure 4- 35 displayed a series of spectra of acetone exposed to 473K treated and 1273K treated Air/HCl treated HiPco sample at 95K. The partial pressure of acetone was plotted as a function of sample temperature. The area under each curve represented the coverage of the surface by molecules. The peak temperature associated with the maximum desorption rate. The acetone desorption from nanotubes occurred in two temperature ranges. One is around 150 K and second one is 300 - 400 K. The acetone boiling temperature is 329 K. The higher temperature peaks appearing right above the boiling temperature indicated a strong interaction of acetone with the nanotubes. The amount of acetone adsorbed on nanotube samples increased almost linearly for the entire exposure region.

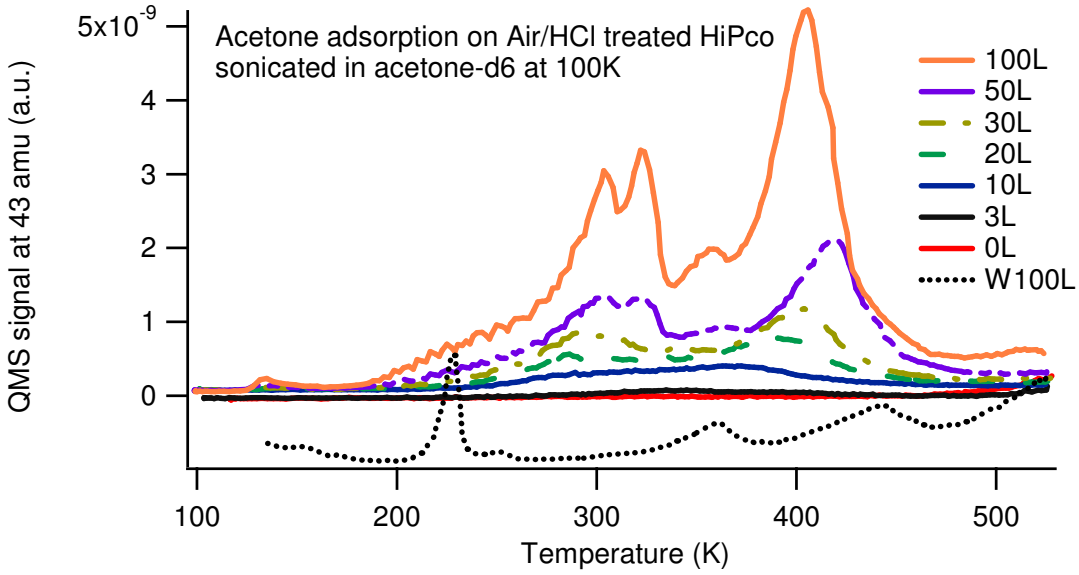

Figure 4- 35 TPD spectra of acetone adsorbed on Air/HCl treated HiPco nanotube surface after 500 K treatment. (W data offset for clarity)

A control experiment on bare W grid was also performed in this study to make sure that acetone desorption does not occurs from W supports and/or other sample mount plate, but from the nanotube, itself. The peaks from bare W are the off-set, dotted line in Figure 4- 34. The biggest peak from W grid at 220 K doesn't appear in the nanotube spectra which mean that peaks in nanotube spectra are not influenced by W grid. In addition, nanotube deposition covered the entire surface of W grid sampled by the QMS aperture was proved.

The acetone carbonyl peak was observed in the infrared spectra (Figure 4- 36) at 1710 cm^{-1}. The extinction coefficient of this vibrational mode was small. The peak was larger than 1 milli.O.D. after the exposure was larger than 80 Langmuir. Desorption of this carbonyl peak (Figure 4- 37) happened 120 to 200 K with a maximum around 150-180 K which agrees with the TPD data for the lower temperature peak.

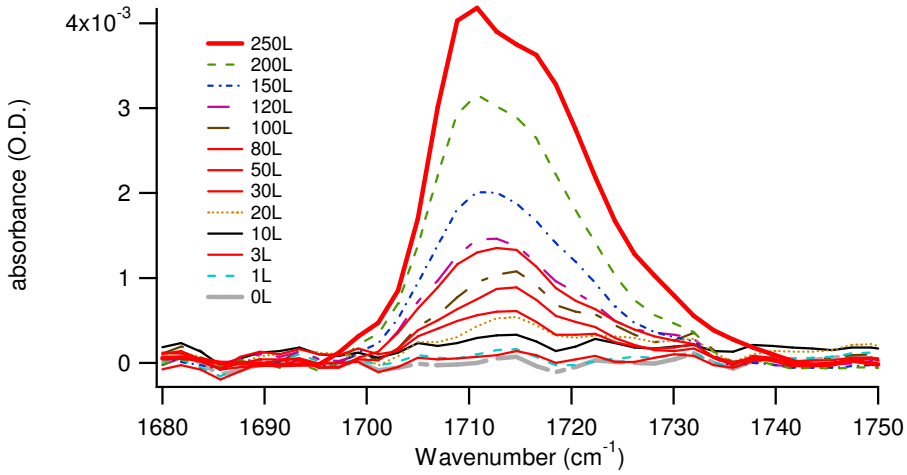

Figure 4- 36 IR spectra of acetone adsorbed on Air/HCl treated HiPco nanotube surface after 473 K treatment

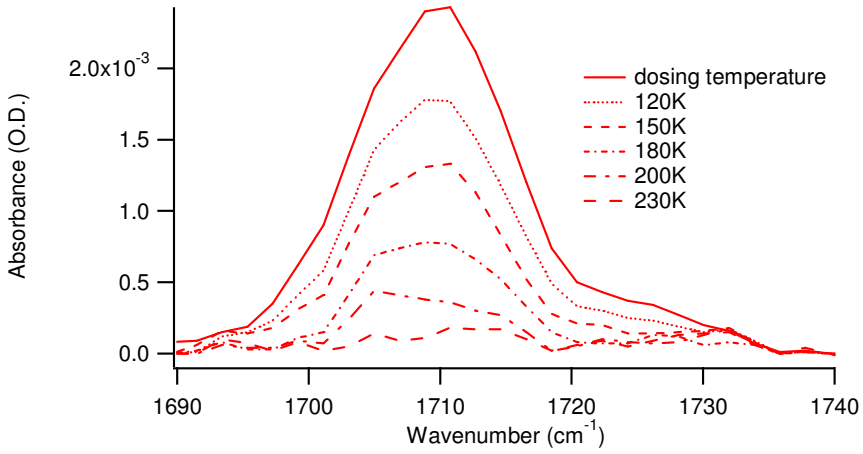

Figure 4- 37 IR desorption spectra of acetone adsorbed on Air/HCl treated HiPco nanotube surface after 473 K treatment

Sonication induced acetone chemisorption by full spectrum TPD and IR The stronger the solvent-nanotube interaction, the higher the temperature at which the solvent should desorb from the nanotube. In order to provide a more complete analysis, and because possible reactions were suspected with unknown products, the TPD were performed by taking 1 to 100 amu spectra at intervals of 10 K while ramping the temperature from 128 K to 828 K (full spectrum TPD). Figure 4- 38 shows the profile of desorbed species from Air/HCl treated HiPco nanotubes sonicated in acetone. Below room temperature, only 2, 18, 28 and 44 amu peaks were observed. Those are all background species (possibly trace H_2, H_2O, CO_2, CO and N_2) above room temperature, additional peaks at 58, 55, 43, 42, 41, 39, 36, 15 amu appear. 58, 43, and 15 amu correspond to the fragmentation products in the acetone mass spectrum (RGA Mass spectrum library, Stanford Research Systems). The temperatures at which the peaks are observed are above the boiling point of acetone, providing evidence of a strong interaction between acetone and nanotubes. Chakrapani et.al., who previously studies the acetone sonication reaction, suggested 41, 39 and 42 amu peaks were similar to propylene fragmentation pattern.[163] These features would result from desorption of adsorbed alkyl fragments of acetone, which further confirms chemisorption.

Control experiments to investigate contribution from the W grid sample support were also performed. As shown in Figure 4- 39, except for the background gases, no species desorbed from W grid during temperature ramping. The influence from W grid on the results shown in Figure 4- 38 was excluded.

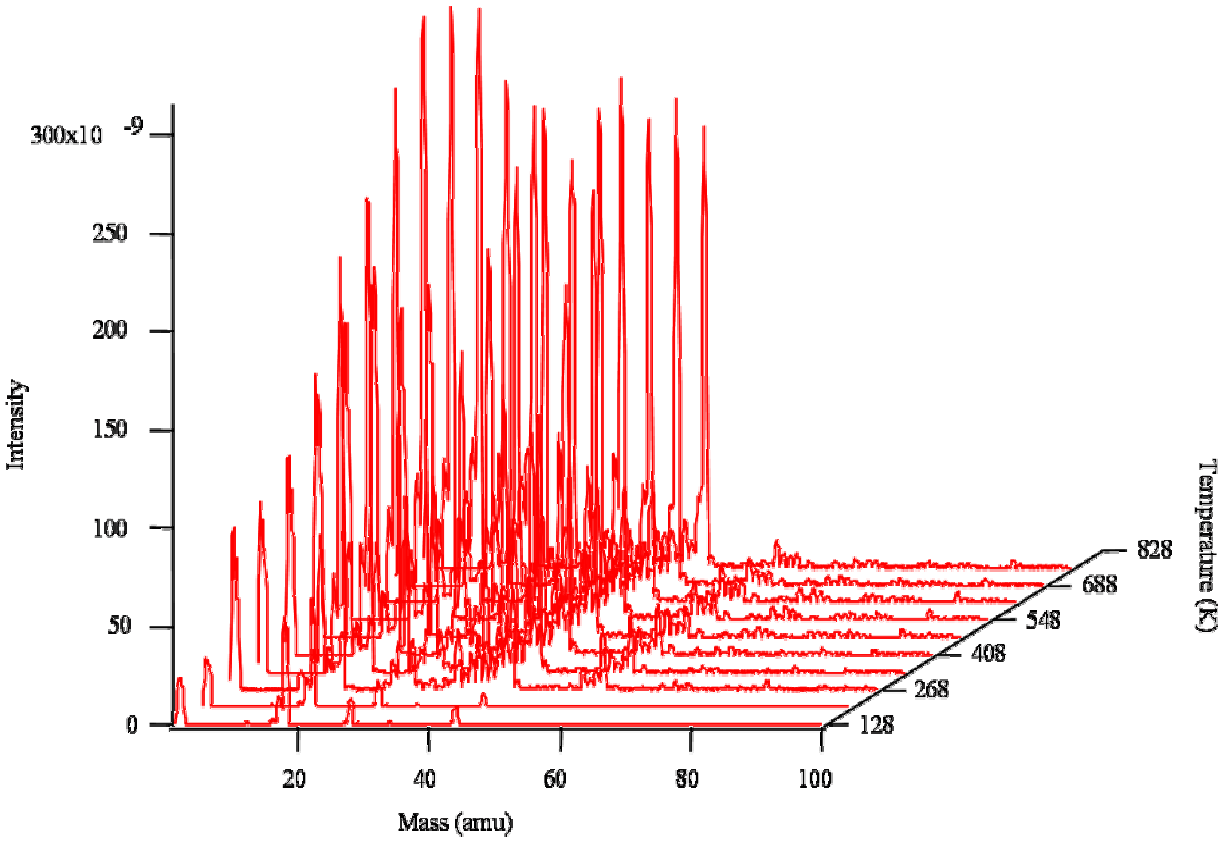

Figure 4- 38 Full spectrum (1-100 amu) TPD of Air/HCl treated HiPco nanotubes sonicated in acetone

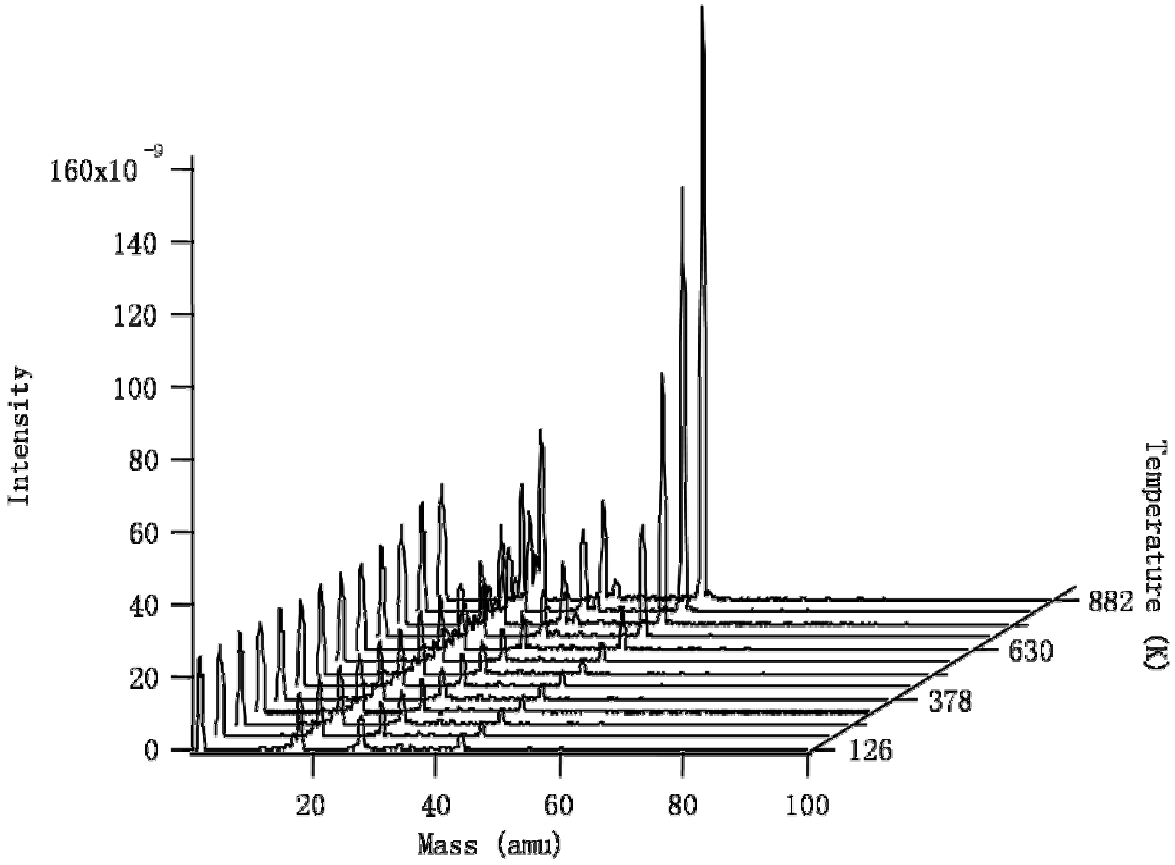

Figure 4- 39 Full spectrum (1-100 amu) TPD of W grid

Acetone was used to disperse air/HCl treated HiPco samples. Besides the persistence of the features in the CH stretch region of the IR spectrum, it was strange to find no increase in the carbonyl peak region of the infrared spectrum of nanotubes sonicated in acetone (solid line in Figure 4- 40). In order to compare acetone sonicated into/onto nanotubes with physisorbed on nanotube surfaces, at 94 K 200 L acetone was dosed onto air/HCl treated HiPco nanotube samples which had been sonicated into acetone. The results in an intense carbonyl peak around 1710 cm^{-1} as shown in the dotted line in Figure 4- 40. Moreover the increase of ether peak on Air/HCl treated nanotube surfaces was observed after sonication into acetone as shown in Figure 4- 41 compared to nanotubes samples sonicated in toluene.

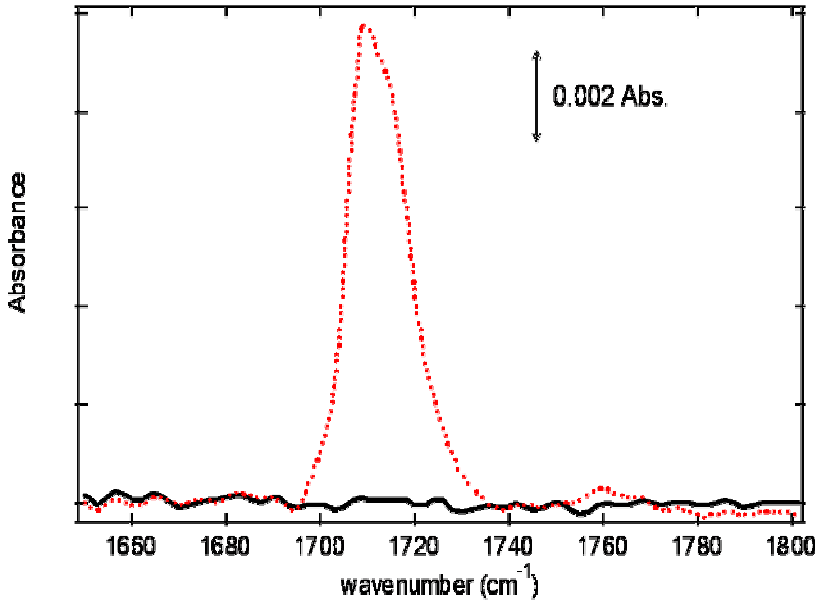

Figure 4- 40 Infrared spectra of the carbonyl peak (around 1710 cm^{-1}) from acetone physisorbed (dotted line) on nanotubes compared sonicated (solid line, dose 200 L at 94 K) into nanotubes

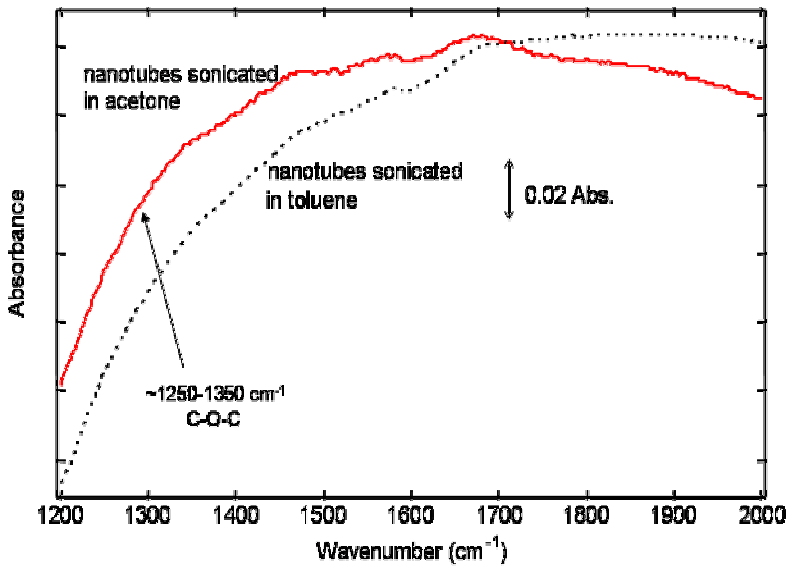

Figure 4- 41 Infrared spectra of oxygen containing functional group region for Air/HCl treated nanotubes sonicated in acetone (solid line) and toluene (dotted line)

The vibrational spectrum of a molecule is considered to be a unique physical property and is characteristic of the molecule. At the very least IR enables the presence of a specific group to be determined. It is also possible to determine its local environment [124]. In Figure 4-42, the CH_2/CH_3 stretch region of mid-IR spectra of nanotubes sonicated in acetone (dashed line), and physisorbed acetone on nanotubes (solid line) was compared. There are two peaks, near 2910 and 2970 cm^{-1}, on the spectrum of nanotubes sonicated in acetone (dashed line). While this is the CH_2/CH_3 region CH_2 peaks from acetone were not expected unless substantial rearrangement of the molecule occurs. Another high intensity peak around 3010 cm^{-1} arose upon the acetone exposure at 94 K. The CH_3 peak from physisorbed acetone is clearly different from chemisorbed acetone.

The preceding discussion suggests that the acetone reacted with nanotubes and formed anther kind of oxygen structure instead of carbonyl, possibly an ether structure. In order to test this hypothesis, a molecule, Methyl Tertiary Butyl Ether (MTBE), with a similar structure to the possible reaction product was selected to adsorb on nanotube samples. The spectrum of MTBE adsorbed on nanotubes was also shown in Figure 4- 42 (dotted line).

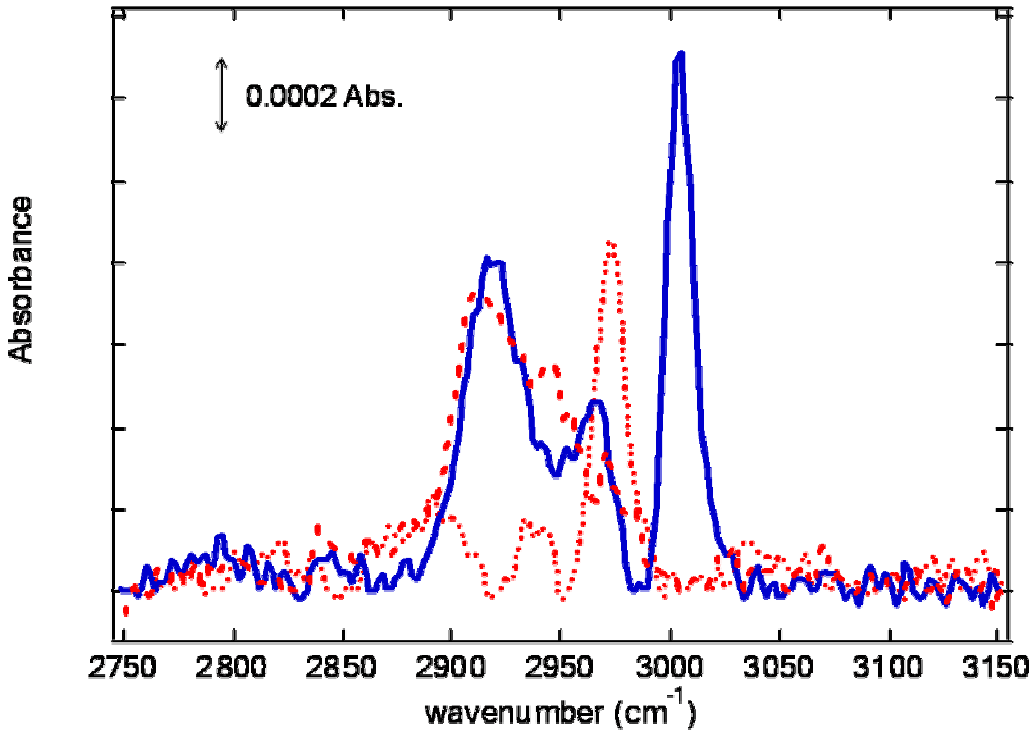

Figure 4- 42 The CH_2/CH_3 stretch region of mid-IR spectra of Air/HCl treated nanotubes sonicated in acetone (dashed line), physisorbed acetone on nanotubes (solid line) and MTBE adsorbed on Air/HCl treated nanotubes (dotted line)

There is similarity between the CH_2/CH_3 peak positions of nanotubes sonicated in acetone and MTBE adsorbed on nanotube surfaces. The CH_2/CH_3 ligand in MTBE connects to ether type oxygen. As the carbonyl oxygen became ether type oxygen after reaction with nanotube the CH_2/CH_3 peaks shift to lower wavenumbers. There is possibility that the CH_2/CH_3 in acetone sonicated nanotubes also connects to ether type oxygen. This further supports the suggestion for an acetone nanotube reaction.

Based on both infrared and TPD studies, one possible scheme for acetone chemisorption on nanotubes during sonication is proposed in Figure 4- 43. The carbonyl group on acetone molecule could react with the dangling bond, on defect sites, on nanotube surfaces and form ether structures[163]. However, because of their chemical properties, hexanes and toluene are not expected to react with nanotubes.

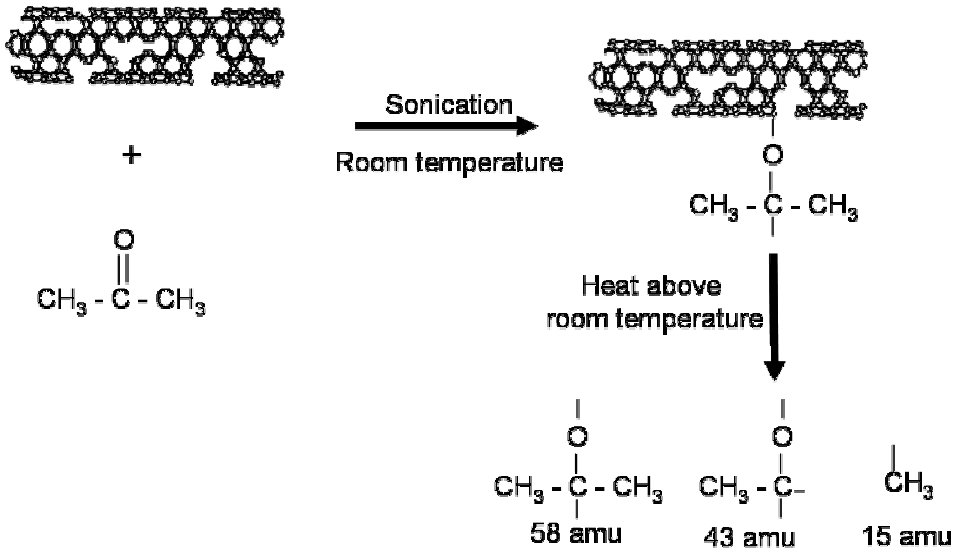

Figure 4- 43 Reaction scheme between acetone and nanotubes

Summary and Conclusions In summary, the interaction between acetone and nanotubes was investigated by TPD and infrared spectroscopy. Both physisorption and chemisorption appeared. A possible reaction scheme was suggested for acetone bonding with nanotubes during sonication. The strong interaction between acetone and nanotube during sonication suggested that one needs to be careful in interpreting experimental data when aggressive sample preparation was applied during sample preparation.

5.0 ENVIRONMENTAL SIGNIFICANCE OF THIS STUDY

The environmental applications and impact of this study can be divided into three topics. The first one is that this study demonstrates a possible method to enhance the performance of nanotube sensors by changing the degree of chemical and physical morphology. The results bridges the controversy between theoretical and experiment studies between the interaction between ammonia and carbon nanotube. Protection of human health and ecosystems requires rapid, precise sensors capable of detecting pollutants at the molecular level. Major improvements in process control, compliance monitoring, and environmental decision-making could be achieved if more accurate, less costly, more sensitive techniques were available. Nanotechnology offers the possibility of sensors enabled to be selective or specific, detect multiple analytes, and monitor their presence in real time. [209]

The second environmental application comes from the finding that nanotubes are potential sorbents for environmental treatments. Through the studies of the interaction between molecules and nanotubes, it was shown that there is a strong interaction between acetone and nanotubes, with desorption occurring at temperatures even higher than the boiling point of acetone. The results illustrated that nanotubes are potential candidates for separating certain molecules, like acetone, from their matrix based on different interaction energies. Cost-effective treatment poses a challenge for the EPA and others in the development of effective risk management strategies. EPA supports research that addresses new treatment approaches that are

more effective in reducing contaminant levels and more cost effective than currently available techniques. Nanotechnology offers the possibility of more effective treatment of soil and water due to the higher surface to volume ratios of nano materials, and it offers the possibility of novel collection and separation protocols imparted due to the unique physical properties of nanomaterials. Specific control and design of materials at the molecular level may impart increased affinity, capacity, and selectivity for pollutants. [210]

The third environmental application comes from the fact that this study successfully demonstrated detection of low concentrations of functionalities on carbonaceous materials by fluorescent labeling (FLOSS). FLOSS indicated the presence of COOH and CHO groups on the ACF25 fiber surface, for which neither the infrared spectrum nor the X-ray photoelectron spectrum showed evidence of their existence. FLOSS detects only exposed functional groups as opposed to functional groups hidden in small pores. This apparent limitation, however, highlights the surface sensitivity and specificity of FLOSS technique. FLOSS revealed that purification processes introduced more groups to purified nanotubes. Moreover, FLOSS showed that the functional groups are distributed heterogeneously on the nanotube surface. New functional groups created through the purification process grew preferentially on the defect sites. Functionality is a key for most of the applications of carbonaceous materials, including sorbents. Determination and quantification of functionalities will help to improve the performance of activated carbon fibers, carbon nanotubes, etc.

6.0 SUMMARY AND CONCLUSIONS

This work investigated the possible environmental application of carbon nanotubes through the study of chemical properties (functionalities) and topological heterogeneity (defects) and their influence on the interaction between small molecules (ammonia, acetone and hydrogen sulfide) and nanotubes. Functionalities/defects on nanotubes surface play an important role on their adsorption ability. This study answered an important question about the influence of different production and purification methods on a variety of functionalities that exist on the nanotube surface. This study also evaluated the possibility of determining functionalities on carbon material surface by fluorescence labeling technique. The key tasks that have been accomplished in this study include:

1. Determination of the impact of oxygen containing functional groups and/or defects on nanotube adsorption abilities. This task was accomplished by the study of ammonia, acetone and hydrogen sulfide adsorption on nanotube surfaces. Thus the adsorption capacity of carbon nanotubes can be controlled by changing the degree of functionalities on nanotube surfaces.
2. Resolving the controversy between theoretical and experimental results about the interaction between ammonia and nanotubes. The key finding of this task suggests a way to improve the sensitivity of nanotube sensors by enhancing the presence of oxygen containing surface functionalities.

3. Illustrating that different purification methods result in different degrees of functionalities on nanotube surface. Air/HCl purification is an effective method to remove metal catalyst without introducing significant functionalities. However, nitric acid oxidation generate significant oxygen containing functionalities while somewhat enhancing metal removal. Thus carbon nanotube purifications methods can be selected based on the requirements for their application.
4. Chemical identification and quantification of functionalities on carbonaceous surface using the FLOSS technique. This technique was successfully applied to activated carbon fiber and single walled carbon nanotubes. The surface sensitivity and specificity of this analytical technique was demonstrated for several classes of carbonaceous materials. Using this technique, it was observed that little OH functionality, compared to CHO or COOH, existed on these materials. This method can be used to detect low concentrations of functionalities which are below the sensitivities of IR and XPS techniques.

7.0 SUGGESTIONS FOR FUTURE WORK

Environmental engineering is often faced with the lack of fundamental understanding of molecular interactions in the complex mixtures that characterize environmental systems. Future studies on adsorption on carbon nanotubes under UHV conditions should utilize multiple analytical techniques (e.g., IR+TPD+XPS) to fully characterize many components of both the nanotubes and adsorbates used in the study. In addition, experimental techniques developed in this study may be applicable to characterization of complex environmental samples that require better understanding of surface phenomena relevant to the behavior of the entire systems.

Additional work would be needed to modify the experimental instrument used in this study and incorporate more experimental analytical methodologies. For instance, it would be useful to perform TPD and obtain IR spectra at the same time on the same sample. It would be advantageous to have the ability to change experimental parameters, e.g. pressures, over ranges that mimic more realistic environmental conditions and the ability to introduce species that might be expected under realistic field conditions (e.g. water and oxygen) into the chamber.

The results of this study indicate that there are strong interactions between molecules, e.g. acetone, and nanotubes. This suggests that carbon nanotubes have potential uses in selective adsorption of toxic species. Separation is a promising future research topic. One may be able to extend the fundamental surface science results to study the possible removal of pollutants, like MTBE from its matrix, like water.

It is well known that the performance of sulfur-impregnated activated carbon fibers for mercury uptake is strongly related to physical and chemical properties of both the sulfur and carbon. The experiment setup in this work offers the potential to understand the surface chemistry of the carbon and the formation of sulfur compound.

APPENDIX A

PHYSICAL CONSTANTS OF METAL CANDIDATES FOR SAMPLE WIRES

Materials	Symbol	Melting Point (℃)	Temperature (℃) for given vapor pressure (torr)		
			10^{-8}	10^{-6}	10^{-4}
Copper	Cu	1083	727	857	1017
Gold	Au	1064	807	947	1132
Nickel	Ni	1455	927	1072	1262
Tungsten	W	3410	2117	2407	2757

All data were obtained from the catalog of the K.J Lesker company.

APPENDIX B

PHYSICAL CONSTANTS OF MOLECULES STUDIED

	Acetone (C_3H_6O)	Hexane (C_6H_{14})	Ammonia (NH_3)	Hydrogen sulfide (H_2S)	MTBE ($C_5H_{12}O$)
Molecular weight (g/mol)	58	86.18	17.03	34.08	88.15
Boiling point (T_b,K)	329	341.9	N/A	212.87	328.2
Melting point (T_m,K)	229	178	194.95	190.85	164.50
Triple point (K)	229	178.0	0.06060 bar	187.66	164.56
Heat of vaporization (kJ/mol)	28.31	28.85	N/A	N/A	27.94

All data were obtained from CRC handbook of chemistry and physics, David R. Lide, 78th edition, CRC press.

BIBLIOGRAPHY

1. www.epa.gov.

2. Masciangioli, T. and W.X. Zhang, *Environmental technologies at the nanoscale.* Environmental Science & Technology, 2003. 37(5): p. 102A-108A.

3. Li, Y.H., S.G. Wang, J.Q. Wei, X.F. Zhang, C.L. Xu, Z.K. Luan, D.H. Wu, and B.Q. Wei, *Lead adsorption on carbon nanotubes.* Chemical Physics Letters, 2002. 357(3-4): p. 263-266.

4. Li, Y.H., S.G. Wang, Z.K. Luan, J. Ding, C.L. Xu, and D.H. Wu, *Adsorption of cadmium(II) from aqueous solution by surface oxidized carbon nanotubes.* Carbon, 2003. 41(5): p. 1057-1062.

5. Iijima, S., *Helical microtubules of graphitic carbon.* Nature, 1991. 354(6348): p. 56.

6. Saito, R., G. Dresselhaus, and M.S. Dresselhaus, *Properties of Carbon Nanotubes.* Imperial Collage Press; Singapore, 1998.

7. Odom, T.W., J.L. Huang, P. Kim, and C.M. Lieber, *Structure and electronic properties of carbon nanotubes.* Journal of Physical Chemistry B, 2000. 104(13): p. 2794-2809.

8. www.pa.msu.edu/cmp/csc/ntproperties/equilibriumstructure.html, 2004.

9. http://es.epa.gov/ncer/nano/index.html.

10. Dionysiou, D., *Environmental applications and implications of nanotechnology and nanomaterials.* Journal of Environmental Engineering-Asce, 2004. 38(3): p. 723-724.

11. Forster, P.M., J. Eckert, J.S. Chang, S.E. Park, G. Ferey, and A.K. Cheetham, *Hydrogen adsorption in nanoporous Nickel(II) phosphates.* Journal of the American Chemical Society, 2003. 125(5): p. 1309-1312.

12. Gordillo, M.C. and J. Marti, *Hydrogen bonding in supercritical water confined in carbon nanotubes.* Chemical Physics Letters, 2001. 341(3-4): p. 250-254.

13. Huang, W.Z., X.B. Zhang, F.Z. Kong, J.P. Tu, J.X. Ma, C.P. Chen, Y.S. Ning, and Y.L. Sun, *Hydrogen storage capacity of potassium-doped multi-walled carbon nanotubes.* Chinese Journal of Chemical Physics, 2002. 15(1): p. 51-55.

14. Zhu, H.W., X.S. Li, L.J. Ci, C.L. Xu, D.H. Wu, and Z.Q. Mao, *Hydrogen storage in heat-treated carbon nanofibers prepared by the vertical floating catalyst method.* Materials Chemistry and Physics, 2003. 78(3): p. 670-675.

15. Jin, Y.X., Z.J. Liu, W.X. Chen, and Z.D. Xu, *Hydrogenation of chlorophyll over carbon nanotubes-supported nickel catalyst at normal temperature and pressure.* Acta Physico-Chimica Sinica, 2002. 18(5): p. 459-462.

16. Dillon, A.C., K.M. Jones, T.A. Bekkedahl, C.H. Kiang, D.S. Bethune, and M.J. Heben, *Storage of hydrogen in single-walled carbon nanotubes.* Nature, 1997. 386(6623): p. 377-379.

17. Hynek, S., W. Fuller, and J. Bentley, *Hydrogen storage by carbon sorption.* International Journal of Hydrogen Energy, 1997. 22(6): p. 601-610.

18. Simonyan, V.V. and J.K. Johnson, *Hydrogen storage in carbon nanotubes and graphitic nanofibers.* Journal of Alloys and Compounds, 2002. 330: p. 659-665.

19. Valentini, L., I. Armentano, L. Lozzi, S. Santucci, and J.M. Kenny, *Interaction of methane with carbon nanotube thin films: role of defects and oxygen adsorption.* Materials Science & Engineering C-Biomimetic and Supramolecular Systems, 2004. 24(4): p. 527-533.

20. Cao, D.P., X.R. Zhang, J.F. Chen, W.C. Wang, and J. Yun, *Optimization of single-walled carbon nanotube arrays for methane storage at room temperature.* Journal of Physical Chemistry B, 2003. 107(48): p. 13286-13292.

21. Tanaka, H., M. El-Merraoui, W.A. Steele, and K. Kaneko, *Methane adsorption on single-walled carbon nanotube: a density functional theory model.* Chemical Physics Letters, 2002. 352(5-6): p. 334-341.

22. Long, R.Q. and R.T. Yang, *Carbon nanotubes as superior sorbent for dioxin removal.* Journal of the American Chemical Society, 2001. 123(9): p. 2058-2059.

23. Peng, X.J., Y.H. Li, Z.K. Luan, Z.C. Di, H.Y. Wang, B.H. Tian, and Z.P. Jia, *Adsorption of 1,2-dichlorobenzene from water to carbon nanotubes.* Chemical Physics Letters, 2003. 376(1-2): p. 154-158.

24. Li, Q.L., D.X. Yuan, and Q.M. Lin, *Evaluation of multi-walled carbon nanotubes as an adsorbent for trapping volatile organic compounds from environmental samples.* Journal of Chromatography A, 2004. 1026(1-2): p. 283-288.

25. Cai, Y., Y. Cai, S. Mou, and Y. Lu, *Multiwalled carbon nanotubes as a solid phase extraction adsorbent for the determination of chlorophenols in environmental water samples.* Journal of Chromatography A, 2005. 1081(2): p. 245-247.

26. Villalpando-Paez, F., A.H. Romero, E. Munoz-Sandoval, L.M. Martinez, H. Terrones, and M. Terrones, *Fabrication of vapor and gas sensors using films of aligned CNx nanotubes.* Chemical Physics Letters, 2004. 386(1-3): p. 137-143.

27. Suehiro, J., G.B. Zhou, and M. Hara, *Fabrication of a carbon nanotube-based gas sensor using dielectrophoresis and its application for ammonia detection by impedance spectroscopy.* Journal of Physics D-Applied Physics, 2003. 36(21): p. L109-L114.

28. Kong, J., N.R. Franklin, C.W. Zhou, M.G. Chapline, S. Peng, K.J. Cho, and H.J. Dai, *Nanotube molecular wires as chemical sensors.* Science, 2000. 287(5453): p. 622-625.

29. Goldoni, A., R. Larciprete, L. Petaccia, and S. Lizzit, *Single-wall carbon nanotube interaction with gases: Sample contaminants and environmental monitoring*. Journal of the American Chemical Society, 2003. 125(37): p. 11329-11333.

30. Collins, P.G., K. Bradley, M. Ishigami, and A. Zettl, *Extreme oxygen sensitivity of electronic properties of carbon nanotubes.* Science, 2000. 287(5459): p. 1801-1804.

31. Kuzmany, H., A. Kukovecz, F. Simon, A. Holzweber, C. Kramberger, and T. Pichler, *Functionalization of carbon nanotubes.* Synthetic Metals, 2004. 141(1-2): p. 113-122.

32. Zhao, J.J., H.K. Park, J. Han, and J.P. Lu, *Electronic properties of carbon nanotubes with covalent sidewall functionalization.* J. Phys. Chem. B, 2004. 108(14): p. 4227-4230.

33. Boul, P.J., J. Liu, E.T. Mickelson, C.B. Huffman, L.M. Ericson, I.W. Chiang, K.A. Smith, D.T. Colbert, R.H. Hauge, J.L. Margrave, and R.E. Smalley, *Reversible sidewall functionalization of buckytubes.* Chem. Phys. Lett., 1999. 310(3-4): p. 367-372.

34. Halicioglu, T. and R.L. Jaffe, *Solvent effect on functional groups attached to edges of carbon nanotubes.* Nano Letters, 2002. 2(6): p. 573-575.

35. Sun, Y.P., W.J. Huang, Y. Lin, K.F. Fu, A. Kitaygorodskiy, L.A. Riddle, Y.J. Yu, and D.L. Carroll, *Soluble dendron-functionalized carbon nanotubes: Preparation, characterization, and properties.* Chem. Mater., 2001. 13(9): p. 2864-2869.

36. Yang, C.M., H. Kanoh, K. Kaneko, M. Yudasaka, and S. Iijima, *Adsorption behaviors of HiPco single-walled carbon nanotube aggregates for alcohol vapors.* J. Phys. Chem. B, 2002. 106(35): p. 8994-8999.

37. Toebes, M.L., F.F. Prinsloo, J.H. Bitter, A.J. van Dillen, and K.P. de Jong, *Influence of oxygen-containing surface groups on the activity and selectivity of carbon nanofiber-supported ruthenium catalysts in the hydrogenation of cinnamaldehyde.* J.Cataly., 2003. 214(1): p. 78-87.

38. Liu, C.G., M. Liu, M.Z. Wang, and H.M. Cheng, *Research and development of carbon materials for electrochemical capacitors - II - The carbon electrode.* New Carbon Materials, 2002. 17(2): p. 64-72.

39. Hafner, J.H., C.L. Cheung, A.T. Woolley, and C.M. Lieber, *Structural and functional imaging with carbon nanotube AFM probes.* Progress in Biophysics & Molecular Biology, 2001. 77(1): p. 73-110.

40. Wong, S.S., E. Joselevich, A.T. Woolley, C.L. Cheung, and C.M. Lieber, *Covalently functionalized nanotubes as nanometre-sized probes in chemistry and biology.* Nature, 1998. 394(6688): p. 52-55.

41. Yang, Y.L., J. Zhang, X.L. Nan, and Z.F. Liu, *Studies on the dissociation behavior of carboxylic groups at the open end of single-walled carbon nanotubes by tip chemistry.* Chemical Journal of Chinese Universities-Chinese, 2002. 23(3): p. 469-471.

42. Nguyen, C.V., L. Delzeit, A.M. Cassell, J. Li, J. Han, and M. Meyyappan, *Preparation of nucleic acid functionalized carbon nanotube Arrays.* Nano Letters, 2002. 2(10): p. 1079-1081.

43. Kuznetsova, A., I. Popova, J.T. Yates, M.J. Bronikowski, C.B. Huffman, J. Liu, R.E. Smalley, H.H. Hwu, and J.G.G. Chen, *Oxygen-containing functional groups on single-wall carbon nanotubes: NEXAFS and vibrational spectroscopic studies.* J. Am. Chem. Soc., 2001. 123(43): p. 10699-10704.

44. Zhang, J., H.L. Zou, Q. Qing, Y.L. Yang, Q.W. Li, Z.F. Liu, X.Y. Guo, and Z.L. Du, *Effect of chemical oxidation on the structure of single-walled carbon nanotubes.* J. Phys. Chem. B, 2003. 107(16): p. 3712-3718.

45. Bower, C., A. Kleinhammes, Y. Wu, and O. Zhou, *Intercalation and partial exfoliation of single-walled carbon nanotubes by nitric acid.* Chem. Phys. Lett., 1998. 288(2-4): p. 481-486.

46. Yang, C.M., K. Kaneko, M. Yudasaka, and S. Iijima, *Effect of purification on pore structure of HiPco single-walled carbon nanotube aggregates.* Nano Letters, 2002. 2(4): p. 385-388.

47. Hernadi, K., A. Siska, L. Thien-Nga, L. Forro, and I. Kiricsi, *Reactivity of different kinds of carbon during oxidative purification of catalytically prepared carbon nanotubes.* Solid State Ionics, 2001. 141: p. 203-209.

48. Chiang, I.W., B.E. Brinson, R.E. Smalley, J.L. Margrave, and R.H. Hauge, *Purification and characterization of single-wall carbon nanotubes.* J. Phys. Chem. B, 2001. 105(6): p. 1157-1161.

49. Vidic, R., M. Suidan, G. Sorial, and R. Brenner, *Molecular-Oxygen and the Adsorption of Phenols - Effect of Functional-Groups.* Water Environ. Res., 1993. 65(2): p. 156-161.

50. Wu, S. and P. Pendleton, *Adsorption of anionic surfactant by activated carbon: Effect of surface chemistry, ionic strength, and hydrophobicity.* J. Colloid Interface Sci., 2001. 243(2): p. 306-315.

51. Kwon, S., R. Vidic, and E. Borguet, *Enhancement of adsorption on graphite (HOPG) by modification of surface chemical functionality and morphology.* Carbon, 2002. 40(13): p. 2351-2358.

52. Kwon, S., R. Vidic, and E. Borguet, *The effect of surface chemical functional groups on the adsorption and desorption of a polar molecule, acetone, from a model carbonaceous surface, graphite.* Surf. Sci., 2003. 522(1-3): p. 17-26.

53. Li, C., K. Yao, and J. Liang, *Influence of acid treatments on the activity of carbon nanotube-supported catalysts.* Carbon, 2003. 41(4): p. 858-860.

54. Toebes, M., F. Prinsloo, J. Bitter, A. van Dillen, and K. de Jong, *Influence of oxygen-containing surface groups on the activity and selectivity of carbon nanofiber-supported ruthenium catalysts in the hydrogenation of cinnamaldehyde.* J. Catal., 2003. 214(1): p. 78-87.

55. Beck, N., S. Meech, P. Norman, and L. Pears, *Characterisation of surface oxides on carbon and their influence on dynamic adsorption.* Carbon, 2002. 40(4): p. 531-540.

56. Li, Y., C. Lee, and B. Gullett, *Importance of activated carbon's oxygen surface functional groups on elemental mercury adsorption.* Fuel, 2003. 82(4): p. 451-457.

57. Liu, J., Z. He, and S. Wang, *Formation mechanism of carbon fiber biofilms - I. effects of carbon fiber surface characteristics on the immobilization of microorganisms.* New Carbon Mater., 2002. 17(3): p. 20-24.

58. Boehm, H., *surface oxides on carbon and their analysis: a critical assessment.* Carbon, 2002. 40: p. 145-149.

59. Boehm, H., *Some Aspects of the Surface-Chemistry of Carbon-Blacks and Other Carbons.* Carbon, 1994. 32(5): p. 759-769.

60. DelaPuente, G., J. Pis, J. Menendez, and P. Grange, *Thermal stability of oxygenated functions in activated carbons.* J. Ana. Appl. Pyrolysis, 1997. 43(2): p. 125-138.

61. Salame, I. and T. Bandosz, *Surface chemistry of activated carbons: Combining the results of temperature-programmed desorption, boehm, and potentiometric titrations.* J. Colloid Interface Sci., 2001. 240(1): p. 252-258.

62. Wang, Z., H. Kanoh, K. Kaneko, G. Lu, and D. Do, *Structural and surface property changes of macadamia nut-shell char upon activation and high temperature treatment.* Carbon, 2002. 40(8): p. 1231-1239.

63. Park, S. and W. Jung, *Effect of KOH activation on the formation of oxygen structure in activated carbons synthesized from polymeric precursor.* J. Colloid Interface Sci., 2002. 250(1): p. 93-98.

64. Chiang, H., C. Huang, and P. Chiang, *The surface characteristics of activated carbon as affected by ozone and alkaline treatment.* Chemosphere, 2002. 47(3): p. 257-265.

65. Park, E. and J. Lee, *Effect of surface treatment of the support on CO oxidation over carbon-supported Wacker-type catalysts.* J. Catal., 2000. 193(1): p. 5-15.

66. Gomezserrano, V., M. Acedoramos, A. Lopezpeinado, and C. Valenzuelacalahorro, *Oxidation of Activated Carbon by Hydrogen-Peroxide - Study of Surface Functional-Groups by Ft-Ir.* Fuel, 1994. 73(3): p. 387-395.

67. Smith, D. and A. Chughtai, *The Surface-Structure and Reactivity of Black Carbon.* Colloids Surf. A, 1995. 105(1): p. 47-77.

68. Biniak, S., G. Szymanski, J. Siedlewski, and A. Swiatkowski, *The characterization of activated carbons with oxygen and nitrogen surface groups.* Carbon, 1997. 35(12): p. 1799-1810.

69. Lee, W., J. Lee, and P. Reucroft, *XPS study of carbon fiber surfaces treated by thermal oxidation in a gas mixture of O-2/(O-2+N-2).* Appl. Surf. Sci., 2001. 171(1-2): p. 136-142.

70. Otake, Y. and R. Jenkins, *Characterization of Oxygen-Containing Surface Complexes Created on a Microporous Carbon by Air and Nitric-Acid Treatment.* Carbon, 1993. 31(1): p. 109-121.

71. Swiatkowski, A., A. Derylo-Marczewska, J. Goworek, and S. Biniak, *Study of adsorption equilibria in the systems ternary liquid mixtures-modified activated carbons.* J. Colloid Interface Sci., 1999. 218(2): p. 480-487.

72. Strelko, V. and D. Malik, *Characterization and metal sorptive properties of oxidized active carbon.* J. Colloid Interface Sci., 2002. 250(1): p. 213-220.

73. Gun'ko, V. and T. Bandosz, *Heterogeneity of adsorption energy of water, methanol and diethyl ether on activated carbons: effect of porosity and surface chemistry.* Phys. Chem. Chem. Phys., 2003. 5(10): p. 2096-2103.

74. Park, S., Y. Jang, J. Shim, and S. Ryu, *Studies on pore structures and surface functional groups of pitch-based activated carbon fibers.* J. Colloid Interface Sci., 2003. 260(2): p. 259-264.

75. Tessmer, C., R. Vidic, and L. Uranowski, *Impact of oxygen-containing surface functional groups on activated carbon adsorption of phenols.* Environ. Sci. & Techn., 1997. 31(7): p. 1872-1878.

76. Jagiello, J., T. Bandosz, and J. Schwarz, *A Study of the Activity of Chemical Groups on Carbonaceous and Model Surfaces by Infinite Dilution Chromatography.* Chromatographia, 1992. 33(9-10): p. 441-444.

77. Salame, II and T.J. Bandosz, *Study of diethyl ether adsorption on activated carbons using IGC at finite concentration.* Langmuir, 2001. 17(16): p. 4967-4972.

78. Fanning, P. and M. Vannice, *A Drifts Study of the Formation of Surface Groups on Carbon by Oxidation.* Carbon, 1993. 31(5): p. 721-730.

79. Zhuang, Q., T. Kyotani, and A. Tomita, *Drift and Tk Tpd Analyses of Surface Oxygen Complexes Formed During Carbon Gasification.* Energy & Fuels, 1994. 8(3): p. 714-718.

80. Garcia, A., A. Cuesta, M. MontesMoran, A. MartinezAlonso, and J. Tascon, *Zeta potential as a tool to characterize plasma oxidation of carbon fibers.* J.Colloid Interface Sci., 1997. 192(2): p. 363-367.

81. Paredes, J.I., A. Martinez-Alonso, and J. Tascon, *Application of scanning tunneling and atomic force microscopies to the characterization of microporous and mesoporous materials.* Microporous and Mesoporous Mater., 2003. 65(2-3): p. 93-126.

82. McArthur, E., T. Ye, J. Cross, S. Petoud, and E. Borguet, *Fluorescence detection of surface bound intermediates produced from UV photoreactivity of alkylsiloxane SAMs.* J. Am. Chem. Soc. (Communication), 2004. 126: p. 2260-2261.

83. Hollander, A., *Labelling techniques for the chemical analysis of polymer surfaces.* Surf. Interface Anal., 2004. 36(8): p. 1023-1026.

84. Ivanov, V., J. Behnisch, A. Hollander, F. Mehdorn, and H. Zimmermann, *Determination of functional groups on polymer surfaces using fluorescence labelling.* Surf. Interface Anal., 1996. 24(4): p. 257-262.

85. Zhou, B., Y. Lin, H.P. Li, W.J. Huang, J.W. Connell, L.F. Allard, and Y.P. Sun, *Absorptivity of functionalized single-walled carbon nanotubes in solution.* Journal of Physical Chemistry B, 2003. 107(49): p. 13588-13592.

86. Wang, S.G., Y.H. Li, X.Y. Gong, H.Z. Zhao, Z.K. Luan, C.L. Xu, and D.H. Wu, *Surface characteristics of modified carbon nanotubes and its application in lead adsorption from aqueous solution.* Chinese Science Bulletin, 2003. 48(5): p. 441-443.

87. Li, Y.H., J. Ding, Z.K. Luan, Z.C. Di, Y.F. Zhu, C.L. Xu, D.H. Wu, and B.Q. Wei, *Competitive adsorption of Pb2+, Cu2+ and Cd2+ ions from aqueous solutions by multiwalled carbon nanotubes.* Carbon, 2003. 41(14): p. 2787-2792.

88. Li, X.S., H.W. Zhu, L.J. Ci, C.L. Xu, Z.Q. Mao, B.Q. Wei, J. Liang, and D.H. Wu, *Effects of structure and surface properties on carbon nanotubes' hydrogen storage characteristics.* Chinese Science Bulletin, 2001. 46(16): p. 1358-1360.

89. Yu, R.Q., L.W. Chen, Q.P. Liu, J.Y. Lin, K.L. Tan, S.C. Ng, H.S.O. Chan, G.Q. Xu, and T.S.A. Hor, *Platinum deposition on carbon nanotubes via chemical modification.* Chemistry of Materials, 1998. 10(3): p. 718-722.

90. Li, C.H., K.F. Yao, and J. Liang, *Influence of acid treatments on the activity of carbon nanotube-supported catalysts.* Carbon, 2003. 41(4): p. 858-860.

91. Li, C.S., D.Z. Wang, J.J. Wu, W.Z. Lu, and J. Liang, *Effect of inorganic acid treatment on ultrahigh capacitor made of carbon nanotubes.* Journal of Inorganic Materials, 2003. 18(5): p. 1010-1016.

92. Joseph, S., R.J. Mashl, E. Jakobsson, and N.R. Aluru, *Electrolytic transport in modified carbon nanotubes.* Nano Letters, 2003. 3(10): p. 1399-1403.

93. Chen, Y., R.C. Haddon, S. Fang, A.M. Rao, W.H. Lee, E.C. Dickey, E.A. Grulke, J.C. Pendergrass, A. Chavan, B.E. Haley, and R.E. Smalley, *Chemical attachment of organic functional groups to single-walled carbon nanotube material.* Journal of Materials Research, 1998. 13(9): p. 2423-2431.

94. Jiang, K.Y., A. Eitan, L.S. Schadler, P.M. Ajayan, R.W. Siegel, N. Grobert, M. Mayne, M. Reyes-Reyes, H. Terrones, and M. Terrones, *Selective attachment of gold nanoparticies to nitrogen-doped carbon nanotubes.* Nano Letters, 2003. 3(3): p. 275-277.

95. Fu, Q., C.G. Lu, and J. Liu, *Selective coating of single wall carbon nanotubes with thin SiO2 layer.* Nano Letters, 2002. 2(4): p. 329-332.

96. Garg, A. and S.B. Sinnott, *Effect of chemical functionalization on the mechanical properties of carbon nanotubes.* Chemical Physics Letters, 1998. 295(4): p. 273-278.

97. Zhang, J., H.L. Zou, Q. Qing, Y.L. Yang, Q.W. Li, Z.F. Liu, X.Y. Guo, and Z.L. Du, *Effect of chemical oxidation on the structure of single-walled carbon nanotubes.* Journal of Physical Chemistry B, 2003. 107(16): p. 3712-3718.

98. Martinez, M.T., M.A. Callejas, A.M. Benito, M. Cochet, T. Seeger, A. Anson, J. Schreiber, C. Gordon, C. Marhic, O. Chauvet, J.L.G. Fierro, and W.K. Maser, *Sensitivity of single wall carbon nanotubes to oxidative processing: structural modification, intercalation and functionalisation.* Carbon, 2003. 41(12): p. 2247-2256.

99. Kuzmany, H., A. Kukovecz, C. Kramberger, T. Pichler, M. Holzinger, and H. Kataura, *Exohedral and endohedral function alization of single wall carbon nanotubes.* Synthetic Metals, 2003. 135(1-3): p. 791-793.

100. Ros, T.G., A.J. van Dillen, J.W. Geus, and D.C. Koningsberger, *Surface oxidation of carbon nanofibres.* Chemistry-a European Journal, 2002. 8(5): p. 1151-1162.

101. Konya, Z., I. Vesselenyi, K. Niesz, A. Kukovecz, A. Demortier, A. Fonseca, J. Delhalle, Z. Mekhalif, J.B. Nagy, A.A. Koos, Z. Osvath, A. Kocsonya, L.P. Biro, and I. Kiricsi,

Large scale production of short functionalized carbon nanotubes. Chemical Physics Letters, 2002. 360(5-6): p. 429-435.

102. Lee, W.H., S.J. Kim, W.J. Lee, J.G. Lee, R.C. Haddon, and P.J. Reucroft, *X-ray photoelectron spectroscopic studies of surface modified single-walled carbon nanotube material.* Applied Surface Science, 2001. 181(1-2): p. 121-127.

103. Mawhinney, D.B., V. Naumenko, A. Kuznetsova, J.T. Yates, J. Liu, and R.E. Smalley, *Infrared spectral evidence for the etching of carbon nanotubes: Ozone oxidation at 298 K.* Journal of the American Chemical Society, 2000. 122(10): p. 2383-2384.

104. Kuznetsova, A., I. Popova, J.T. Yates, M.J. Bronikowski, C.B. Huffman, J. Liu, R.E. Smalley, H.H. Hwu, and J.G.G. Chen, *Oxygen-containing functional groups on single-wall carbon nanotubes: NEXAFS and vibrational spectroscopic studies.* Journal of the American Chemical Society, 2001. 123(43): p. 10699-10704.

105. Chiu, P.W., G.S. Duesberg, U. Dettlaff-Weglikowska, and S. Roth, *Interconnection of carbon nanotubes by chemical functionalization.* Applied Physics Letters, 2002. 80(20): p. 3811-3813.

106. Koos, A.A., Z.E. Horvath, Z. Osvath, L. Tapaszto, K. Niesz, Z. Konya, I. Kiricsi, N. Grobert, M. Ruhle, and L.P. Biro, *STM investigation of carbon nanotubes connected by functional groups.* Materials Science & Engineering C-Biomimetic and Supramolecular Systems, 2003. 23(6-8): p. 1007-1011.

107. Jiang, L.Q. and L. Gao, *Modified carbon nanotubes: an effective way to selective attachment of gold nanoparticles.* Carbon, 2003. 41(15): p. 2923-2929.

108. Mawhinney, D.B., V. Naumenko, A. Kuznetsova, J.T. Yates, J. Liu, and R.E. Smalley, *Surface defect site density on single walled carbon nanotubes by titration.* Chemical Physics Letters, 2000. 324(1-3): p. 213-216.

109. Xu, H., M. Zheng, D.R. Dai, P. Xie, F.L. Bai, and R.B. Zhang, *Structural investigation of a new polyorganosiloxane containing nanotubular cavities using organic fluorescent probes.* Chinese Journal of Polymer Science, 1999. 17(4): p. 383-389.

110. Riggs, J.E., Z.X. Guo, D.L. Carroll, and Y.P. Sun, *Strong luminescence of solubilized carbon nanotubes.* Journal of the American Chemical Society, 2000. 122(24): p. 5879-5880.

111. Bulusheva, L.G., A.V. Okotrub, A. Fonseca, and J.B. Nagy, *Electronic structure of multiwall carbon nanotubes.* Synthetic Metals, 2001. 121(1-3): p. 1207-1208.

112. Funaki, T., T. Simomura, and K. Ito, *Inclusion-dissociation behavior between non-ionic surfactants and molecular nanotubes in aqueous solution.* Kobunshi Ronbunshu, 2001. 58(6): p. 299-303.

113. Fu, K.F., R.B. Martin, A.M. Rao, and Y.P. Sun, *Spectroscopic probing of organic molecules encapsulated in functionalized carbon nanotubes in solution.* Journal of Nanoscience and Nanotechnology, 2003. 3(1-2): p. 127-131.

114. Moore, V.C., M.S. Strano, E.H. Haroz, R.H. Hauge, R.E. Smalley, J. Schmidt, and Y. Talmon, *Individually suspended single-walled carbon nanotubes in various surfactants.* Nano Letters, 2003. 3(10): p. 1379-1382.

115. Murakami, H., T. Nomura, and N. Nakashima, *Noncovalent porphyrin-functionalized single-walled carbon nanotubes in solution and the formation of porphyrin-nanotube nanocomposites.* Chemical Physics Letters, 2003. 378(5-6): p. 481-485.

116. Nakashima, N., Y. Tomonari, and H. Murakami, *Water-soluble single-walled carbon nanotubes via noncovalent sidewall-functionalization with a pyrene-carrying ammonium ion.* Chemistry Letters, 2002(6): p. 638-639.

117. Otobe, K., H. Nakao, H. Hayashi, F. Nihey, M. Yudasaka, and S. Iijima, *Fluorescence visualization of carbon nanotubes by modification with silicon-based polymer.* Nano Letters, 2002. 2(10): p. 1157-1160.

118. Qu, L.W., R.B. Martin, W.J. Huang, K.F. Fu, D. Zweifel, Y. Lin, Y.P. Sun, C.E. Bunker, B.A. Harruff, J.R. Gord, and L.F. Allard, *Interactions of functionalized carbon nanotubes with tethered pyrenes in solution.* Journal of Chemical Physics, 2002. 117(17): p. 8089-8094.

119. Hazani, M., R. Naaman, F. Hennrich, and M.M. Kappes, *Confocal fluorescence imaging of DNA-functionalized carbon nanotubes.* Nano Letters, 2003. 3(2): p. 153-155.

120. Zhang, C.F., X.H. Shen, and H.C. Gao, *Studies on the formation of cyclodextrin nanotube by fluorescence and anisotropy measurements.* Spectroscopy and Spectral Analysis, 2003. 23(2): p. 217-220.

121. Ito, T., L. Sun, and R.M. Crooks, *Observation of DNA transport through a single carbon nanotube channel using fluorescence microscopy.* Chemical Communications, 2003(13): p. 1482-1483.

122. Prakash, R., S. Washburn, R. Superfine, R.E. Cheney, and M.R. Falvo, *Visualization of individual carbon nanotubes with fluorescence microscopy using conventional fluorophores.* Applied Physics Letters, 2003. 83(6): p. 1219-1221.

123. Zhu, W.H., N. Minami, S. Kazaoui, and Y. Kim, *Fluorescent chromophore functionalized single-wall carbon nanotubes with minimal alteration to their characteristic one-dimensional electronic states.* Journal of Materials Chemistry, 2003. 13(9): p. 2196-2201.

124. Coates, J., *Interpretation of infrared spectra, a practical approach.* Encyclopedia of analytical chemistry, 2000: p. 10815-10837.

125. Wingrave, J.A. and A.V. Teplyakov, *Infrared spectrometer attachment assembly for use with vacuum and high-pressure cells.* Journal of Vacuum Science & Technology A, 2003. 21(5): p. 1800-1801.

126. Lichtfers, U. and B. Rumpf, *Infrared spectroscopic studies for determining species concentrations in aqueous solutions containing ammonia and carbon dioxide.* Chemie Ingenieur Technik, 2000. 72(12): p. 1526-+.

127. Fuente, E., J.A. Menendez, M.A. Diez, D. Suarez, and M.A. Montes-Moran, *Infrared spectroscopy of carbon materials: A quantum chemical study of model compounds.* Journal of Physical Chemistry B, 2003. 107(26): p. 6350-6359.

128. Kuhlmann, U., H. Jantoljak, N. Pfander, P. Bernier, C. Journet, and C. Thomsen, *Infrared active phonons in single-walled carbon nanotubes.* Chemical Physics Letters, 1998. 294(1-3): p. 237-240.

129. Xie, H.Q., H. Lee, W. Youn, and M. Choi, *Nanofluids containing multiwalled carbon nanotubes and their enhanced thermal conductivities.* Journal of Applied Physics, 2003. 94(8): p. 4967-4971.

130. Kang, S.Z., Q.D. Zeng, C. Wang, S.D. Xu, H.M. Zhang, Z.G. Wang, L.J. Wan, and C.L. Bai, *Towards total dissolution of full length unmodified carbon nanotubes (CNT) and its application to fabrication of ultra-thin CNT films at the water/air interface.* Journal of Materials Chemistry, 2003. 13(6): p. 1244-1247.

131. Wilson, T. and O.E. Vilches, *Adsorption of He-4 on carbon nanotube bundles.* Physica B-Condensed Matter, 2003. 329: p. 278-279.

132. Matranga, C. and B. Bockrath, *Permanent Trapping of CO2 in Single-Walled Carbon Nanotubes Synthesized by the HiPco Process.* J. Phys. Chem. B, 2004. 108: p. 6170-6174.

133. Matranga, C., L. Chen, M. Smith, E. Bittner, J.K. Johnson, and B. Bockrath, *Trapped CO2 in carbon nanotube bundles.* Journal of Physical Chemistry B, 2003. 107(47): p. 12930-12941.

134. Yim, W.L., O. Byl, J.T. Yates, and J.K. Johnson, *Vibrational behavior of adsorbed CO2 on single-walled carbon nanotubes.* Journal of Chemical Physics, 2004. 120(11): p. 5377-5386.

135. Byl, O., P. Kondratyuk, S.T. Forth, S.A. FitzGerald, L. Chen, J.K. Johnson, and J.T. Yates, *Adsorption of CF4 on the internal and external surfaces of opened single-walled carbon nanotubes: A vibrational spectroscopy study.* Journal of the American Chemical Society, 2003. 125(19): p. 5889-5896.

136. Byl, O., P. Kondratyuk, and J.T. Yates, *Adsorption and dimerization of NO inside single-walled carbon nanotubes - An infrared spectroscopic study.* Journal of Physical Chemistry B, 2003. 107(18): p. 4277-4279.

137. Yang, C.M., H. Kanoh, K. Kaneko, M. Yudasaka, and S. Iijima, *Adsorption behaviors of HiPco single-walled carbon nanotube aggregates for alcohol vapors.* Journal of Physical Chemistry B, 2002. 106(35): p. 8994-8999.

138. Toebes, M.L., F.F. Prinsloo, J.H. Bitter, A.J. van Dillen, and K.P. de Jong, *Influence of oxygen-containing surface groups on the activity and selectivity of carbon nanofiber-supported ruthenium catalysts in the hydrogenation of cinnamaldehyde.* Journal of Catalysis, 2003. 214(1): p. 78-87.

139. Valentini, L., I. Armentano, D. Puglia, L. Lozzi, S. Santucci, and J.M. Kenny, *A deeper understanding of the photodesorption mechanism of aligned carbon nanotube thin films by impedance spectroscopy.* Thin Solid Films, 2004. 449(1-2): p. 105-112.

140. Liang, W. and Z.B. Yuan, *Direct electrochemistry of glucose oxidase at a gold electrode modified with single-wall carbon nanotubes.* Sensors, 2003. 3(12): p. 544-554.

141. Wang, Z.M., H. Kanoh, K. Kaneko, G.Q. Lu, and D. Do, *Structural and surface property changes of macadamia nut-shell char upon activation and high temperature treatment.* Carbon, 2002. 40(8): p. 1231-1239.

142. Ellison, M.D., M.J. Crotty, D. Koh, R.L. Spray, and K.E. Tate, *Adsorption of NH3 and NO2 on single-walled carbon nanotubes.* Journal of physical Chemistry B, 2004. 108(23): p. 7938-7943.

143. Kwon, S., *Environmentally relevant adsorption on carbonaceous surfaces studied by optical differential reflectance and temperature programmed desorption.* Ph.D proposal, University of Pittsburgh, 2002.

144. Habenschaden, E. and J. Kuppers, *Evaluation of Flash Desorption Spectra.* Surface Science, 1984. 138: p. L147-L150.

145. Redhead, P.A., *Thermal desorption of Gases.* Vacuum, 1962. 12: p. 203-211.

146. Kwon, S., E. Borguet, and R.D. Vidic, *Impact of surface heterogeneity on mercury uptake by carbonaceous sorbents under UHV and atmospheric pressure.* Environmental Science & Technology, 2002. 36(19): p. 4162-4169.

147. Kwon, S., J. Russell, X.C. Zhao, R.D. Vidic, J.K. Johnson, and E. Borguet, *Combined experimental and theoretical investigation of polar organic adsorption/desorption from model carbonaceous surfaces: Acetone on graphite.* Langmuir, 2002. 18(7): p. 2595-2600.

148. Kwon, S., R. Vidic, and E. Borguet, *The effect of surface chemical functional groups on the adsorption and desorption of a polar molecule, acetone, from a model carbonaceous surface, graphite.* Surface Science, 2003. 522(1-3): p. 17-26.

149. http://www.kynol.com.

150. Chiang, I.W., B.E. Brinson, A.Y. Huang, P.A. Willis, M.J. Bronikowski, J.L. Margrave, R.E. Smalley, and R.H. Hauge, *Purification and characterization of single-wall carbon nanotubes (SWNTs) obtained from the gas-phase decomposition of CO (HiPco process).* Journal of Physical Chemistry B, 2001. 105(35): p. 8297-8301.

151. Thess, A., R. Lee, P. Nikolaev, H.J. Dai, P. Petit, J. Robert, C.H. Xu, Y.H. Lee, S.G. Kim, A.G. Rinzler, D.T. Colbert, G.E. Scuseria, D. Tomanek, J.E. Fischer, and R.E. Smalley, *Crystalline ropes of metallic carbon nanotubes.* Science, 1996. 273(5274): p. 483-487.

152. Smith, M.R., S.W. Hedges, R. LaCount, D. Kern, N. Shah, G.P. Huffman, and B. Bockrath, *Selective oxidation of single-walled carbon nanotubes using carbon dioxide.* Carbon, 2003. 41(6): p. 1221-1230.

153. Boehm, H.P., *surface oxides on carbon and their analysis: a critical assessment.* Carbon, 2002. 40: p. 145-149.

154. Matranga, C., L. Chen, M. Smith, E. Bittner, J.K. Johnson, and B. Bockrath, *Trapped CO2 in carbon nanotube bundles.* J. Phys. Chem. B, 2003. 107(47): p. 12930-12941.

155. Nakanishi, K., *Infrared absorption spectroscopy-practical*. 1962: Holden-Day Inc. San Francisco and Nankodo Company Limited, Tokyo.

156. Li, X.H., J.L. Niu, J. Zhang, H.L. Li, and Z.F. Liu, *Labeling the defects of single-walled carbon nanotubes using titanium dioxide nanoparticles.* J. Phys. Chem. B, 2003. 107(11): p. 2453-2458.

157. Kuznetsova, A., D.B. Mawhinney, V. Naumenko, J.T. Yates, J. Liu, and R.E. Smalley, *Enhancement of adsorption inside of single-walled nanotubes: opening the entry ports.* Chem. Phys. Lett., 2000. 321(3-4): p. 292-296.

158. Hennrich, F., R. Wellmann, S. Malik, S. Lebedkin, and M.M. Kappes, *Reversible modification of the absorption properties of single-walled carbon nanotube thin films via nitric acid exposure.* Phys. Chem. Chem. Phys., 2003. 5(1): p. 178-183.

159. Furtado, C.A., U.J. Kim, H.R. Gutierrez, L. Pan, E.C. Dickey, and P.C. Eklund, *Debundling and Dissolution of Single-Walled Carbon Nanotubes in Amide Solvents.* J. Am. Chem. Soc., 2004. 126: p. 6095 - 6105.

160. Mathauer, K. and C. Frank, *Naphthalene chromophore tethered in the constrained environment of a self-assembled monolayer.* Langmuir, 1993. 9: p. 3002-3008.

161. Wang, Y., H. Viswanathan, A. Audi, and P. Sherwood, *X-ray photoelectron spectroscopic studies of carbon fiber surfaces. 22. comparison between surface treatment of untreated and previously surface-treated fibers.* Chem. Mater., 2000. 12: p. 1100-1107.

162. Shin, S., J. Jang, S. Yoon, and I. Mochida, *A study on the effect of heat treatment on functional groups of pitch based activated carbon fiber using FTIR.* Carbon, 1997. 35(12): p. 1739-1743.

163. Chakrapani, N., Y.M.M. Zhang, S.K. Nayak, J.A. Moore, D.L. Carroll, Y.Y. Choi, and P.M. Ajayan, *Chemisorption of acetone on carbon nanotubes.* Journal of Physical Chemistry B, 2003. 107(35): p. 9308-9311.

164. Kukovecz, A., C. Kramberger, V. Georgakilas, M. Prato, and H. Kuzmany, *A detailed Raman study on thin single-wall carbon nanotubes prepared by the HiPCO process.* European Physical Journal B, 2002. 28(2): p. 223-230.

165. Karachevtseva, V.A., A.Y. Glamazda, U. Dettlaff-Weglikowska, V.S. Kurnosov, E.D. Obraztsova, A.V. Peschanskii, V.V. Eremenko, and S. Roth, *Raman spectroscopy of HiPCO single-walled carbon nanotubes at 300 and 5 K.* Carbon, 2003. 41(8): p. 1567-1574.

166. Georgakilas, V., D. Voulgaris, E. Vazquez, M. Prato, D.M. Guldi, A. Kukovecz, and H. Kuzmany, *Purification of HiPCO carbon nanotubes via organic functionalization.* Journal of the American Chemical Society, 2002. 124(48): p. 14318-14319.

167. Yudasaka, M., H. Kataura, T. Ichihashi, L.C. Qin, S. Kar, and S. Iijima, *Diameter enlargement of HiPco single-wall carbon nanotubes by heat treatment.* Nano Letters, 2001. 1(9): p. 487-489.

168. Masciangioli, T. and W.X. Zhang, *Environmental technologies at the nanoscale.* Environ. Sci. Technol., 2003. 37(5): p. 102A-108A.

169. Zhu, H.W., X.S. Li, L.J. Ci, C.L. Xu, D.H. Wu, and Z.Q. Mao, *Hydrogen storage in heat-treated carbon nanofibers prepared by the vertical floating catalyst method.* Mater. Chem. Phys., 2003. 78(3): p. 670-675.

170. Kuznetsova, A., J.T. Yates, J. Liu, and R.E. Smalley, *Physical adsorption of xenon in open single walled carbon nanotubes: Observation of a quasi-one-dimensional confined Xe phase.* J. Chem. Phys., 2000. 112(21): p. 9590-9598.

171. Chang, H., J.D. Lee, S.M. Lee, and Y.H. Lee, *Adsorption of NH3 and NO2 molecules on carbon nanotubes.* Appl. Phys. Lett., 2001. 79(23): p. 3863-3865.

172. Ellison, M.D., M.J. Crotty, D. Koh, R.L. Spray, and K.E. Tate, *Adsorption of NH3 and NO2 on single-walled carbon nanotubes.* J. Phys. Chem. B, 2004. 108(23): p. 7938-7943.

173. Valentini, L., C. Cantalini, I. Armentano, J.M. Kenny, L. Lozzi, and S. Santucci, *Highly sensitive and selective sensors based on carbon nanotubes thin films for molecular detection.* Diamond Relat. Mater., 2004. 13(4-8): p. 1301-1305.

174. Bradley, K., J.C.P. Gabriel, M. Briman, A. Star, and G. Gruner, *Charge transfer from ammonia physisorbed on nanotubes.* Phys. Rev. Lett., 2003. 91(21): p. 218301.

175. Zhao, J.J., A. Buldum, J. Han, and J.P. Lu, *Gas molecule adsorption in carbon nanotubes and nanotube bundles.* Nanotechnology, 2002. 13(2): p. 195-200.

176. Bauschlicher, C. and A. Ricca, *Binding of NH3 to graphite and to a (9,0) carbon nanotube.* Phys. Rev. B, 2004. 70(115409).

177. Elstner, M., D. Porezag, G. Jungnickel, J. Elsner, M. Haugk, T. Frauenheim, S. Suhai, and G. Seifert, *Self-consistent-charge density-functional tight-binding method for simulations of complex materials properties.* Phys. Rev. B, 1998. 58(11): p. 7260-7268.

178. Elstner, M., P. Hobza, T. Frauenheim, S. Suhai, and E. Kaxiras, *Hydrogen bonding and stacking interactions of nucleic acid base pairs: A density-functional-theory based treatment.* J. Chem. Phys., 2001. 114(12): p. 5149-5155.

179. Irle, S., G.S. Zheng, M. Elstner, and K. Morokuma, *From C-2 molecules to self-assembled fullerenes in quantum chemical molecular dynamics.* Nano Lett., 2003. 3(12): p. 1657-1664.

180. Kumar, A., M. Elstner, and S. Suhai, *SCC-DFTB-D study of intercalating carcinogens: Benzo(a)pyrene and its metabolites complexed with the G-C base pair.* Int. J. Quantum. Chem., 2003. 95(1): p. 44-59.

181. Lubezky, A., L. Chechelnitsky, and M. Folman, *Fourier transform infrared spectrum of ammonia adsorbed on C-60 films.* Surf. Sci., 2000. 454: p. 147-151.

182. Binbrek, O.S. and A. Anderson, *Raman spectra of molecular crystals. Ammonia and ammonia-d3.* Chem. Phys. Lett., 1972. 15(3): p. 421-7.

183. Krungleviciute, V., L. Heroux, S. Talapatra, and A.D. Migone, *Gas adsorption on HiPco nanotubes: Surface area determinations, and neon second layer data.* nano Lett., 2004. 4(6): p. 1133-1137.

184. Yang, C.M., K. Kaneko, M. Yudasaka, and S. Iijima, *Effect of purification on pore structure of HiPco single-walled carbon nanotube aggregates.* Nano Lett., 2002. 2(4): p. 385-388.

185. Rowntree, P., G. Scoles, and J. Xu, *The Structure of Ammonia Overlayers Physisorbed onto the Surface of Single-Crystal Graphite, Determined by Means of Atomic-Beam Diffraction.* J. Chem. Phys., 1990. 92(6): p. 3853-3857.

186. Peng, S., K.J. Cho, P.F. Qi, and H.J. Dai, *Ab initio study of CNT NO2 gas sensor.* Chem. Phys. Lett., 2004. 387(4-6): p. 271-276.

187. Feng, X., C. Matranga, R. Vidic, and E. Borguet, *A Vibrational Spectroscopic Study of the Fate of Oxygen-Containing Functional Groups and Trapped CO2 in Single-Walled Carbon Nanotubes During Thermal Treatment.* J. Phys. Chem. B, 2004. 108(52): p. 19949-19954.

188. Chiang, I.W., B.E. Brinson, A.Y. Huang, P.A. Willis, M.J. Bronikowski, J.L. Margrave, R.E. Smalley, and R.H. Hauge, *Purification and characterization of single-wall carbon nanotubes (SWNTs) obtained from the gas-phase decomposition of CO (HiPco process).* J. Phys. Chem. B, 2001. 105(35): p. 8297-8301.

189. Zhao, W., C.H. Song, B. Zheng, J. Liu, and T. Viswanathan, *Thermal recovery behavior of fluorinated single-walled carbon nanotubes.* J. Phys. Chem. B, 2002. 106(2): p. 293-296.

190. Valentini, L., L. Lozzi, S. Picozzi, C. Cantalini, S. Santucci, and J.M. Kenny, *Adsorption of oxidizing gases on multiwalled carbon nanotubes.* J. Vac. Sci. Technol., 2004. 22(4): p. 1450-1454.

191. Valentini, L., C. Cantalini, L. Lozzi, S. Picozzi, I. Armentano, J.M. Kenny, and S. Santucci, *Effects of oxygen annealing on cross sensitivity of carbon nanotubes thin films for gas sensing applications.* Sens. Actuators, B, 2004. 100(1-2): p. 33-40.

192. Zettlemoyer, A.C., J.J. Chessick, and A. Chand, *Sorption by organic substances. II. effect of funtional groups on ammonia sorption.* J. Phys. Chem., 1955. 59: p. 375-8.

193. Liu, C.Y. and K. Aika, *Effect of surface oxidation of active carbon on ammonia adsorption.* Bull. Chem. Soc. Japan, 2003. 76(7): p. 1463-1468.

194. Mangun, C.L., R.D. Braatz, J. Economy, and A.J. Hall, *Fixed bed adsorption of acetone and ammonia onto oxidized activated carbon fibers.* Ind. Eng. Chem. Res., 1999. 38(9): p. 3499-3504.

195. Goldoni, A., R. Larciprete, L. Petaccia, and S. Lizzit, *Single-wall carbon nanotube interaction with gases: Sample contaminants and environmental monitoring.* J. Am. Chem. Soc., 2003. 125(37): p. 11329-11333.

196. Irle, S., D.M. Stanley, and K. Morokuma, *Application of the ONIOM method in carbon nanotube chemistry: Ozonolysis.* in preparation, 2004.

197. You, X., Master thesis, University of Pittsburgh, 2002.

198. Bittner, E.W., M.R. Smith, and B.C. Bockrath, *Characterization of the surfaces of single-walled carbon nanotubes using alcohols and hydrocarbons: a pulse adsorption technique.* Carbon, 2003. 41(6): p. 1231-1239.

199. Cai, L.T., J.L. Bahr, Y.X. Yao, and J.M. Tour, *Ozonation of single-walled carbon nanotubes and their assemblies on rigid self-assembled monolayers.* Chemistry of Materials, 2002. 14(10): p. 4235-4241.

200. Kuznetsova, A., J.T. Yates, V.V. Simonyan, J.K. Johnson, C.B. Huffman, and R.E. Smalley, *Optimization of Xe adsorption kinetics in single walled carbon nanotubes.* Journal of Chemical Physics, 2001. 115(14): p. 6691-6698.

201. Kuznetsova, A., D.B. Mawhinney, V. Naumenko, J.T. Yates, J. Liu, and R.E. Smalley, *Enhancement of adsorption inside of single-walled nanotubes: opening the entry ports.* Chemical Physics Letters, 2000. 321(3-4): p. 292-296.

202. Wang, Z.H., G.A. Luo, J.F. Chen, S.F. Xiao, and Y.M. Wang, *Carbon nanotubes as separation carrier in capillary electrophoresis.* Electrophoresis, 2003. 24(24): p. 4181-4188.

203. Saito, Y. and S. Uemura, *Field emission from carbon nanotubes and its application to electron sources.* Carbon, 2000. 38(2): p. 169-182.

204. Zhu, C.C., W.H. Liu, and L.J. Huangfu, *Flat-panel structure for field-emission displays with carbon nanotube cathode.* Journal of Vacuum Science & Technology B, 2001. 19(5): p. 1691-1693.

205. Fu, K.F. and Y.P. Sun, *Dispersion and solubilization of carbon nanotubes.* Journal of Nanoscience and Nanotechnology, 2003. 3(5): p. 351-364.

206. Koshio, A., M. Yudasaka, M. Zhang, and S. Iijima, *A simple way to chemically react single-wall carbon nanotubes with organic materials using ultrasonication.* Nano Letters, 2001. 1(7): p. 361-363.

207. Sun, Y., S.R. Wilson, and D.I. Schuster, *High dissolution and strong light emission of carbon nanotubes in aromatic amine solvents.* Journal of the American Chemical Society, 2001. 123(22): p. 5348-5349.

208. Ausman, K.D., R. Piner, O. Lourie, R.S. Ruoff, and M. Korobov, *Organic solvent dispersions of single-walled carbon nanotubes: Toward solutions of pristine nanotubes.* Journal of Physical Chemistry B, 2000. 104(38): p. 8911-8915.

209. http://es.epa.gov/ncer/nano/research/nano_sensors.html.

210. http://es.epa.gov/ncer/nano/research/nano_treatment.html.